Feedback control for mechanical cooling and squeezing in cavity quantum optomechanics

PhD Dissertation
Frederik Werner Isaksen

Supervised by
Professor Ulrik Lund Andersen, DTU Physics
Senior Adviser Ulrich Busk Hoff, DTU Physics

DTU Physics
Technical University of Denmark

October 2022

Feedback control for mechanical cooling and squeezing in cavity quantum optomechanics

Phd Dissertation
October 2022

By
Frederik Werner Isaksen

Supervisor:	Professor Ulrik Lund Andersen, DTU Physics
Co-supervisor:	Senior Adviser Ulrich Busk Hoff, DTU Physics
Period:	September 2019 – October 2022
University:	Technical University of Denmark
Department:	DTU Physics, Department of Physics Section of Quantum Physics and Information Technology, QPIT bigQ - Center for Macroscopic Quantum States

Abstract (English)

Cavity optomechanics is a hugely popular research field in which the interaction between photons of light and phonons of mechanical oscillators is studied. It is a promising platform for generating non-classical quantum states at a macroscopic scale and for making devices suitable for photonic quantum computers and quantum communication protocols.

A central challenge in optomechanics is the large amount of noise present in mechanical oscillators at room temperature. In order to be able to observe quantum phenonema, this noise must be eliminated. A well-established method for doing so is feedback cooling, in which a strong probe field interacting with the cavity optomechanical system is used to measure the mechanical position which is then used to apply a feedback force back onto the mechanical oscillator in order to stop its motion, thereby reducing the mechanical noise (quantified by its phonon number) and cooling it down. Such a feedback scheme may also potentially be used to prepare the mechanical oscillator in a squeezed state. In this dissertation, we theoretically investigate two types of feedback cooling schemes.

In one scheme, we use conditional estimation of the quantum state of the optomechanical system to apply feedback using optimal control. We calculate the minimal phonon number and maximum squeezing levels that may be obtained using this feedback scheme. We highlight the inherent difference between the so-called conditional state and unconditional state of the mechanics — a difference which it is often falsely assumed can be brought to zero. We also compare the performance of the scheme under different approximations of the mechanical interaction with its environment and with an adiabatic approximation of the cavity field. Furthermore, we investigate how much the phonon numbers and squeezing levels may be improved using a squeezed probe field.

We also investigate an entirely different feedback scheme, where the output field from the cavity is not measured, but instead sent through a delay line before it is fed back directly into the cavity. This feedback scheme is potentially simpler to set up experimentally. We find that this feedback scheme produces phonon numbers comparable to, but not as low as the previous scheme.

Together, these results pave the way for achieving ground state cooling and squeezing at room temperature in optomechanical systems, which opens the possibility for more interesting quantum information applications.

Abstract (Dansk)

Kavitets-optomekanik er et enormt populært forskningsfelt hvor interkationen mellem fotoner af lys og fononer af mekaniske oscillatorer studeres. Det er en lovende platform til at generere ikke-klassiske kvantetilstande på en makroskopisk skala og for at lave devices til fotoniske kvantecomputere og kvantekommunikationsprotokoller.

En central udfordring inden for optomekanik er den store mængde støj som mekaniske oscillatorer er påvirket af ved stuetemperatur. Denne støj skal elimineres, for at man er i stand til at observere kvantefænomener. En veletableret måde at reducere støjen på er feedback-køling: Her lader man det kavitets-optomekaniske system interagere med et stærkt probelysfelt som bruges til at måle den mekaniske position, som så bruges til at påtrykke en feedback-kraft på mekanikken således at dens bevægelse ophører. Herved reduceres den mekaniske støj (kvantificeret ved dens fonontal) og mekanikken køles ned. sådan et feedbacksystem kan også potentielt bruges til at forberede mekanikken i en såkaldt klemt tilstand. I denne afhandling laves en teoretisk undersøgles af to typer af feedbacksystemer.

I et af systemerne bruges betinget estimering af det optomekaniske systems kvantetilstand til at påtrykke feedback ved brug af optimal kontrol. vi udregner det minimal fonontal og maksimale squeezing nivea som kan opnås ved brug af dette feedbacksystem. Vi fremhæver de iboende forskelle mellem de såkaldte betingede og ubetingede tilstand af mekanikken – en forskel som det ofte forkert antages kan bringes til nul. Vi sammenligner også virkningsgraden af af feedbacksystemet under forskellige approksimationer af den mekaniske interaktion med sit termiske miljø og med en adiabatisk approksimation af kavitetsfeltet. Derudover undersøger vi hvor meget fonontallet og squeezingniveauet kan forbedres ved at bruge et klemt probefelt.

Vi undersøger også et helt anderledes feedbacksystem, hvor udgangsfeltet fra kaviteten ikke måles, men i stedet sendes gennem en delay line før det sendes tilbage inde i kaviteten. Dette feedbacksystem er potentielt simplere at opsætte eksperimentelt. Vi lærer at dette feedbacksystem resulterer i fonontal sammenlignelige med, men ikke så lave som under det foregående system.

Tilsammen baner disse resultater vejen for at opnå køling til grundtilstanden og squeezing i optomekaniske systemer ved stuetemperatur, hvilket låser op for flere mulige interessante anvendelser i kvanteinformationssammenhæng.

Contents

Chapter 1

Introduction

This dissertation is about cavity quantum optomechanics. This research field has evolved tremendously in the past 20 years and has become an exciting platform for exploring quantum mechanical phenonena at a macroscopic level and developing quantum technology [1, 2, 3].

The word optomechanics, a combination of the words 'optics' and 'mechanics', is used to describe physical interactions between light and mechanical elements, typically mechanical harmonic oscillators. In this work, we are mainly talking about so-called radiation-pressure interactions, which describes the situation where momentum is exchanged between the mechanical oscillator and photons. In cavity optomechanics, this interaction takes place between photons and a mechanical element inside a cavity, for instance as a vibrating end mirror. The advantage of using a cavity is that each photon will interact with the mechanics multiple times, as the photons are circulating back and forth between the cavity mirrors, thus increasing the applied force on the mechanics. As this force is applied, the position of the mechanical element changes (in an oscillating fashion), which in turn will change the resonance frequency of the light inside the cavity. This interplay between the cavity light field mode and the mechanical mode allows for some rich and interesting physics. From the perspective of a quantum physicist, one of the motivations behind building optomechanical experiments is that both the mechanical oscillator and the cavity light field are adequately described as quantum harmonic oscillators. That these two seemingly very different physical entities may be modeled using the same mathematical framework is not only convenient from a theoretical perspective, but also means that the mechanics and the light are able to carry the same type of quantum states. This, for example, opens the door to mapping or transferring quantum information between the mechanics and the cavity, using the optomechanical system as a quantum memory for light [4, 5, 6, 7]. This is particularly relevant as we today are able to generate quite sophisticated quantum states of light in the laboratory [8], and a number of platforms for building a photonic quantum computer are starting to show promise [9, 10, 11]. At the same time, our ability to engineer small high quality mechanical oscillators using nanofabrication is also continually increasing [12, 13, 14]. As a results, some of the experimental achievements of the fields is observing quantum entanglement between two mechanical oscillators [15, 16], performing an optomechanical Bell test [17], and creating single-phonon added and subtracted states [18].

If one wants to observe quantum mechanical effects of the mechanical oscillator, it is necessary to eliminate the noise added to the mechanical vibrations from the external environment. This noise is quantified by the so-called mechanical phonon number, a dimensionless number n that counts the number of energy quanta (phonons) carried by the oscillator. If the mechanical

oscillator is left at a temperature T without any other interactions than with its thermal environment, its n is equal to the *thermal* phonon number $\bar{n} = \left[\exp\left(\frac{\hbar\Omega_m}{k_\mathrm{B}T}\right) - 1\right]^{-1}$, where Ω_m is the oscillator angular resonance frequency, $\hbar$ is the reduced Planck constant and k_B is the Boltzmann constant. Depending on the details of the optomechanical setup, the resonance frequency may be as low as $\Omega_m \approx 3\,\mathrm{Hz}$ ($\bar{n} \approx 10^{13}$ at room temperature, $T = 300\,\mathrm{K}$) [19] to as high as $\Omega_m \approx 10\,\mathrm{GHz}$ ($\bar{n} \approx 10^4$) [20]. We generally want to remove as many thermal phonons from the oscillator as possible; this is referred to as *cooling* of the mechanics. If $n = 0$, we have reached the quantum ground state of the oscillator. As reaching exactly $n = 0$ is not possible due to the laws of thermodynamics, a phonon number of $n < 1$ is typically considered 'ground state cooling' of the oscillator. Achieving ground state cooling of a macroscopic mechanical oscillator is a research goal in itself, but minimizing the phonon number as much as possible will in general pave the way for generating more interesting quantum states or quantum interactions, as this is often a requirement in theoretical proposals thereof [21, 22, 23]. For mechanical oscillators with large mechanical frequencies, ground state cooling may be achievable simply by putting the optomechanical setup into a dilution fridge that can cool the environment down to around $\sim 10\,\mathrm{mK}$. However, for low frequency oscillators that will not be enough. Furthermore, if the optomechanical system is to be used as a device in a quantum computer or quantum communication system, storing it in a freezer is impractical.

This is the main motivation behind mechanical cooling via the optomechanical interaction with the light field. Generally, there are two methods of optomechanical cooling. The first one is so-called laser cooling, in which a laser drives the optomechanical cavity at a frequency detuned from from the laser cavity frequency. If the cavity linewidth κ is far below Ω_m (the so-called *sideband-resolved regime*), this process will exchange phonons and photons between the mechanics and the light, such that phonons are taken out of the mechanics, thereby resulting in cooling. This method has been used extensively through the literature, and was recently used to achieve ground state cooling of a levitated nanoparticle in an optomechanical setup [24]. The second method, which instead works in the so-called *bad-cavity regime* where κ is much larger than Ω_m, is *feedback cooling*. With this method, a probe laser field is used to measure the phase quadrature of the cavity field, which due to the nature of the optomechanical interaction will be correlated with the mechanical position. This measurement is then used to generate a feedback force applied to the mechanics such as to stop the mechanical motion, thereby reducing its motional energy and thus its phonon number. The feedback cooling methods can be further divided into two categories: The first and so far most popular method is *cold damping*, in which the mechanical position signal from the probe field is used as input to a negative-derivative feedback filter, such that the feedback signal is proportional to the negative momentum. Cold damping in optomechanics was first proposed in Ref. [25], and the development of the theory has matured since then [26, 27, 28], and it has since been widely experimentally applied, including to bring the mechanics to the ground state both at helium-cooled ($\sim 4\,\mathrm{K}$) temperatures [29] and at room temperature [30]. A second, less widely-used method is feedback based on conditional state estimation and optimal control. Here, the mechanical quantum state is continuously estimated based on the probe field measurement [31, 32], and the estimated *conditional* quantum state is used to generate a feedback signal that is optimal with respect to minimizing the phonon number [33, 34]. This method is in many cases more experimentally challenging to implement than cold damping due to the computational speed required to do the state estimation in real-time, but is on the other hand guaranteed to minimize the achievable phonon number using a linear (homodyne) measurement of the probe field. The method of using conditional state estimation in an optomechanical system was first used in Ref. [35], and the first example of using both

state estimation and feedback in Ref. [36]. The method has since been successfully applied to reach the ground state [37]. Other interesting experiments based on the ideas of conditional state estimation and feedback control in optomechanics have been carried out [38, 39], and there exists many interesting theoretical proposals on the subject as well [40, 41, 42, 43, 44, 45]. Most notably, it has been suggested that conditional state estimation may be used to generate single-mode squeezing of the mechanical degrees of freedom, an important milestone that is yet to be achieved in an optomechanics experiment. At this point, the reader might conclude that the field of optomechanical ground state cooling has reached a sort of conclusion, since this goal has been experimentally achieved. It should however at this point be noted that the experiments that have demonstrated room-temperature ground state cooling to this date [24, 30, 37], whether it is using sideband cooling or any kind of feedback cooling, are all optomechanical platforms based on levitating nanoparticles. At room temperature, platforms based on other types of mechanical oscillators with different advantages and trade-offs have only come close to the ground state [19, 46, 47]. Thus, there is still work to be done.

1.1 Thesis structure

The main purpose of this dissertation is to try and answer some questions regarding how low a phonon number and how much mechanical squeezing can be achieved using optomechanical feedback cooling. In this dissertation, some measurement and feedback strategies in an optomechanical setup are explored.

In Chapter 2, we review the basic theoretical foundations upon which the work of this PhD project is built. This includes some fundamentals of quantum mechanics, harmonic oscillators, quantum optomechanics, open quantum systems, and some Itō calculus.

In Chapter 3, we present theoretical work on a measurement-based feedback scheme for optomechanical cooling and squeezing, based on continuous conditional dynamics, optimal state estimation and optimal control.

In Chapter 4, the model presented in chapter 3 is extended to encompass squeezed probe fields rather than just coherent probe fields.

In Chapter 5, we propose and analyse an optomechanical feedback scheme based on coherent, direct feedback using the output field from the cavity without an intermediate measurement.

Finally, in Chapter 6, the dissertation is concluded.

Chapter 2

Basics

This chapter contains the basic theoretical concepts upon which the work in this dissertation is built.

2.1 Basic quantum mechanics

It is assumed that the reader is familiar with basic quantum mechanics. Nevertheless, a brief review of the central axioms of the theory is presented below for the sake of completeness. We expect that the reader is familiar with linear algebra in finite and infinite-dimensional Hilbert spaces.

According to quantum mechanics, a physical system is fully described by a *state vector* $|\psi\rangle$ which lies in a (separable) Hilbert space $\mathcal{H}$. We use the standard Dirac notation where $\langle\psi|$ is the dual vector of $|\psi\rangle$ and $\langle\phi|\psi\rangle$ is the inner product between the vectors $|\psi\rangle$ and $|\phi\rangle$. A requirement of the state vector $|\psi\rangle$ is that it is normalized, i.e. that $\langle\psi|\psi\rangle = 1$.

Physical *observables* (e.g. position, momentum, energy...) are represented by linear operators $\hat{A}$ acting on vectors lying in $\mathcal{H}$. Note that throughout this dissertation, any symbol with a hat ($\hat{}$) on top of it denotes am operator. The possible outcomes of measuring the observable $\hat{A}$ are given by the operators eigenvalues $\{a_j\}_{j\in J}$ with associated eigenvectors $\{|\psi_j\rangle\}_{j\in J}$, i.e. $\hat{A}\,|\psi_j\rangle = a_j\,|\psi_j\rangle$ for all $j \in J$. In order for these outcomes to correspond to values of a physical measurement, we require that all eigenvalues a_j of $\hat{A}$ must be real numbers, from which it follows that all physical observables $\hat{A}$ are Hermitian, i.e. $\hat{A}^\dagger = \hat{A}$, where the superscript $\dagger$ ('dagger') denotes the Hermitian conjugate. From this it also follows that the eigenvectors are orthogonal, i.e. that $\langle\psi_j|\psi_k\rangle = 0$ for $j \neq k$. We usually also take the eigenvectors to be normalized, but this is not always possible.

The probability of measuring the outcome a_j of the physical observable $\hat{A}$ is given by

$$\Pr(a_j) = |\langle\psi_j|\psi\rangle|^2 \tag{2.1.1}$$

The act of performing the measurement with outcome a_j changes the system's state vector (or simply, its state) from $|\psi\rangle$ to $|\psi_j\rangle$. This is referred to as a *measurement collapse* or *collapse of the wave function.* Note that some observables $\hat{A}$ may have several linearly independent eigenvectors corresponding to the same eigenvalue, e.g. there may exist $j_1, j_2, ... \in J$ such that $a_{j_1} = a_{j_2} = ... =: a$. In this case, we have that

$$\Pr(a) = \sum_i |\langle \psi_{j_i} | \psi \rangle|^2 , \tag{2.1.2}$$

and the state collapses to

$$|\psi_{\text{after}}\rangle = \frac{\sum_i \langle \psi_{j_i} | \psi \rangle \, |\psi_{j_i}\rangle}{\sqrt{\Pr(a)}}. \tag{2.1.3}$$

From these relations, it follows that the *expectation value* of the observable $\hat{A}$ is given by

$$\langle A \rangle := \sum_j a_j \Pr(a_j) = \langle \psi | \hat{A} | \psi \rangle . \tag{2.1.4}$$

It is far from always the case that one knows the state vector of the system with certainty. Generally, the system is known to be in some state $|\phi_1\rangle$ with probability p_1, $|\phi_2\rangle$ with probability p_2 and so on. In this case, the state of the system is associated with its *density matrix* (also called its *state operator*)

$$\hat{\rho} = \sum_i p_i \, |\phi_i\rangle \langle \phi_i| , \tag{2.1.5}$$

where all $p_i \geq 0$ and $\sum_i p_i = 1$. From the above definition, one finds that the density matrix has the following properties:

1. $\hat{\rho}$ is Hermitian.
2. $\hat{\rho}$ is positive-semi-definite, i.e. $\langle \phi | \hat{\rho} | \psi \rangle \geq 0$ for any two vectors $|\phi\rangle , |\psi\rangle \in \mathcal{H}$.
3. $\text{Tr}(\hat{\rho}) = 1$, where Tr is the trace operation, i.e. $\text{Tr}(...) = \sum_i \langle \psi_j | ... | \psi_j \rangle$ for any complete, orthonormal set $\{|\psi_j\rangle\}_{j=1}^{\infty}$ of $\mathcal{H}$.

Conversely, one can show that any operator satisfying the properties 1.-3. is a valid density matrix, i.e. that it can be written in the of form Eq. (2.1.5). It is often useful to check if a given density matrix actually fulfills the properties 1.-3. This is done in order to verify calculations, for example to check numerical results from computer code, or to investigate if a physical model is a valid description of reality.

It is clear that a density matrix is a more general way of representing a physical system than a state vector. This is seen by noting that physical states which are adequately described by a single state vector $|\psi\rangle$ with probability 1 has the associated density matrix $\hat{\rho} = |\psi\rangle \langle \psi|$. This is referred to as a *pure* state. A necessary and sufficient condition that a state is pure is that $\text{Tr}(\hat{\rho}^2) = 1$. The number $\text{Tr}(\hat{\rho}^2)$ is always between 0 and 1 and is therefore also called the *purity* of the state. States that are not pure are called *mixed states*.

When a system is in the state $\hat{\rho}$, the expectation value of the operator $\hat{A}$ is given by

$$\langle A \rangle = \sum_i p_i \langle \phi_i | \hat{A} | \phi_i \rangle = \text{Tr}[\hat{A}\hat{\rho}]. \tag{2.1.6}$$

Measuring the observable $\hat{A}$ with outcome a_j now has probability

$$\Pr(a_j) = \begin{cases} \sum_i p_i \, |\langle \phi_i | \psi_j \rangle|^2 = \langle \psi_j | \hat{\rho} | \psi_j \rangle , & \text{if } a_j \text{ has one eigenvector } |\psi_j\rangle , \\ \sum_i p_i \sum_k |\langle \phi_i | \psi_{j_k} \rangle|^2 = \sum_k \langle \psi_{j_k} | \hat{\rho} | \psi_{j_k} \rangle & \text{if } a_j \text{ has multiple eigenvectors } \{|\psi_{j_k}\rangle\}_k . \end{cases} \tag{2.1.7}$$

The measurement probabilities may be reformulated in terms of *projection operators*: Assume that the set of eigenvectors associated with the eigenvalue a_j of observable $\hat{A}$ be $\{|\psi_{j_k}\rangle\}_k$, which may or may not contain only a single vector. Let

$$\hat{\Pi}_j = \sum_k |\psi_{j_k}\rangle \langle\psi_{j_k}| \tag{2.1.8}$$

be the projection operator associated with the measurement outcome a_j. We can then write the measurement probability as

$$\Pr(a_j) = \mathrm{Tr}\left[\hat{\Pi}_j \hat{\rho}\right] = \langle \Pi_j \rangle , \tag{2.1.9}$$

which collapses the state into the density matrix

$$\hat{\rho}_{\text{after}} = \frac{\hat{\Pi}_j \hat{\rho} \hat{\Pi}_j}{\Pr(a_j)}. \tag{2.1.10}$$

An important concept related to the measurement of states in quantum mechanics is *compatible* and *incompatible* observables. Define the *commutator* between two operators $\hat{A}$ and $\hat{B}$ as $[\hat{A}, \hat{B}] := \hat{A}\hat{B} - \hat{B}\hat{A}$. if any two observables $\hat{A}$ and $\hat{B}$, have a commutator $[\hat{A}, \hat{B}] = 0$, then a common set of eigenstates exists between them, which means that any measurement of both $\hat{A}$ and $\hat{B}$ simultaneously can be carried out to arbitrary precision. In this case, the observables are called compatible. by contrast if $[\hat{A}, \hat{B}] \neq 0$, the observables are called incompatible, and a measurement of both observable is inherently uncertain. Specifically, defining the standard deviation of some observable $\hat{O}$ as $\sigma_O = \sqrt{\langle O^2 \rangle - \langle O \rangle^2}$, the *Heisenberg uncertainty relation* holds for any observables $\hat{A}$ and $\hat{B}$:

$$\sigma_A \sigma_B \geq \frac{1}{2} \left| \langle [\hat{A}, \hat{B}] \rangle \right| \tag{2.1.11}$$

Finally, we discuss the time evolution of the system. For pure states, the time evolution is governed by the *Schrödinger equation*:

$$i\hbar \frac{d}{dt} |\psi(t)\rangle = \hat{H}(t) |\psi(t)\rangle , \tag{2.1.12}$$

where $i = \sqrt{-1}$ and $\hbar$ is the reduced Planck constant. $\hat{H}(t)$ is the so-called *Hamiltonian* operator, which is also the observable for the energy of the system. In many cases, the Hamiltonian is constant over time, but we keep it explicitly time-dependent here for generality. For mixed states, we use the *von Neumann equation*:

$$i\hbar \frac{d}{dt} \hat{\rho}(t) = [\hat{H}(t), \hat{\rho}(t)] \tag{2.1.13}$$

The above equations are used when working in the so-called Schrödinger picture, in which the state of the system evolves over time, while the observables are constant (Except for explicit time-dependencies). An alternative to this is the *Heisenberg picture*, in which the states are constant, but the observables evolve over time according to the *Heisenberg equation*:

$$\frac{d}{dt} \hat{A}(t) = \frac{i}{\hbar} [\hat{H}(t), \hat{A}(t)] + \frac{\partial \hat{A}(t)}{\partial t}, \tag{2.1.14}$$

where the partial derivative accounts for explicit time-dependencies. The two pictures are physically equivalent since they produce the same expectation values of any observable $\hat{A}$ at time t:

$$\langle A(t)\rangle = \underbrace{\mathrm{Tr}\left[\hat{A}\hat{\rho}(t)\right]}_{\text{Schrödinger picture}} = \underbrace{\mathrm{Tr}\left[\hat{A}(t)\hat{\rho}\right]}_{\text{Heisenberg Picture}} \tag{2.1.15}$$

The time evolution of the system may equivalently be described by a *time evolution operator* $\hat{U}(t)$, defined to fulfill the differential equation

$$i\hbar\frac{d}{dt}\hat{U}(t) = \hat{H}(t)\hat{U}(t), \quad U(0) = \hat{I}, \tag{2.1.16}$$

where $\hat{I}$ is the identity operator. An important property of the time evolution operator is that it is unitary, meaning that $\hat{U}^\dagger(t)\hat{U}(t) = \hat{U}(t)\hat{U}^\dagger(t) = \hat{I}$. It is, however, *not* an observable since it is not Hermitian. In the Schrödinger picture, the time evolution of the states can now be written as the application of the time evolution operator on the state. Namely, we have that

$$|\psi(t)\rangle = \hat{U}(t)\,|\psi(0)\rangle\,, \text{ for pure states,} \tag{2.1.17}$$

$$\hat{\rho}(t) = \hat{U}(t)\hat{\rho}(0)\hat{U}^\dagger(t), \text{ for mixed states.} \tag{2.1.18}$$

The time evolution operator can also be used in the Heisenberg picture, where we have that

$$\hat{A}(t) = \hat{U}^\dagger(t)\hat{A}(0)\hat{U}(t). \tag{2.1.19}$$

Thus, the time evolution operator is a convenient way to connect the two pictures.

Finally, we consider the case in which the Hamiltonian is constant and we can write it as $\hat{H}(t) = \hat{H}$. Consider an eigenstate $|E\rangle$ of $\hat{H}$ with eigenvalue (also called *eigenenergy*) E:

$$\hat{H}\,|E\rangle = E\,|E\rangle \tag{2.1.20}$$

The energy eigenstates are hugely important in almost any analysis of a quantum mechanical problem. For one, if the initial state of the system is $|\psi(0)\rangle = |E\rangle$, then its time evolution is given simply by

$$|\psi(t)\rangle = e^{-iEt/\hbar}\,|E\rangle\,. \tag{2.1.21}$$

Also of particular importance is the energy *ground state*, that is, the energy eigenstate corresponding to the lowest energy of the system.

We finally remark that up until this point it has been implicitly assumed that the operators and observables in question have a discrete set of eigenvalues. However, it is quite often the case that the set of eigenvalues are continuous. In these cases, the formulas involving sums in this section are replaced with formulas involving integrals in a straightforward way. For example, the position operator $\hat{q}$ of a free point particle in one dimension has a continuous set of eigenvalues and eigenstates, $\hat{q}\,|q\rangle = q\,|q\rangle$, where q spans the whole real number line. This is also a case where the eigenstates can not be normalized: the inner product $\langle q|q\rangle$ is equal to the peak of a Dirac delta function. Given a pure state $|\psi\rangle$, $p(q) = |\langle q|\psi\rangle|^2$ is now the probability *density* function of the position. This means that e.g. the probability that q lies in the interval $[a, b]$ is given by

$$\Pr(q \in [a,b]) = \int_a^b |\langle q|\psi\rangle|^2\, dq \tag{2.1.22}$$

The function $\psi(q) := \langle q|\psi\rangle$ is commonly referred to as the position *wavefunction* or the position representation of $|\psi\rangle$.

2.2 Quantum harmonic oscillators

The vast majority of this dissertation is concerned with two types of physical systems: mechanical oscillators and optical cavity fields. Both of these systems are adequately modeled as quantum harmonic oscillators. It is adequate for most types of mechanical oscillators to model them as a point particle of mass m attached to a spring. The Hamiltonian governing such a system is

$$\hat{H} = \frac{\hat{p}^2}{2m} + \frac{1}{2}m\omega^2\hat{q}^2 \tag{2.2.1}$$

Here, $\hat{q}$ and $\hat{p}$ are the canonical observables for position and momentum, respectively, and ω is the resonance frequency of the mechanical oscillations. This Hamiltonian describes a quantum harmonic oscillator in its simplest form. Note that $\hat{q}$ and $\hat{p}$ satisfies the following fundamental *commutation relation*:

$$[\hat{q}, \hat{p}] = i\hbar \tag{2.2.2}$$

The Hamiltonian in Eq. (2.2.1) can be recast in the form

$$\hat{H} = \hbar\omega(\hat{a}^\dagger\hat{a} + 1/2), \tag{2.2.3}$$

where

$$a = \sqrt{\frac{m\omega}{2\hbar}}\hat{q} + \frac{i}{\sqrt{2\hbar m\omega}}p \tag{2.2.4}$$

The operator $\hat{a}^\dagger$ is called a *raising operator* or a *creation operator*, while its Hermitian conjugate $\hat{a}$ is called a *lowering* or *annihilation* operator. These operators satisfy the following commutation relation:

$$[\hat{a}, \hat{a}^\dagger] = 1 \tag{2.2.5}$$

We remark that when modeling an optical cavity field of resonance frequency ω using equation Eq. (2.2.3), the *number operator* $\hat{n} = \hat{a}^\dagger\hat{a}$ describes the number of photons in the cavity field. When it describes a mechanical oscillator, $\hat{n}$ instead denotes a similar quantity called *phonons*, the quanta of energy carried by the oscillator.

The eigenstates of the harmonic oscillator Hamiltonian $\hat{H}$ are the so-called *number states* or *Fock states* $\{|n\rangle\}_{n=0}^{\infty}$. These states are orthonormal, i.e. $\langle n|n'\rangle = \delta_{n,n'}$. Their corresponding eigenenergies are $E_n = \hbar\omega(n + 1/2)\,|n\rangle$, $n = 0, 1, ...$, and form a complete basis for the Hilbert space. The number states and the creation/annihilation operators satisfy the following important properties:

$$\begin{aligned} \hat{a}^\dagger\,|n\rangle &= \sqrt{n+1}\,|n+1\rangle\,, \quad n \geq 0 \\ \hat{a}\,|n\rangle &= \sqrt{n}\,|n-1\rangle\,, \qquad n \geq 1 \\ \hat{a}\,|0\rangle &= 0 \end{aligned} \tag{2.2.6}$$

Thus, $\hat{a}^\dagger$ raises a given number state by 1, while $\hat{a}$ decreases the number by 1. When modeling an optical cavity field of resonance frequency ω using equation Eq. (2.2.3), the *number operator* $\hat{n} = \hat{a}^\dagger\hat{a}$ describes the number of photons in the cavity field. if the field is in a number state $|n\rangle$, it contains a definite amount of photons $|n\rangle$. When we are dealing with a mechanical oscillator $\hat{n}$ instead denotes a similar quantity called *phonons*. In both cases, the observable $\hat{n}$ counts the quanta of energy stored in the system.

The number state $|0\rangle$ is the ground state of $\hat{H}$ and is customarily called the *vacuum state*, as it describes the physics when no photons are contained in the cavity field.

We end this section by mentioning that it is often convenient to work with a non-dimensionalized version of the operators q and p, called *quadrature operators* or *phase space operators*:

$$\hat{Q} = \frac{\hat{a} + \hat{a}^\dagger}{\sqrt{2}} \quad , \hat{P} = \frac{\hat{a} - \hat{a}^\dagger}{i\sqrt{2}}, \tag{2.2.7}$$

satisfying the commutation relation $[\hat{Q}, \hat{P}] = i$. When dealing with mechanical oscillators, $\hat{Q}$ and $\hat{P}$ are called the *position quadrature* and *momentum quadrature*, respectively. When dealing with an optical field, they are the *amplitude* and *phase* quadrature, respectively. The Hamiltonian may be rewritten in terms of these quadratures as

$$\hat{H} = \frac{\hbar\omega}{2}\left(\hat{Q}^2 + \hat{P}^2\right) \tag{2.2.8}$$

Throughout this dissertation, we will almost exclusively use the symbols $\hat{Q}$ and $\hat{P}$ to refer to the quadratures of a mechanical oscillator, whereas when describing an optical cavity field, we will replace $\hat{Q}$ and $\hat{P}$ with the symbols $\hat{X}$ and $\hat{Y}$, respectively.

2.3 Gaussian quantum states

Consider a harmonic oscillator mode with annihilation operator $\hat{a}$ and corresponding phase space operators $\hat{Q}$ and $\hat{P}$ given as in Eq. (2.2.7). Furthermore, consider the eigenstates $\{|Q\rangle\}_{Q\in\mathbb{R}}$ of $\hat{Q}$ normalized such that $\langle Q'|Q\rangle = \delta(Q' - Q)$, where δ is the Dirac delta function. An important way of representing states $\hat{\rho}$ of the harmonic oscillator is by its *quantum Wigner function* (or simply *Wigner function*):

$$W(Q, P) = \frac{1}{2\pi}\int_{-\infty}^{\infty} \langle Q - y/2|\,\hat{\rho}\,|Q + y/2\rangle\, e^{iPy} dy \tag{2.3.1}$$

It can be shown that the quantum Wigner function $W(Q, P)$ is a one-to-one mapping of the density matrix $\hat{\rho}$. It is often called a *quasi-probability distribution function*, since it shares many similar qualities to a 2D probability density function. For instance, the Wigner function is normalized in the sense that $\int_{-\infty}^{\infty}\int_{-\infty}^{\infty} W(Q, P)dQdP = 1$. Furthermore, the probability distributions of Q and P are given by the marginal distributions $\Pr(Q) = \int_{-\infty}^{\infty} W(Q, P)dP$ and $\Pr(P) = \int_{-\infty}^{\infty} W(Q, P)dQ$. However, the most important way in which it is *different* from a regular 2D probability distribution is that it may take on negative values.

The Wigner function may be generalized to a system consisting of many harmonic oscillators [48]: Given a set of n harmonic oscillator modes with annihilation operators $\hat{a}_1, \hat{a}_2, ..., \hat{a}_n$, satisfying the commutation relations $[\hat{a}_i, \hat{a}_j^\dagger] = \delta_{i,j}$, where $\delta_{i,j}$ is the Kronecker delta. Note that we will refer to such physical systems as *multi-mode* systems, while systems described by only a single harmonic oscillator as *single-mode* systems. We collect their corresponding quadrature operators into a column vector of dimension $2n$:

$$\hat{\mathbf{X}} = (\hat{Q}_1, \hat{P}_1, \hat{Q}_2, \hat{P}_2, ..., \hat{Q}_n, \hat{P}_n)^T \tag{2.3.2}$$

where $\hat{Q}_i = (\hat{a}_i + \hat{a}_i^\dagger)/\sqrt{2}$ and $\hat{P}_i = (\hat{a}_i - \hat{a}_i^\dagger)/(i\sqrt{2})$. Furthermore, for any vector $\mathbf{v}$ denote by $(\mathbf{v})_i$ the i'th entry in the vector, e.g. $(\hat{\mathbf{X}})_3 = \hat{Q}_2$. Define the *characteristic function*

$$\boldsymbol{\chi}(\mathbf{Y}) = \mathrm{Tr}[\hat{\rho}\exp(i\hat{\mathbf{X}}\boldsymbol{\Omega}\mathbf{Y})], \tag{2.3.3}$$

where $\mathbf{Y} \in \mathbb{R}^{2n}$ and $\mathbf{\Omega}$ is called the *symplectic matrix* and is defined as a $2n \times 2n$ block-diagonal matrix consisting of n copies of the matrix $\begin{bmatrix} 0 & 1 \\ -1 & 0 \end{bmatrix}$ along the diagonal and 0 otherwise. The Wigner function is then defined as:

$$W(\mathbf{X}) = \frac{1}{(2\pi)^n} \int_{\mathbb{R}^{2n}} \exp(-\mathbf{X}^T \mathbf{\Omega} \mathbf{Y}) \boldsymbol{\chi}(\mathbf{Y}) d^{2n}\mathbf{Y}, \tag{2.3.4}$$

where $\mathbf{X} \in \mathbb{R}^{2n}$.

A *Gaussian* quantum state is a harmonic oscillator state whose Wigner function follows a multivariate Gaussian distribution:

$$W(\mathbf{X}) = W(\mathbf{X}; \boldsymbol{\mu}, \mathbf{V}) = \frac{1}{(2\pi)^n \sqrt{\det \mathbf{V}}} \exp\left[\frac{1}{2}(\mathbf{X} - \boldsymbol{\mu})^T \mathbf{V}^{-1} (\mathbf{X} - \boldsymbol{\mu})\right] \tag{2.3.5}$$

The Wigner function above is fully determined by two parameters: the mean

$$\boldsymbol{\mu} = \langle \mathbf{X} \rangle = (\langle Q_1 \rangle, \langle P_1 \rangle, ..., \langle Q_n \rangle, \langle P_n \rangle)^T \tag{2.3.6}$$

and the variance $\mathbf{V} =: \mathrm{Var}[\mathbf{X}]$, a $2n \times 2n$ symmetric matrix where each entry $(\mathbf{V})_{i,j}$ in the i'th row and j'th column is given by

$$(\mathbf{V})_{i,j} = \frac{1}{2} \langle \{(\hat{\mathbf{X}} - \langle \hat{\mathbf{X}} \rangle)_i, (\hat{\mathbf{X}} - \langle \hat{\mathbf{X}} \rangle)_j\} \rangle, \tag{2.3.7}$$

where $\{\hat{A}, \hat{B}\} := \hat{A}\hat{B} + \hat{B}\hat{A}$ is the *anticommutator* of the operators $\hat{A}$ and $\hat{B}$. Note that $(\mathbf{V})_{i,i} = \sigma^2_{(\mathbf{X})_i}$ is the variance of $(\mathbf{X})_i$.

From a theoretical perspective, the main appeal of Gaussian quantum states is that they are fully characterised by their mean $\boldsymbol{\mu}$ and variance $\mathbf{V}$. A harmonic oscillator state $|\psi\rangle$ is an infinite-dimensional vector and so is determined by infinitely many parameters in the worst case. On the other hand, a state which you know is Gaussian is characterised by a finite set of real numbers and therefore simpler to deal with. Gaussian states are also typically stable over time: For any physical system described by a Hamiltonian that is at most second order in the quadrature operators in $\hat{\mathbf{X}}$, the quantum state will remain Gaussian if the initial state is Gaussian [48].

We will now go through some important examples of Gaussian single-mode quantum states: The first one is the already encountered vacuum state $|\psi\rangle = |0\rangle$. Its mean and variance are given by

$$\boldsymbol{\mu} = \begin{bmatrix} 0 \\ 0 \end{bmatrix}, \quad \mathbf{V} = \begin{bmatrix} \frac{1}{2} & 0 \\ 0 & \frac{1}{2} \end{bmatrix}. \quad \text{(vacuum state)} \tag{2.3.8}$$

We note that any state with the above variance is called a *minimum uncertainty* state. This is because a variance of $\sigma^2_Q = \sigma^2_P = \frac{1}{2}$ saturates the Heisenberg uncertainty relation in Eq. (2.1.11) for the observables $\hat{P}$ and $\hat{Q}$.

The second one is the so-called *coherent* states, also called *displaced vacuum* states. These are given by $|\psi\rangle = |\alpha\rangle = \hat{D}(\alpha)|0\rangle$, where

$$\hat{D}(\alpha) = \exp(\alpha \hat{a}^\dagger - \alpha^* \hat{a}) \tag{2.3.9}$$

is the so-called *displacement* operator, and α is a complex number. These states are often described as the 'most classical' of all pure states, as the expectation value of the electric field

under these states oscillates sinusoidally [49]. They are also the states that describe laser light inside a cavity. The mean and variance of such states are given by

$$\boldsymbol{\mu} = \begin{bmatrix} \sqrt{2}\mathrm{Re}(\alpha) \\ \sqrt{2}\mathrm{Im}(\alpha) \end{bmatrix}, \quad \mathbf{V} = \begin{bmatrix} \frac{1}{2} & 0 \\ 0 & \frac{1}{2} \end{bmatrix}. \quad \text{(coherent state)} \tag{2.3.10}$$

Thirdly, we have so-called *thermal* states. These are the thermal-equilibrium states of the harmonic oscillator with Hamiltonian $\hat{H} = \hbar\omega(\hat{a}^\dagger\hat{a} + 1/2)$, given by

$$\hat{\rho} = \frac{1}{\bar{n}+1}\sum_{n=0}^{\infty}\left(\frac{\bar{n}}{\bar{n}+1}\right)^n |n\rangle\langle n|, \tag{2.3.11}$$

where $\bar{n}$ is the average photon (or phonon) number given by $\bar{n} = \langle\hat{n}\rangle$. For an external environmental temperature of T, we have that $\bar{n} = \left[\exp\left(\frac{\hbar\omega}{k_B T}\right) - 1\right]^{-1}$. Note that contrary to the previous two states, the thermal state is inherently mixed. Its mean and variance is given by

$$\boldsymbol{\mu} = \begin{bmatrix} 0 \\ 0 \end{bmatrix}, \quad \mathbf{V} = \begin{bmatrix} \bar{n}+\frac{1}{2} & 0 \\ 0 & \bar{n}+\frac{1}{2} \end{bmatrix}. \quad \text{(thermal state)} \tag{2.3.12}$$

Finally, we have the *squeezed* state $|\psi\rangle = \hat{S}(\xi)|0\rangle$, where

$$\hat{S}(\xi) = \exp\left\{\frac{1}{2}\left[\xi^*\hat{a}^2 - \xi(\hat{a}^\dagger)^2\right]\right\} \tag{2.3.13}$$

is the *squeezing* operator. The complex number ξ can be rewritten as $re^{i\theta}$, where r is called the squeezing parameter and θ the squeezing angle. The mean and variance for $\theta = 0$ is

$$\boldsymbol{\mu} = \begin{bmatrix} 0 \\ 0 \end{bmatrix}, \quad \mathbf{V} = \begin{bmatrix} \frac{e^{-2r}}{2} & 0 \\ 0 & \frac{e^{2r}}{2} \end{bmatrix}. \quad \text{(thermal state)} \tag{2.3.14}$$

and the variance for $\theta \neq 0$ is obtained by applying a rotation matrix transformation with angle θ. The fundamental property of squeezed states is that the variance along one of the phase space quadratures is less than that of a coherent state. For this reason, squeezed states are often considered as *nonclassical* states.

2.4 Basics of cavity optomechanics

A cavity optomechanical system (See sketch in Fig. 2.1) consists of a mechanical oscillator coupled to a mode of the electrical field in a cavity of length L. The mechanical element is modeled as an end mirror of the cavity attached to a spring. The cavity is driven by a laser driving field of frequency ω_L with annihilation operator $\hat{a}_{\mathrm{in}}$, decomposed into a mean value α_{in} and a fluctuation term $\delta\hat{a}_{\mathrm{in}}$ such that $\langle\delta a_{\mathrm{in}}\rangle = 0$. Denoting the cavity mode annihilation operator by $\hat{a}$ and that of the mechanical oscillator by $\hat{b}$, the Hamiltonian is of the following form:

$$\hat{H} = \underbrace{\hbar\Omega_m\hat{b}^\dagger\hat{b}}_{\hat{H}_m} + \underbrace{\hbar\omega_c\hat{a}^\dagger\hat{a}}_{\hat{H}_c} + \underbrace{\hat{H}\hbar g_0\hat{a}^\dagger\hat{a}(\hat{b}+\hat{b}^\dagger)}_{\hat{H}_{\mathrm{int}}} + \underbrace{i\hbar\kappa_{\mathrm{in}}(\alpha_{\mathrm{in}}\hat{a}^\dagger - \alpha_{\mathrm{in}}^*\hat{a})}_{\hat{H}_{\mathrm{drive}}} \tag{2.4.1}$$

where Ω_m is the mechanical resonance frequency and ω_c is the frequency of the cavity mode. The first two $\hat{H}_m$ and $\hat{H}_c$ terms represent the Hamiltonians for the individual harmonic oscillator

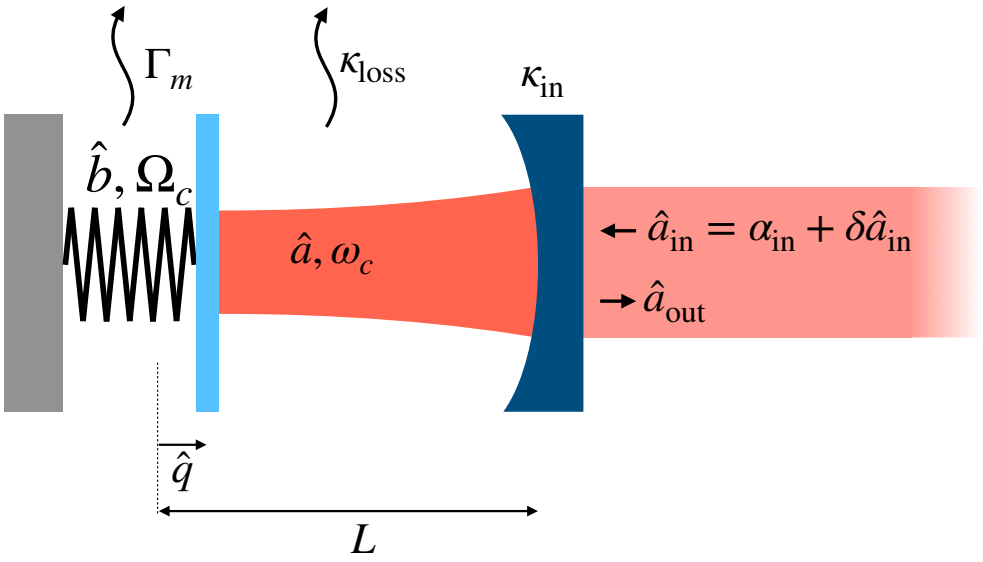

Figure 2.1: Sketch of an cavity optomechanical system. Figure created by the author.

systems while the term $\hat{H}_{\text{int}}$ represents the optomechanical interaction Hamiltonian with g_0 being the optomechanical single-photon coupling strength: $g_0 = \omega_c x_{\text{ZPF}}/L$. This parameter basically represents the optical frequency shift that is produced by a displacement of the mechanical position q by its zero-point motion $x_{\text{ZPF}} = \sqrt{\hbar/(2m\Omega_m)}$, where m is the effective mass of the oscillator. This interaction Hamiltonian was first derived in Ref. [50], and is called a *radiation pressure* interaction. In essence, the interaction term describes a parametric coupling in which a mechanical displacement of an oscillator controls the frequency of the cavity resonance. The last term $\hat{H}_{\text{drive}}$ accounts for the drive of the cavity by a laser through one of the cavity mirrors with rate κ_{in}. Note that light will dissipate from the cavity at a total rate κ, called *the cavity dissipation rate* or *cavity linewidth*. It holds that $\kappa = \kappa_{\text{in}} + \kappa_{\text{loss}}$, where κ_{loss} describes the dissipation rate due to other mechanisms than the mirror dissipation rate κ_{in}. We will describe how to account for these losses in the next section. The system is rather generic and can be realized in many different physical systems. Just to name a few, the Hamiltonian can be realized by movable mirrors on a cantilever or suspended mirrors in a cavity, in microtoroidal and photonic crystal cavities simultaneously hosting optical and phononic modes, by a mechanical membrane placed in the middle of a cavity and by bulk acoustic modes in crystalline materials.

The Hamiltonian in Eq. (2.4.1) inherently represents a nonlinear interaction between light and mechanics, but in most experiments on optomechanics performed to date, the coupling strength has been weak and thus the interaction can be safely described as linear. We therefore consider a linearized model of the optomechanical system. This can be done by assuming a strong drive laser, i.e. a large α_{in}. One can then decompose the mode operators into mean values and fluctuation terms: $\hat{a} = (\alpha + \delta\hat{a})e^{i\omega_L t}$, and $\hat{b} = \beta + \delta\hat{b}$, where the complex exponential is introduced in order to move into a frame rotating with the laser frequency. By inserting this into the Hamiltonian in Eq. (2.4.1) and subsequently applying a linearization approximation

(neglecting terms second order in $\delta\hat{a}$) we arrive at the following linearized Hamiltonian[1]:

$$\hat{H}_{\text{lin}} = \hbar\Delta\hat{a}^\dagger\hat{a} + \hbar\Omega_m\hat{b}^\dagger\hat{b} + \hbar g_0(\alpha^*\hat{a} + \alpha\hat{a}^\dagger)(\hat{b} + \hat{b}^\dagger) \tag{2.4.2}$$

Here we have also defined a frame rotating with the laser frequency and introduced the detuning: $\Delta_0 = \omega_c - \omega_L$ and the effective detuning $\Delta = \Delta_0 +$ (small correction term). Notice that the driving term has disappeared as a result of the linearization. It is also customary to introduce the drive-enhanced coupling strength: $g = \alpha g_0$ which represents the coupling strengths (boosted by the amplitude of the drive field) between a mechanical oscillator, $\hat{b}$, and a laser-driven cavity mode, $\delta\hat{a}$, at frequencies Ω_m and Δ. Therefore, in this linearized regime, it is possible to attain an arbitrarily large coupling strength between light and mechanics by increasing the drive amplitude. The linearized Hamiltonian in Eq. (2.4.2) captures some rich physics that we will briefly discuss in the following.

When the system is driven on resonance ($\Delta = 0$), we have that

$$\begin{aligned}\hat{H}_{\text{lin}} &= \hbar\Omega_m\hat{b}^\dagger\hat{b} + \hbar g(\hat{a} + \hat{a}^\dagger)(\hat{b} + \hat{b}^\dagger) \\ &= \hbar\Omega_m\hat{b}^\dagger\hat{b} + \hbar 2g\hat{X}\hat{Q},\end{aligned} \tag{2.4.3}$$

where $\hat{X} = (\hat{a} + \hat{a}^\dagger)/\sqrt{2}$ and $\hat{Q} = (\hat{a} + \hat{a}^\dagger)/\sqrt{2}$ are the amplitude and position quadrature of the light and mechanics, respectively. In this case, the interaction Hamiltonian induces a phase shift of the light depending on the position of the mirror. This is the case that we will be concerned with for almost all of this dissertation. Two other important cases are when the laser drive is red-detuned such that $\Delta = \Omega_m$ and blue-detuned such that $\Delta = -\Omega_m$. In the red-detuned case, the interaction Hamiltonian resembles a beamsplitter-type interaction between the mechanical mode and the cavity mode. This interaction may be used to cool the mechanics using a strong driving laser (a procedure called sideband cooling), and to perform a quantum state transfer between the cavity mode and mechanical mode. In the blue-detuned case, the interaction Hamiltonian has the approximate form of a two-mode squeezing operation between the mechanics and the cavity mode. It should be noted, that both the two-mode squeezing interaction and the beamsplitter interactions are only approximately realized when the system is in the *sideband-resolved regime*, that is, when the cavity dissipation rate is much smaller than the mechanical frequency, i.e. $\kappa \ll \Omega_m$. In this case, a photon inside the cavity circulates over multiple mechanical oscillation periods before exiting the cavity. By contrasts, the regime that we will be concerned with for the most part in this work is the *bad cavity regime*, when $\kappa \gg \Omega_m$. In this case, a photon will only interact with the mechanics for a short period of time relative to the mechanical period. In this case, when the system is driven on resonance, light exiting the cavity will contain information about the mechanical position encoded in its phase. Therefore, by measuring the phase quadrature of the output field (denoted in the sketch by annihilation operator $\hat{a}_{\text{out}}$), one can get information about the immediate position of the mechanics. This is the main ingredient for performing *feedback cooling* experiments, in which the information about the mechanical position is converted into a feedback signal sent to the mechanics in order to cool it down, i.e. to decrease its phonon number. There are a number of ways in which this feedback force may be applied, but in this work we will mainly consider the case in which the feedback signal is an amplitude-modulated light beam sent into the cavity and interacts with the mechanics through radiation pressure.

[1] More detailed descriptions on how to derive $\hat{H}_{\text{lin}}$ are be given in Chapters 3 and 5 under two different sets of circumstances.

2.5 Coupling to the environment: Quantum Langevin equations and master equations

When analysing quantum optomechanical systems, we must account for losses to the environment. In this dissertation, this is modeled using two approaches: Quantum Langevin equations and quantum master equations. Both of these approaches are based on a model of an open quantum system, in which the external environment is modeled as a large ensemble of experimentally inaccessible quantum systems, called a *bath*, which is coupled to the *system* in question (here the optomechanical modes). By virtue of this coupling, the system will thermalize to the temperature of the bath, and noise will be added.

Note that this section uses some of the same structure and wording from my master's thesis [51].

2.5.1 Quantum Langevin equations

The quantum Langevin equations are a form of modifications to the Heisenberg equations of motion of system operators. We will here merely state these equations without going through the derivations but we will highlight one of the main assumption they are based on: The *first Markov approximation*, that states that the coupling to the bath is independent of frequency. This assumption implies that the coupling to the environment is memory-less, and that the autocorrelation function of the bath operators is proportional to a delta function.

For a system operator $\hat{O}$ pertaining to the mechanical mode, we use the so-called independent oscillator model, originating from Ref. [52]. In this model, the harmonic oscillator is surrounded by an external bath of infinitely many other harmonic oscillators attached to it by springs. The quantum Langevin equations are given by [52, 2]:

$$\dot{\hat{O}} = \frac{1}{i\hbar}[\hat{O}, \hat{H}] + i\sqrt{2\Gamma_m}[\hat{O}, \hat{Q}]\hat{P}_{\text{in}} + \frac{\Gamma_m}{2i\Omega_m}\left\{[\hat{O}, \hat{Q}], \dot{\hat{Q}}\right\} \tag{2.5.1}$$

where Γ_m is the damping rate of the mechanics. For most of this dissertation, we will instead of Γ_m work with the mechanical *quality factor* $Q_m = \Omega_m/\Gamma_m$. We note that this is a non-rotating wave approximation of the mechanical interaction with the bath.

For the cavity field, we use a model similar to the independent oscillator model developed by Gardiner and Collett [53], that also relies on the first Markov approximation. In this case, the quantum Langevin equation is given by:

$$\dot{\hat{O}} = \frac{1}{i\hbar}[\hat{O}, \hat{H}] - [\hat{O}, \hat{a}^\dagger]\left(\frac{\kappa}{2}\hat{a} - \sqrt{\kappa}\hat{a}_{\text{in}}(t)\right) + \left(\frac{\kappa}{2}\hat{a}^\dagger - \sqrt{\kappa}\hat{a}^\dagger_{\text{in}}(t)\right)[\hat{O}, \hat{a}] \tag{2.5.2}$$

where κ is the cavity damping rate. The operators $\hat{a}_{\text{in}} = \hat{a}_{\text{in}}(t)$ and the operator $\hat{P}_{\text{in}} = \hat{P}_{\text{in}}(t) = (\hat{b}_{\text{in}}(t) - \hat{b}^\dagger_{\text{in}}(t))/i\sqrt{2}$ represents input (noise) operators of the bath. Unlike $\hat{a}$ and $\hat{b}$, these operators are not dimensionless, but have SI units $\sqrt{\text{s}^{-1}}$. They fulfil the commutation relations

$$[\hat{a}_{\text{in}}(t), \hat{a}^\dagger_{\text{in}}(t')] = \delta(t - t') \tag{2.5.3}$$

$$[\hat{b}_{\text{in}}(t), \hat{b}^\dagger_{\text{in}}(t')] = \delta(t - t'), \tag{2.5.4}$$

where $\delta(t)$ is the Dirac delta function. Throughout the dissertation, we will assume $\hat{b}_{\text{in}}(t)$ to be in a thermal state, and $\hat{a}_{\text{in}}(t)$ will generally, though not always, be a vacuum state.

While $\hat{a}_{\text{in}}(t)$ is the incident field on the cavity, the outgoing (or output) field from the mechanics $\hat{a}_{\text{out}}(t)$ is given by

$$\hat{a}_{\text{out}}(t) = \hat{a}_{\text{in}}(t) - \sqrt{\kappa}a(t) \tag{2.5.5}$$

2.5.2 Quantum master equations

Like the quantum Langevin equations in essence are modifications to Heisenberg's equation of motion for operators, quantum master equations may be regarded as modifications to the von Neumann equation for density matrices.

$$\frac{d\hat{\rho}}{dt} = -\frac{i}{\hbar}[\hat{H}, \hat{\rho}] + \mathcal{L}_m\hat{\rho} + \mathcal{L}_c\hat{\rho} \tag{2.5.6}$$

The superoperators $\mathcal{L}_m$ and $\mathcal{L}_c$ are describing the interaction between the environment and the mechanics and cavity field, respectively. For the mechanics, we substitute $\mathcal{L}_m$ for one of two interactions, $\mathcal{L}_{\text{RWA}}$ or $\mathcal{L}_{\text{nonRWA}}$, given by

$$\mathcal{L}_{\text{RWA}}\hat{\rho} = \Gamma_m(\bar{n}+1)\mathcal{D}[\hat{b}]\hat{\rho} + \Gamma_m\bar{n}\mathcal{D}[\hat{b}^\dagger]\hat{\rho}, \tag{2.5.7a}$$

$$\mathcal{L}_{\text{nonRWA}}\hat{\rho} = \frac{i\Gamma_m}{2\Omega_m}[\hat{Q}, \{\dot{Q}, \hat{\rho}\}] - \Gamma_m(\bar{n}+1/2)[Q, [Q, \hat{\rho}]], \tag{2.5.7b}$$

where the superoperator $\mathcal{D}$ is defined as

$$\mathcal{D}[\hat{c}]\hat{\rho} := \hat{c}\hat{\rho}\hat{c}^\dagger - \frac{1}{2}\left(\hat{c}^\dagger\hat{c}\hat{\rho} + \rho\hat{c}^\dagger\hat{c}\right), \tag{2.5.8}$$

For the cavity field, again assuming that the environment is in a vacuum state,

$$\mathcal{L}_c\hat{\rho} = \kappa\mathcal{D}[\hat{a}]\hat{\rho} \tag{2.5.9}$$

A discussion of the superoperators $\mathcal{L}_{\text{RWA}}$ and $\mathcal{L}_{\text{nonRWA}}$ is given in Chapter 3.

2.6 Itō stochastic calculus

The subject of Itō stochastic calculus is a mathematical underpinning continuous measurement theory, upon which a lot of this thesis is based on. We shall therefore present the basics of the subject below. In the following, $\mathrm{E}[Z]$ and $\mathrm{Var}[Z]$ denote the expectation value and variance, respectively, of the stochastic variable Z.

A *stochastic process* is a function $X(t)$ that takes a time t as input and gives a (typically real) stochastic variable as output. The outputs are not necessarily independent, but may be correlated in time.

An important stochastic process is the *Wiener process*[2] $W(t)$, $t \geq 0$. It is defined by the following properties:

1. $W(0) = 0$
2. For any three times $t_0 \leq t_1 \leq t_2$, $W(t_0)$ is independent of the increment $W(t_2) - W(t_1)$.

[2]Sometimes also referred to as *mathematical Brownian motion* and denoted as $B(t)$, $t \geq 0$.

3. For any two times $t_1 \leq t_2$, the increment $W(t_2) - W(t_1)$ is normally distributed (or Gaussian) with mean 0 and variance $t_2 - t_1$.

4. $W(t)$ is continuous in time t.

A key property of a Wiener process is that while it is continuous in time, it is nowhere differentiable. This comes from the fact that the increment $W(t + \Delta t) - W(t)$ is Gaussian at every step size Δt and thus will not approach a definite value as Δt approaches 0. The difference quotient $(W(t+\Delta t) - W(t))/\Delta t$ therefore has no well-defined limit and thus the derivative does not exists.

We are now in a position to define the *Itō integral*. Let $X(t)$ be a stochastic process and $W(t)$ a Wiener process. Furthermore, let $[a, b]$ be an interval, let $T = \{t_1, t_2, ..., t_n\}$ be a partition of the interval such that $a = t_1 \leq t_2 \leq ... \leq t_n = b$, and let the largest increment in the partition be $|T| := \max_i(t_{i+1} - t_i)$. The Itō integral is defined as:

$$\int_a^b X(t)dW(t) := \lim_{|T|\to 0} \sum_{i=1}^{n-1} X(t_i)[W(t_{i+1}) - W(t_i)] \tag{2.6.1}$$

Intuitively, an Itō integral is similar to an ordinary Riemann integral, but where the integrand $X(t_i)$ is multiplied by stochastic increments $W(t_{i+1}) - W(t_i)$ instead of time increments $t_{i+1} - t_i$. The Itō increment satisfies the following important properties:

1. $\mathrm{E}\left[\int_a^b X(t)dW(t)\right] = 0$ (zero expectation value)

2. $\left(\int_a^b X(t)dW(t)\right)^2 = \int_a^b X(t)^2 dt$ (Itō isometry)

An *Itō stochastic differential equation* is an equation of the form

$$dX(t) = f(t, X(t))dt + g(t, X(t))dW(t) \tag{2.6.2}$$

In the above, t is time and dt is the differential time increment, $X(t)$ is the unknown function to be solved for and f and g are real functions of two real variables. The above equation is really a shorthand notation for the Itō integral equation:

$$X(t) = \int_{t_0}^{t} f(t, X(t))dt + \int_{t_0}^{t} g(t, X(t))dW(t), \tag{2.6.3}$$

One can, however, work with the differential form Eq. (2.6.2) by introducing some rules for calculations with the so-called *Wiener increment* $dW(t)$. It is, heuristically, a stochastic infinitesimal object: It is normally distributed with mean value 0 and variance dt. It is a function of t in the sense that, for two times $t_1 \neq t_2$, $dW(t_1)$ and $dW(t_2)$ are two independent identically distributed Wiener increments. It also has the unique property $dW(t)^2 = dt$, which is a different way of expressing the Itō isometry. As an example to illustrate why these relations are useful, consider the following two stochastic processes X and Y governed by the Itō equations:

$$\begin{aligned} dX(t) &= f_1 dt + g_1 dW(t) \\ dY(t) &= f_2 dt + g_2 dW(t) \end{aligned} \tag{2.6.4}$$

We wish to write the Ito equation for the product $Z(t) = X(t)Y(t)$. We have that

$$\begin{aligned} Z(t+dt) &= Z(t) + dZ(t) = (X(t) + dX(t))(Y(t) + dY(t)) \\ \iff dZ(t) &= X(t)dY(t) + dX(t)Y(t) + dX(t)dY(t) \\ &= X(t)(f_2dt + g_2dW(t)) + (f_1dt + g_1dW(t))Y(t) + (f_1dt + g_1dW(t))(f_2dt + g_2dW(t)) \end{aligned} \tag{2.6.5}$$

In the final term, we use the heuristics $dW(t)^2 = dt$, $dt^2 = 0$ and $dtdW(t) = 0$ to simplify and get

$$dZ(t) = X(t)(f_2dt + g_2dW(t)) + (f_1dt + g_1dW(t))Y(t) + g_1g_2dt \tag{2.6.6}$$

This example shows how one can manipulate Itō equations. These principles are used extensively to derive optomechanical equations of motions throughout this dissertation.

Chapter 3

Mechanical cooling and squeezing using optimal control

In this chapter, we present the paper 'Mechanical cooling and squeezing using optimal control' [54]. This paper was authored by Frederik Werner Isaksen and Ulrik Lund Andersen. It is available at arxiv.org (arXiv:2207.07785).

A couple of addendums to the paper is listed below:

- By mistake, the momentum quadrature variable $\hat{P}$ is never explicitly defined in the text. it is given by $\hat{P} = (\hat{b} - \hat{b}^\dagger)/(i\sqrt{2})$.
- By mistake, some of the parameters used to generate the plots in Figs. 3.4 and 3.5 are left out in the text. These parameters are $Q_m = 10^8$, $\kappa = 10^8$ Hz, $\eta = 1$, and $T = 300\,\mathrm{K}$.

3.1 Abstract

A mechanical system can be optimally controlled through continuous measurements of its position followed by feedback. We revisit the complete formalism for predicting the performance of such as system without invoking the standard rotating wave approximations and the adiabatic approximation. Using this formalism we deduce both the conditional and unconditional state of a mechanical oscillator using the optimal control and feedback that leads to mechanical cooling and mechanical squeezing. We find large discrepancies between the exact solutions and the approximate solutions stressing the importance of using the complete model.

3.2 Introduction

Fueled by the dramatic progress in developing high-quality nano- and micromechanical oscillators, there has recently been a surge of interest in controlling the motion of such oscillators at the quantum level for testing fundamental physics and for realizing novel quantum technologies[1, 3]. A promising strategy for the optimal quantum control of a mechanical oscillator is by monitoring its motional dynamics through optimized measurements and subsequently use this information to drive the oscillator into a certain target state [33, 40]. Such a strategy has for

example by now been used to prepare a mechanical oscillator near its quantum mechanical ground state[24, 37, 29, 55, 30]. In addition to these experimental endeavours, there exists a vast theoretical literature on preparing mechanical oscillators in various quantum states via measurement-based feedback control including the ground state, the squeezed state [56, 45] and more exotic states [42, 22].

The formalism of optimal feedback control of continuously measured quantum systems has been originally developed by Belavkin [57, 58, 59] and later refined by Wiseman & Milburn [34]. It includes a complete quantum mechanical description of the control system and is often formulated in terms of a master equation for the density matrix representing the system. The formalism includes a real-time estimation algorithm that provides the optimal information about the measured state conditioned on previous measurements, and finally produces a conditional state which can be subsequently used to drive the mechanical oscillator into the desired state via feedback[33, 56, 34, 40, 60, 42, 43, 35, 36, 38, 37].

When using the master equation formalism to simulate an optomechanical system, several different approximations are often invoked. Possibly the two most important approximations are the rotating wave approximation (RWA) and the adiabatic approximation. The RWA can be applied when the dynamics of the mechanical system is much faster than all interactions with the environment and the measurement, while the adiabatic approximation is valid if the oscillator dynamics can be adiabatically followed by the probing system. While for some systems these two approximations can be taken, for others, however, they are not valid. As an example, the complete model predicts the formation of squeezed mechanical states via optimal feedback control while an approximative model based on the RWA of the interaction with the measurement apparatus cannot predict its appearance [45].

Moreover, it is important to distinguish the mechanical state that is inferred from the measurement record - known as the conditional state - and the mechanical state that is actually produced through active feedback control - known as the unconditional state. In much of the literature, these two states are often taken to be identical assuming that the feedback control can be done without any noise penalty. This is however a very crude assumption as decoherence of the mechanics plays an important role during feedback, rendering the unconditional state in a state that is more noisy than the conditional state.

In this work we revisit the formalism for optimal feedback control using the master equation framework without using the RWA and the adiabatic approximation, and we apply the formalism to deduce the conditional and unconditional states of the mechanical oscillator. Our control parameters will be optimised for driving the mechanical oscillator into either a ground state or a squeezed state. We find, for example, that if the RWA of the interaction with the environment is applied, the optimal residual phononic occupancy when preparing the oscillator near its ground state is overestimated while when applying the adiabatic approximation, the squeezing degree is underestimated in certain regimes. Moreover, we show that the optimally prepared conditional and unconditional states are different, even if infinitely strong feedback is available. We discuss the consequences thereof, including for example how this changes the optimal measurement quadrature.

The rest of the paper is organized in three sections: In Sec. II we present the model for optimal feedback control using the master equation framework while in Sec. III we present and discuss the results of preparing mechanical ground states and squeezed states using our formalism with a special emphasis on the validity of the RWA and the adiabatic approximation. The work is shortly summarized and concluded in Sec. IV.

3.3 The Physical Model

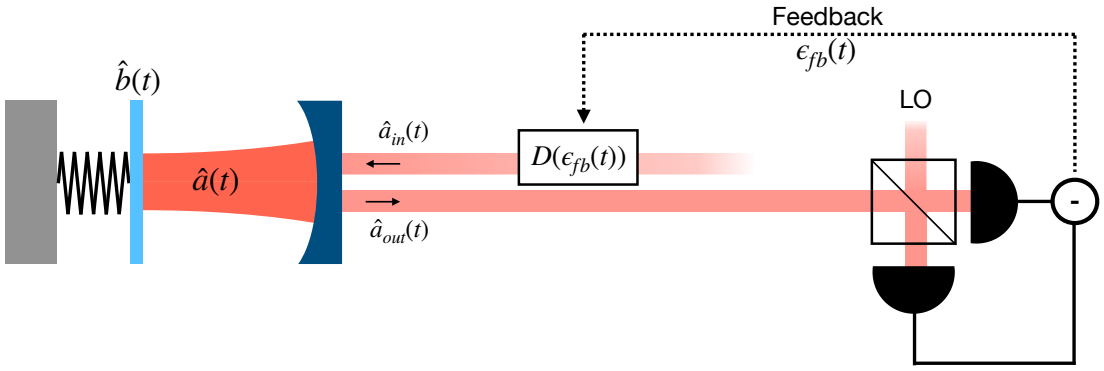

Figure 3.1: Sketch of the optomechanical setup; a cavity mode $\hat{a}$ is interacting with a mechanical mode $\hat{b}$. The output field is detected with a homodyne detector with a local oscillator (LO) with a phase corresponding to measurement of the output quadrature $\hat{X}^{\theta}_{\rm out}(t) = (\hat{a}_{\rm out}(t)e^{-i\theta} + \hat{a}^{\dagger}_{\rm out}(t)e^{i\theta})/\sqrt{2}$. The homodyne detector has detection efficiency η. Based on the homodyne measurement signal, an optical feedback signal of complex amplitude $\epsilon_{\rm fb}(t)$ is applied through a displacement operation $D(\epsilon_{\rm fb}(t)) = \exp[\epsilon_{\rm fb}(t)\hat{a}^{\dagger}_{\rm in} - \epsilon^{*}_{\rm fb}(t)\hat{a}^{\dagger}_{\rm in}]$ on the input field.

We start by considering a standard model for the state of a mechanical oscillator which is conditioned on the continuous measurement of its position as illustrated in Figure 3.1: A cavity mode with annihilation operator $\hat{a}$ and (angular) frequency ω_c is interacting through radiation-pressure forces with a mechanical oscillator with annihilation operator $\hat{b}$ and frequency Ω_m. An input field $\hat{a}_{\rm in}$ of frequency ω_L is injected into the cavity with rate κ. This input coherently drives the cavity field with frequency ω_L and time-dependent complex amplitude $\epsilon(t) = \epsilon_{\rm probe} + \epsilon_{\rm fb}(t)$. Here, the constant term $\epsilon_{\rm probe}$ is applied to enhance the optomechanical coupling and measurement strength, while the time-dependent term $\epsilon_{fb}(t)$ is a feedback induced control field. It is convenient to divide the latter contribution into real and imaginary parts, $\epsilon_{\rm fb}(t) = (x_{\rm fb} + iy_{\rm fb})/\sqrt{2}$. Working in a displaced frame rotating at the cavity field frequency ω_c and using a linearized approximation of the optomechanical radiation-pressure interaction, the full Hamiltonian of the system can be written as

$$\begin{aligned}\hat{H} =& \hbar\Delta\hat{a}^{\dagger}\hat{a} + \hbar\Omega_m\hat{b}^{\dagger}\hat{b} + 2\hbar g\hat{Q}\hat{X} \\ &+ \hbar\sqrt{\kappa}\,[x_{fb}(t)Y - y_{fb}(t)X]\end{aligned} \tag{3.3.1}$$

where g is the probe-enhanced optomechanical coupling rate, $\hbar$ is Planck's reduced constant, $\hat{Q} = (\hat{b} + \hat{b}^{\dagger})/\sqrt{2}$ is the dimensionless position operator of the mechanics, and $\hat{X} = (\hat{a} + \hat{a}^{\dagger})/\sqrt{2}$ and $\hat{Y} = (\hat{a} - \hat{a}^{\dagger})/i\sqrt{2}$ are the cavity field amplitude and phase quadrature representations, respectively. Finally, Δ is the effective detuning, a parameter controlled by the laser frequency ω_L. Throughout this paper, ω_L is chosen such that $\Delta = 0$. The reader is referred to the supplement Section 3.6 for a detailed derivation of the Hamiltonian in equation (3.3.1) as well as expressions for g and Δ. Having specified the Hamiltonian of the cavity optomechanical system,

we are now in a position to discuss the dissipative dynamics of the system. This will be done by using a stochastic master equation of the density matrix ρ representing the system.

Both the cavity mode and the mechanical mode are inevitably subjected to loss and decoherence, and in this paper, we assume all these mechanisms to be Markovian. The cavity mode decays with rate κ due to coupling to the input field. The mechanical mode is coupled to a thermal reservoir of average phonon occupation number $\bar{n}$ with damping rate Γ_m. As a result of this coupling, the quality factor or the mechanical oscillator is $Q_m = \Omega_m/\Gamma_m$.

Finally, the output field, represented by the field operator $\hat{a}_{\text{out}}$, is measured with a homodyne detector which is able to measure an arbitrary quadrature of the field given by $\hat{X}^{\theta}_{\text{out}}(t) = (\hat{a}_{\text{out}}(t)e^{-i\theta} + \hat{a}^{\dagger}_{\text{out}}(t)e^{i\theta})/\sqrt{2}$ where θ is the phase of the detector's local oscillator. We will henceforth refer to θ as the *phase* or the *measurement angle* of the homodyne detector. The output field is related to the input field as per the usual input-output relations $\hat{a}_{\text{out}} = \hat{a}_{\text{in}} - \sqrt{\kappa}\hat{a}$ [53]. We assume that the detection efficiency of the homodyne detector is η.

The information obtained by the continuous homodyne measurement produces a *conditional* density matrix $\hat{\rho}_c$ of the joint system containing the cavity and the mechanical mode. As is customary in the literature, conditional dynamics will be explicitly indicated by a subscript c, i.e. $\hat{\rho}_c$ is the conditional density matrix and $\langle \hat{A} \rangle_c = \text{Tr}[\hat{A}\hat{\rho}_c]$ is the conditional expectation value of the operator $\hat{A}$ w.r.t. $\hat{\rho}_c$. This conditioning, combined with the Hamiltonian evolution including loss and decoherence, can be modeled by the following stochastic master equation [61, 42]:

$$\begin{aligned} d\hat{\rho}_c = &-\frac{i}{\hbar}[\hat{H}, \hat{\rho}_c]dt + \mathcal{L}_{\text{env}}\hat{\rho}_c dt \\ &+ \kappa\mathcal{D}[\hat{a}]\hat{\rho}_c dt + \sqrt{\eta\kappa}\mathcal{H}[\hat{a}e^{-i\theta}]\hat{\rho}_c dW. \end{aligned} \tag{3.3.2}$$

The superoperator $\mathcal{L}_{\text{env}}$ describing the mechanical interaction with the environment is either $\mathcal{L}_{\text{RWA}}$ or $\mathcal{L}_{\text{nonRWA}}$, given by

$$\mathcal{L}_{\text{RWA}}\hat{\rho} = \Gamma_m(\bar{n}+1)\mathcal{D}[\hat{b}]\hat{\rho} + \Gamma_m\bar{n}\mathcal{D}[\hat{b}^{\dagger}]\hat{\rho}, \tag{3.3.3a}$$

$$\mathcal{L}_{\text{nonRWA}}\hat{\rho} = \frac{i\Gamma_m}{2\Omega_m}[Q, \{\dot{Q}, \hat{\rho}\}] - \Gamma_m(\bar{n}+1/2)[Q,[Q,\hat{\rho}]], \tag{3.3.3b}$$

where $[\cdot,\cdot]$, and $\{\cdot,\cdot\}$ denote the commutator and anti-commutator, respectively, and the superoperators $\mathcal{D}$ and $\mathcal{H}$ are defined as

$$\mathcal{D}[\hat{c}]\hat{\rho} := \hat{c}\hat{\rho}\hat{c}^{\dagger} - \frac{1}{2}\left(\hat{c}^{\dagger}\hat{c}\hat{\rho} + \rho\hat{c}^{\dagger}\hat{c}\right), \tag{3.3.4}$$

$$\mathcal{H}[\hat{c}]\hat{\rho} := (\hat{c} - \text{Tr}[\hat{c}\hat{\rho}])\hat{\rho} + \hat{\rho}(\hat{c}^{\dagger} - \text{Tr}[\hat{c}^{\dagger}\hat{\rho}]). \tag{3.3.5}$$

The individual terms in Eqs. (3.3.2) and (3.3.3) deserve some comments: The term $\mathcal{L}_{\text{RWA}}\hat{\rho}$ is the Markovian rotating wave approximation to the environmental interaction with the mechanics, and is the most often used in the literature when modeling optomechanics with a master equation approach. On the other hand, the term $\mathcal{L}_{\text{nonRWA}}\hat{\rho}$, first introduced in [62] does not assume the rotating wave approximation, but also does not in general preserve positivity of the density matrix since it is not on Lindblad form. We refer the reader to ref. [63] for a discussion of some of the inadequacies of this system-environment master equation including attempts at amending it to be on Lindblad form (See also the supplement Section 3.8). The terms in the second line

of Eq. (3.3.2) account for the effect on the master equation of cavity dissipation and subsequent homodyne detection of the output field when the measurement angle is θ [42]. $dW = dW(t)$ is the Wiener increment, a stochastic normally distributed variable satisfying the properties $dW(t')dt = 0$, $dW(t)dW(t') = \delta_{t,t'}dt$, and $\mathrm{E}\left[dW(t)\right] = 0$, where $\mathrm{E}\left[dW(t)\right]$ denotes the (classical) expectation value. The measured photocurrent corresponding to the above conditional evolution is [42]

$$\begin{aligned} I(t)dt &= \sqrt{\eta\kappa}\langle ae^{-i\theta} + a^\dagger e^{i\theta}\rangle_c dt + dW(t) \\ &= \sqrt{2\eta\kappa}\langle X\cos(\theta) + Y\sin(\theta)\rangle_c dt + dW(t). \end{aligned} \tag{3.3.6}$$

Using the master equation in Eq. (3.3.2), equations of motion for the system operators $\hat{\mathbf{X}} = (\hat{Q}, \hat{P}, \hat{X}, \hat{Y})$ can now be derived. Assuming that the Wigner function of the initial state is Gaussian (e.g. a thermal state), the system will stay Gaussian. This follows from the fact that homodyne detection preserves Gaussian states, as does time evolution under a Hamiltonian that is a second order polynomial of creation and annihilation operators [48]. Under this assumption, the quantum state $\hat{\rho}_c = \hat{\rho}_c(t)$ is then fully characterised by the mean vector $\langle\hat{\mathbf{X}}\rangle_c$ and the covariance matrix $\mathbf{V}^c_{\mathbf{XX}} = (V^c_{Z_1Z_2})_{\hat{Z}_1,\hat{Z}_2\in\hat{\mathbf{X}}} = \mathrm{Re}(\langle\hat{\mathbf{X}}\hat{\mathbf{X}}^T\rangle_c - \langle\hat{\mathbf{X}}\rangle_c\langle\hat{\mathbf{X}}^T\rangle_c)$, the equations of motion of which may be derived using the formula $d\langle\hat{O}\rangle_c = \mathrm{Tr}[\hat{O}d\hat{\rho}_c]$. We find (See the supplement Section 3.7):

$$\begin{aligned} d\langle\hat{\mathbf{X}}\rangle_c &= \left(\mathbf{A}\langle\hat{\mathbf{X}}\rangle_c + \mathbf{Bu}\right)dt \\ &\quad + (\mathbf{V}^c_{\mathbf{XX}}\mathbf{C}^T + \mathbf{\Gamma}^T)dW \end{aligned} \tag{3.3.7a}$$

$$\begin{aligned} \frac{d\mathbf{V}^c_{\mathbf{XX}}}{dt} &= \mathbf{A}\mathbf{V}^c_{\mathbf{XX}} + \mathbf{V}^c_{\mathbf{XX}}\mathbf{A}^T + \mathbf{D} \\ &\quad - (\mathbf{V}^c_{\mathbf{XX}}\mathbf{C}^T + \mathbf{\Gamma}^T)(\mathbf{C}\mathbf{V}^c_{\mathbf{XX}} + \mathbf{\Gamma}) \end{aligned} \tag{3.3.7b}$$

Here, $\mathbf{u} = \mathbf{u}(t) = [x_{fb}(t) \quad y_{fb}(t)]^T$ is a time-dependent vector describing the feedback of the system. The matrices $\mathbf{A}$ and $\mathbf{D}$ depend on which of the two dissipation models in Eq. 3.3.3 is used:

$$\mathbf{A}_{\mathrm{RWA}} = \begin{bmatrix} -\Gamma_m/2 & \Omega_m & 0 & 0 \\ -\Omega_m & -\Gamma_m/2 & -2g & 0 \\ 0 & 0 & -\kappa/2 & 0 \\ -2g & 0 & 0 & -\kappa/2 \end{bmatrix} \tag{3.3.8a}$$

$$\mathbf{D}_{\mathrm{RWA}} = \begin{bmatrix} \Gamma_m(\bar{n}+1/2) & 0 & 0 & 0 \\ 0 & \Gamma_m(\bar{n}+1/2) & 0 & 0 \\ 0 & 0 & \kappa/2 & 0 \\ 0 & 0 & 0 & \kappa/2 \end{bmatrix} \tag{3.3.8b}$$

$$\mathbf{A}_{\mathrm{nonRWA}} = \begin{bmatrix} 0 & \Omega_m & 0 & 0 \\ -\Omega_m & -\Gamma_m & -2g & 0 \\ 0 & 0 & -\kappa/2 & 0 \\ -2g & 0 & 0 & -\kappa/2 \end{bmatrix} \tag{3.3.9a}$$

$$\mathbf{D}_{\mathrm{nonRWA}} = \begin{bmatrix} 0 & 0 & 0 & 0 \\ 0 & 2\Gamma_m(\bar{n}+1/2) & 0 & 0 \\ 0 & 0 & \kappa/2 & 0 \\ 0 & 0 & 0 & \kappa/2 \end{bmatrix} \tag{3.3.9b}$$

On the other hand, $\mathbf{B}$, $\mathbf{C}$ and $\mathbf{\Gamma}$ are the same for both models:

$$\mathbf{B} = \begin{bmatrix} 0 & 0 \\ 0 & 0 \\ \sqrt{\kappa} & 0 \\ 0 & \sqrt{\kappa} \end{bmatrix} \tag{3.3.10a}$$

$$\mathbf{C} = \sqrt{2\eta\kappa}\begin{bmatrix} 0 & 0 & \cos(\theta) & \sin(\theta) \end{bmatrix} \tag{3.3.10b}$$

$$\mathbf{\Gamma} = \sqrt{\frac{\eta\kappa}{2}}\begin{bmatrix} 0 & 0 & -\cos(\theta) & -\sin(\theta) \end{bmatrix} \tag{3.3.10c}$$

We note that Eqs. (3.3.7) are formally equivalent to a Kalman Filter [34]. For the rest of this paper, we will mainly be concerned with the steady-state dynamics of $\mathbf{V}^c_{\mathbf{XX}}$, i.e. the solution when $\frac{d}{dt}\mathbf{V}^c_{\mathbf{XX}} = 0$. Equation (3.3.7b) then reduces to an algebraic equation in $\mathbf{V}^c_{\mathbf{XX}}$ known as the algebraic Riccati equation. Onwards, $\mathbf{V}^c_{\mathbf{XX}}$ will therefore almost exclusively refer to the steady-state solution.

Up to this point, we have considered the conditional state of the system, $\hat{\rho}_c$. However, of equal importance is the *unconditional* state $\hat{\rho} := \mathrm{E}[\hat{\rho}_c]$. The difference between the two is as follows: ρ_c depends on (i.e. is conditioned on) the outcome of the homodyne measurements up to time t. As these measurement outcomes are probabilistic in nature, the trajectory of the state will follow a random path in phase space (customarily called *quantum trajectory*). On the other hand, the unconditional state is the average over all possible trajectories from the beginning of the experiment up to time t, and basically corresponds to state of system in which the measurement outcomes are ignored. Mathematically, this is equivalent to removing the term proportional to dW in Eq. (3.3.2), which means that the dW term in Eq. (3.3.7a) and the term $-(\mathbf{V}^c_{\mathbf{XX}}\mathbf{C}^T + \mathbf{\Gamma}^T)(\mathbf{C}\mathbf{V}^c_{\mathbf{XX}} + \mathbf{\Gamma})$ in Eq.(3.3.7b) will vanish. The result is that the mean vector is identically zero for all t, but that the covariance is much larger due to large contributions from both thermal noise and backaction noise. The difference between the conditional and unconditional states of the mechanical mode (with the cavity mode traced out) is illustrated in phase space in Figure 3.2a. Note that *both* $\hat{\rho}$ and $\hat{\rho}_c$ are depicted as having zero mean in Fig. 3.2 for easier comparison, even though $\hat{\rho}_c$ in general will be displaced from the origin by some amount conditional on the measurement record.

To prepare the unconditional state into a state that resembles the conditional state, we need to actively control the motion of the mechanical oscillator based on the homodyne measurement outcomes. As illustrated in Fig. 3.2, the results of the homodyne measurements are fed back onto the opto-mechanical system, thereby driving it into a low-entropy unconditional state as described by the Hamiltonian in Eq. (3.3.1). A phase space representation of the unconditional state with feedback is shown in Fig. 3.2b where it is compared to the conditional state for a particular representative example. The resulting unconditional state depends critically on the estimation and feedback strategy which in turn depends on the state one aims to prepare. In the following we consider the optimal feedback strategies applied for the preparation of an unconditional state with a minimal phonon number (corresponding to mechanical cooling) as well as the optimal strategy for minimizing the variance of one of the mechanical quadratures (corresponding to mechanical squeezing).

3.3.1 Optimal control formalism

In this section we consider the optimal control schemes for mechanical cooling and squeezing. We use the framework of linear-quadratic-Gaussian (LQG) optimal control which is tailored to

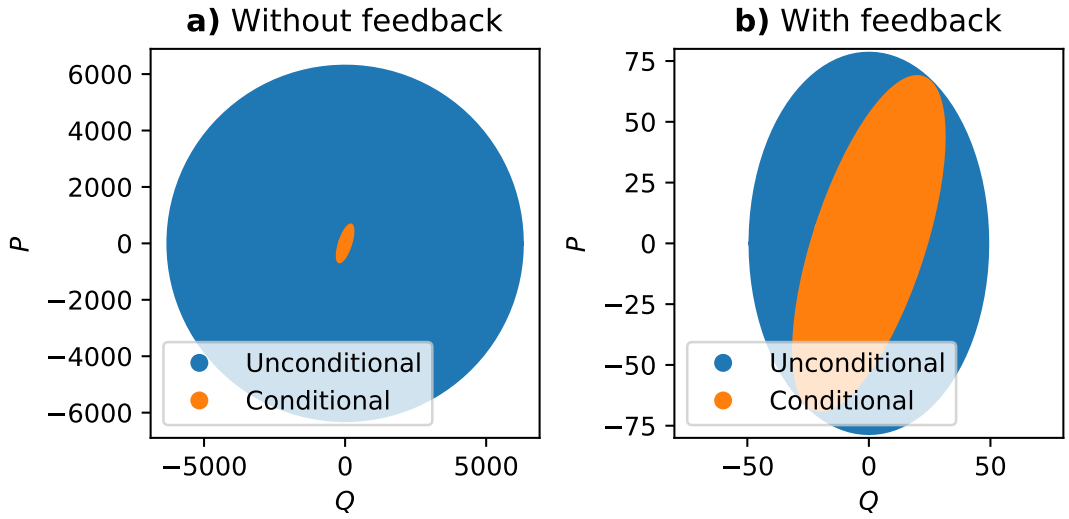

Figure 3.2: The mechanical covariance matrix in steady-state depicted as an uncertainty ellipsis (1 standard deviation) in (Q, P) phase space. Without feedback (Fig. 3.2a), the unconditional state is much larger compared to when feedback is applied (Fig. 3.2b), but the conditional state is unchanged. In Fig. 3.2a, the area of the conditional uncertainty ellipse have been artificially scaled up by a factor of 100 to make it more visible. Plotted for $\Omega_m = 10^6\,\text{Hz}$, $Q_m = 10^4$, $g = 10^5\,\text{Hz}$, $\kappa = 10^8\,\text{Hz}$, $T = 300\,\text{K}$, $\eta = 1$, $q = 10^{-5}$, $p = 10^3$, using the nonRWA model and with feedback that minimizes the phonon number.

minimize a quadratic *cost function* [34]:

$$j = \int_{t_0}^{t_1} \langle h(\hat{\mathbf{X}}(t), \mathbf{u}(t), t) \rangle \, dt. \tag{3.3.11}$$

Here, $\langle ... \rangle$ denotes the expectation value with respect to the unconditional density matrix $\hat{\rho}$, t_0 and t_1 denote the start and end time of the run, respectively, and

$$\begin{aligned} h(\hat{\mathbf{X}}(t), \mathbf{u}(t), t) =& \hat{\mathbf{X}}(t)^T \mathbf{P} \hat{\mathbf{X}}(t) + \mathbf{u}(t)^T \mathbf{Q} \mathbf{u}(t) \\ &+ 2\delta(t - t_1) \hat{\mathbf{X}}(t)^T \mathbf{P}_1 \hat{\mathbf{X}}(t), \end{aligned} \tag{3.3.12}$$

where $\mathbf{P}$, $\mathbf{P}_1$ and $\mathbf{Q}$ are matrices that are specified according to the problem one wants to solve, for example minimizing the mechanical phonon occupancy or minimizing a specific quadrature variance of the mechanical oscillator. The value of $\mathbf{P}_1$ is associated with a terminal cost, i.e. a cost related to $\hat{\mathbf{X}}(t_1)$. However, since we are only interested in the dynamics at steady state, the value of $\mathbf{P}_1$ is irrelevant. This is commonly referred to as an *asymptotic* or *infinite horizon* LQG problem.

According to standard optimal control theory, the optimal feedback is then given by

$$\mathbf{u}(t) = -\mathbf{Q}^{-1} \mathbf{B}^T \mathbf{Y}(t) \langle \hat{\mathbf{X}} \rangle_c(t), \tag{3.3.13}$$

where $\mathbf{K}(t) = \mathbf{Q}^{-1} \mathbf{B}^T \mathbf{Y}(t)$ is the Kalman gain and $\mathbf{Y}(t)$ is a symmetric, positive semi-definite matrix satisfying the differential equation

$$-\frac{d\mathbf{Y}(t)}{dt} = \mathbf{A}^T \mathbf{Y}(t) + \mathbf{Y}(t)\mathbf{A} + \mathbf{P} - \mathbf{Y}(t)\mathbf{B}\mathbf{K}(t) \tag{3.3.14}$$

with the terminal condition $\mathbf{Y}(t_1) = \mathbf{P}_1$.

For asymptotic LQG-problems, $t_1 - t_0$ is very large compared with all other rates of our system. Within this time period, it can be shown that there exists a steady-state solution $\mathbf{Y}$ to Eq. (3.3.14) (i.e. with $-\frac{d}{dt}\mathbf{Y} = 0$) assuming certain stabilization conditions [34]. Given these conditions and with this choice of feedback, the steady-state *unconditional variance* $\mathbf{V_{XX}} = \mathrm{Re}(\langle\hat{\mathbf{X}}\hat{\mathbf{X}}^T\rangle) - \langle\hat{\mathbf{X}}\rangle\langle\hat{\mathbf{X}}^T\rangle)$ of the system is given by the relation $\mathbf{V_{XX}} = \mathbf{V^c_{XX}} + \mathbf{V^E_{XX}}$, where $\mathbf{V^E_{XX}}$ is an excess noise contribution stemming from imperfect feedback. This excess noise variance satisfies the equation

$$\mathbf{N}\mathbf{V^E_{XX}} + \mathbf{V^E_{XX}}\mathbf{N}^T + \mathbf{F}^T\mathbf{F} = 0, \tag{3.3.15}$$

where $\mathbf{N} = \mathbf{A} - \mathbf{BK}$ and $\mathbf{F} = \mathbf{CV^c_{XX}} + \mathbf{\Gamma}$. The expressions Eq. (3.3.14) and Eq. (3.3.15), together with the conditional dynamics in Eq. (3.3.7) gives the complete unconditional steady-state dynamics of the system, and in particular the steady-state unconditional variances, $\mathbf{V_{XX}}$.

3.3.2 Optimal control for mechanical cooling

Having outlined the overall strategy of optimal control, we will now consider two specific examples of optimal control associated with mechanical cooling and mechanical squeezing.

A minimization of the phonon number is obtained by setting $\mathbf{P} = \mathrm{diag}(p\Omega_m, p\Omega_m, 0, 0)$ and $\mathbf{Q} = \mathrm{diag}(q, q)$ where p and q are arbitrary dimensionless parameters. Note that $\mathbf{Q}$ specifies the cost associated with the feedback scheme, and that the fraction p/q is a measure of the feedback power for minimizing the oscillator energy. By using these particular matrices for $\mathbf{P}$ and $\mathbf{Q}$ as well as the formalism in Eqs. (3.3.14) and (3.3.15), we find $\mathbf{V_{XX}}$, and subsequently the minimized phonon number $n = (V_{QQ} + V_{PP} - 1)/2$.

3.3.3 Optimal control for mechanical squeezing

The above procedure can also be used for minimizing the mechanical variance. Specifically, in order to minimize $V_{Q_\nu Q_\nu}$, that is, the variance along $\hat{Q}_\nu = \cos(\nu)\hat{Q} + \sin(\nu)\hat{P}$ for some angle ν, it is straightforward to show that the appropriate cost function is given as in Eqs. (3.3.11) and (3.3.12), but with

$$\mathbf{P} = p\Omega_m \begin{bmatrix} \cos^2(\nu) & \cos(\nu)\sin(\nu) & 0 & 0 \\ \cos(\nu)\sin(\nu) & \sin^2(\nu) & 0 & 0 \\ 0 & 0 & 0 & 0 \\ 0 & 0 & 0 & 0 \end{bmatrix}, \tag{3.3.16}$$

while $\mathbf{Q}$ is identical to the case of mechanical cooling. The minimum variance is then $\min_\nu(V_{Q_\nu Q_\nu}) =: V_{Q_\phi Q_\phi}$ and ϕ, referred to as the squeezing angle, is the optimal choice of ν. Note that we will also investigate the minimum conditional variance $V^c_{Q_{\phi^c} Q_{\phi^c}}$, which in general has a different squeezing angle ϕ^c.

3.3.4 Asymptotic feedback

In general, analytical solutions to the steady-state equations governing the conditional and unconditional covariance matrices do exists, but are unwieldy large and thus too impractical. However, simple expressions for the excess covariance matrix elements in $\mathbf{V_{XX}}$ can be derived in the important limit where $p/q \to \infty$, i.e. when the feedback cost is negligible. In this section

we will be presenting such solutions for the two cases discussed in the previous sections. We will be assuming the generally valid conditions: $g, \kappa, \Omega_m > 0$, $Q_m > 1/2$ and $V^c_{Q,X_\theta} \neq 0$. This last condition is naturally obeyed due to the opto-mechanical coupling. Detailed derivations are found in the supplement Section 3.9.

We first consider the feedback strategy that minimizes the phonon number n. Applying the RWA, we find the steady-state Kalman gain $\mathbf{K} = \mathbf{Q}^{-1}\mathbf{B}^T\mathbf{Y}$ to leading order in p/q:

$$\mathbf{K}^T = \begin{bmatrix} \frac{1}{2}(Q_m^{-1} - \sqrt{4+Q_m^{-2}})\sqrt{\frac{p}{q}} + O\left[\left(\frac{p}{q}\right)^{1/4}\right] & 0 \\ \frac{1}{2}\sqrt{\frac{p}{q}} + O\left[\left(\frac{p}{q}\right)^{1/4}\right] & 0 \\ 2\sqrt{\frac{g}{\sqrt{\kappa}\Omega_m}}\left(\frac{p}{q}\right)^{1/4} + O(1) & 0 \\ 0 & 0 \end{bmatrix} \tag{3.3.17}$$

We note that $\mathbf{K}$ grows unboundedly with p/q, implying that infinite feedback strength is required in that particular limit. We also note that the entries of the fourth row and column are all zero, implying that information about the phase quadrature $\langle \hat{Y} \rangle$ will not be used in the Kalman gain, and that the feedback will not be applied to the phase input quadrature, i.e. $y_{fb}(t) = 0$.

Inserting this expression into Eq. (3.3.15), and taking the limit $p/q \to \infty$, we find the excess covariance matrix elements relevant for the phonon numbers to

$$V^E_{QQ} \to \frac{2}{\sqrt{4+Q_m^{-2}}}\frac{\eta\kappa}{\Omega_m}(V^c_{QX_\theta})^2 \tag{3.3.18}$$

$$V^E_{PP} \to \frac{\left(2 + Q_m^{-2} - Q_m^{-1}\sqrt{4+Q_m^{-2}}\right)}{\sqrt{4+Q_m^{-2}}}\frac{\eta\kappa}{\Omega_m}(V^c_{QX_\theta})^2, \tag{3.3.19}$$

for $p/q \to \infty$.

Without applying the RWA, similar calculations yield

$$V^E_{QQ} \to \frac{\eta\kappa}{\Omega_m}(V^c_{QX_\theta})^2, \tag{3.3.20}$$

$$V^E_{PP} \to \frac{\eta\kappa}{\Omega_m}(V^c_{QX_\theta})^2. \tag{3.3.21}$$

for $p/q \to \infty$. It is clear from these expressions that both for the RWA and nonRWA, the excess noise associated with the preparation of an unconditional state is quadratically proportional to the correlations between the position of the mechanics and the quadrature, X_θ of light.

If we instead choose the feedback strategy that minimizes the minimum variance $V_{Q_\nu Q_\nu}$

(corresponding to the choice of $\mathbf{P}$ in Eq. (3.3.16)), we find for the nonRWA case that:

$$V^E_{Q_\nu Q_\nu} \to \frac{\eta\kappa}{\Omega_m}(V^c_{QX_\theta})^2 \begin{cases} -2\sin(2\nu), & \nu \in]-\pi/2, 0[\\ 0, & \nu = [0, \pi/2] \end{cases} \tag{3.3.22}$$

$$V^E_{P_\nu P_\nu} \to \frac{\eta\kappa}{\Omega_m}(V^c_{QX_\theta})^2 \begin{cases} -\frac{\cos(4\nu)+1}{\sin(2\nu)}, & \nu \in]-\pi/2, 0[\\ \infty, & \nu = 0 \\ 2\csc(2\nu), & \nu \in]0, \pi/2[\\ \infty, & \nu = \pi/2 \end{cases} \tag{3.3.23}$$

$$V^E_{Q_\nu P_\nu} \to \frac{\eta\kappa}{\Omega_m}(V^c_{QX_\theta})^2 \begin{cases} -2\cos(2\nu), & \nu \in]-\pi/2, 0[\\ -1, & \nu = 0, \\ 0, & \nu \in]0, \pi/2[\\ 1, & \nu = \pi/2, \end{cases} \tag{3.3.24}$$

for $p/q \to \infty$. The above expressions are provided only for $\nu \in]-\pi/2, \pi/2]$ since they are π-periodic.

A number of important observations can be made from these results. The Kalman filter and optimal control stratedy applied here with $p/q \to \infty$ yields the lowest possible unconditional phonon number or minimum variance, given that we are able to measure the output field through homodyne detection and apply feedback by displacing the input field as described. However, even in this optimal limit the unconditional dynamics do not match the conditional dynamics. The unconditional phonon number for mechanical cooling as well as the minimized variance for mechanical squeezing will have an extra contribution quantified by the excess noise term in Eqs. (3.3.20)-(3.3.21) and Eqs. (3.3.22)-(3.3.24), respectively as also illustrated in Fig. 3.2b. This is in contrast to what appears to be a common belief in the literature, namely that the unconditional state may always approach the conditional state under feedback.

3.4 Results and discussion

In this section we will be using the mathematical framework for optimal quantum control derived in the previous section for estimating the minimum phonon occupancy as well as the maximum amount of squeezing of the mechanical oscillator. We will both investigate the conditional as well as the unconditional state, and consider the effects of the rotating wave approximation and the adiabatic approximation.

3.4.1 Mechanical cooling

In this section we will consider the effect of measurement induced cooling both on the conditional state where the state of the mechanical system is inferred by the measurements, and the unconditional state where the measured information is actively fed back onto the oscillator to drive it into a low entropy state. By using the formalism in the previous section, we plot in Figure 3.3 the minimum mechanical phonon occupancy against the opto-mechanical coupling strength both in terms of the coupling parameter, g, and the quantum cooperativity, $C_q = 4g^2/\kappa\Gamma_m\bar{n}$ where $\bar{n} = \{\exp(\hbar\Omega_m/k_\mathrm{B}T) - 1\}^{-1}$. The environmental temperature T is set to 300 K throughout the article. The plots in Fig. 3.3 have been numerically optimized (that is, the phonon number has

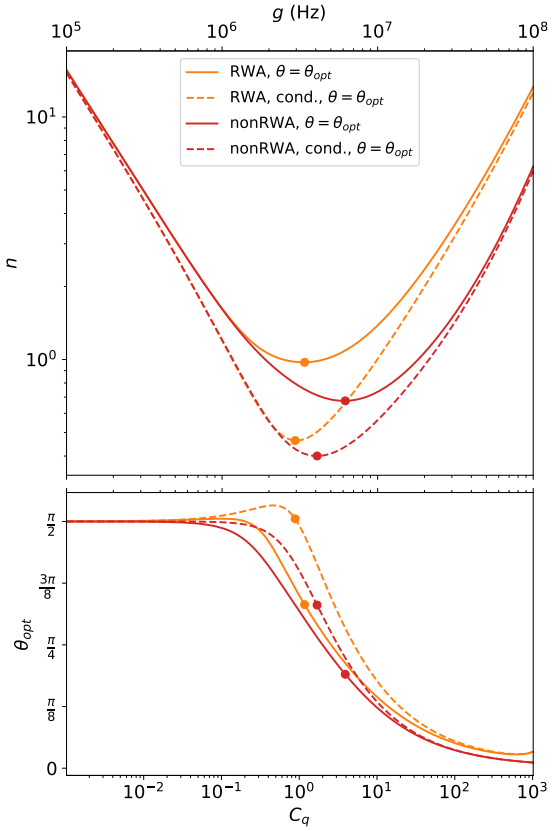

Figure 3.3: Top: Conditional (cond.) and unconditional phonon numbers n vs coupling strength g for the RWA and nonRWA model for $\theta = \theta_{\text{opt}}$. The minimum values of n as a function of g are marked with filled-in circles. Parameters used for this plot is $\Omega_m = 10^6\,\text{Hz}$, $\kappa = 10^8\,\text{Hz}$, $Q_m = 10^8$, $\eta = 1$, and $T = 300\,\text{K}$. Bottom: corresponding values of θ_{opt} versus g. The values at which n is minimal are marked with filled-in circles.

been minimized) over the measurement angle θ of the local oscillator. These optimal phases θ_{opt} are also shown in Fig. 3.3.

It is clear that for low coupling strengths, the optimal measurement angle is $\pi/2$ as expected since in that case all the information about the mechanical oscillator is transferred to the phase quadrature of the probe field. However, for larger coupling strengths, the radiation pressure force creates correlations between the amplitude quadrature of light and the mechanical position, which can be advantageously used for cooling by rotating the phase angle away from $\pi/2$. For very strong coupling, the optimal angle θ_{opt} tends to 0 which corresponds to an amplitude quadrature measurement.

We also clearly see from Fig. 3.3 that by imposing the RWA between the oscillator and the environment, the phononic occupancy is in general underestimated, in particular in the strong coupling regime. For weak coupling, the measurement rate will be low, which means that several mechanical oscillations will be required to resolve its motion. As a result, detailed information about the position and momentum of the mechanical oscillator is being washed out,

and thus a potential asymmetry in phase space of the mechanical state due to its coupling to the environment is not visible. In this regime, the RWA is therefore completely valid. However, when the measurement rate becomes large (that is, stronger coupling), the two mechanical quadratures can be better resolved, and thus a potential asymmetry imposed by the coupling to the environment becomes visible in the measurement. To capture these phase space correlations imposed by the environment, only the model without the RWA is valid, and as seen by Fig. 3.3 (comparing the RWA with non-RWA curves), the knowledge of these correlation indeed improves the cooling rate. The deviation between the RWA and nonRWA models naturally depends on the strength of the coupling of the mechanics to the environment (relative to the mechanical frequency) which is dictated by the thermalization rate, $\gamma_{th} = \Gamma_m(\bar{n} + 1/2)$.

It is clear from Fig. 3.3 that the phonon occupancy is minimized for a certain value of the cooperativity (measurement rate). This is attributed to the fact that a large measurement rate will make the measurement sharp and thus prepare the mechanical state in a squeezed state which inevitably adds phonons to the state. The difference between the conditional and unconditional state is also clearly evident from Fig. 3.3, and as expected the conditional state has a lower entropy than the unconditional state. The feedback required for the generation of the unconditional state imposes a noise penalty due to decoherence of the mechanics during feedback. This extra excess noise is however small, and plays only a role for small phonon occupancy: When the cooperativity is large, the phonon occupancy becomes large and the extra feedback-induced excess noise is negligible.

In Figure 3.4, top, we show the minimized phonon occupancy against the thermal decoherence rate in which we have optimized the values of the coupling strength, g (or C_q) (shown in Fig. 3.4, middle) and the measurement angle, θ (shown in Fig. 3.4, bottom). The phonon occupancy is again illustrated both for the approximative model applying the RWA as well as the complete solution without relying on the RWA. As expected, we observe a large deviation between the two models when the thermal decoherence rate is large (or equivalently when the mechanical frequency is low). This is caused by the establishment of mechanical quadrature correlation due to the strong environmental coupling which is neglected by the RWA model. We also again observe a large difference between the conditional and the unconditional states which is attributed to decoherence during feedback, and which is negligible for low decoherence rates. It is also interesting to note the large difference in the optimal measurement phases for the conditional and unconditional cases which is caused by the complex dynamics that the mechanics undergo during feedback.

We finally consider the effect that the adiabatic approximation might have on phonon occupancy. To illustrate this, in Figure 3.5 we plot the conditional phonon occupancy as a function of the frequency and thermalization rate both for the exact solution and for the one applying the adiabatic approximation. In this plot, we have optimized the coupling strength but set the measurement angle to $\pi/2$. As expected, the adiabatic approximation breaks down when the mechanical frequency approaches the cavity bandwidth which is set to $\kappa = 10^8$ Hz. The effect is further illustrated in the inset where we plot the phonon occupancy against the coupling strength.

3.4.2 Mechanical squeezing

In this section we investigate the potential of generating a squeezed state of the mechanical oscillator, conditionally and unconditionally, without resorting to the conventional RWA and the adiabatic approximation. While the analysis of generating squeezed mechanical state without resorting to the RWA has already been performed by Meng et al [45], here we will extend the

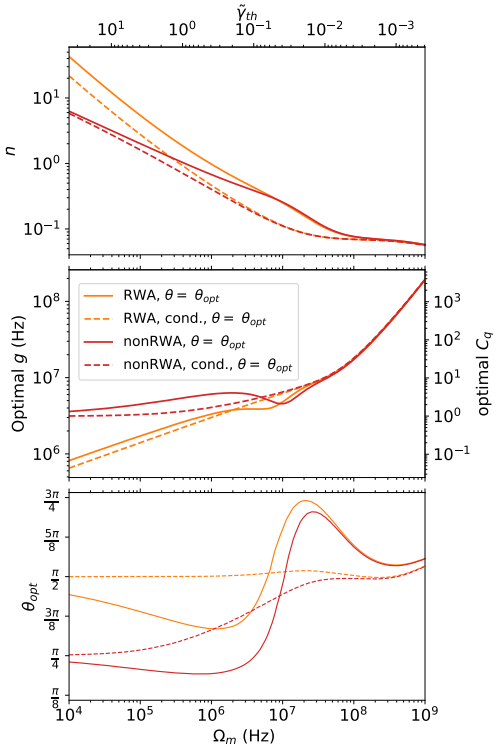

Figure 3.4: Plots of conditional (cond., dashed lines) and unconditional (solid lines) phonon numbers n at the optimal coupling strength g versus mechanical frequency Ω_m. Top: phonon number n is plotted. Middle: Plots of the optimal values of g and equivalent values of the optimal quantum cooperativity C_q. Bottom: Plots of the optimal value of the measurement angle θ.

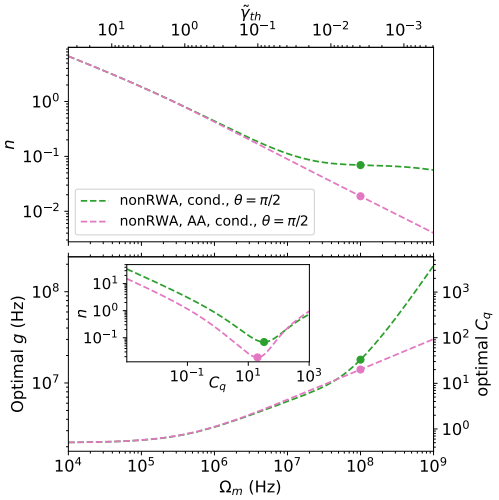

Figure 3.5: Plots of conditional (cond.) phonon number n at the optimal coupling strength g versus mechanical frequency Ω_m. for the nonRWA, with or without the adiabatic approximation (AA.), for $\theta = \pi/2$. Top: Mechanical phonon number n is plotted. Bottom: Plots of the optimal value of C_q. Inset: Conditional phonon number n vs C_q for $\Omega_m = 10^8$ Hz. circular dots on the plots mark points of optimal C_q for $\Omega_m = 10^8$ Hz.

analysis by considering the effect of optimizing the measurement angle, θ, exploring the validity of the adiabatic approximation and estimating the unconditional quantum state including feedback.

We start by illustrating the shortcomings of the adiabatic approximation in Figure 3.6. Here we plot the conditional minimum variance as a function of the coupling strength and the mechanical frequency with and without applying the adiabatic approximation. We observe that the two models completely agree for low frequencies and coupling strengths, but deviate when either Ω_m or g approaches or exceeds κ. In these cases the adiabatic approximation overestimates the achievable minimum variance compared to the full solution. E.g. for $g = 10^7$ Hz and $\Omega_m = 10^8$ Hz, the exact solution does not predict squeezing ($V^c_{Q_{\phi^c} Q_{\phi^c}} = 0.61$) while the approximate solution does ($V^c_{Q_{\phi^c} Q_{\phi^c}} = 0.48$). At the breakdown of the adiabatic approximation, we observe a significant increase in the minimum variance for increasing Ω_m. This is caused by the

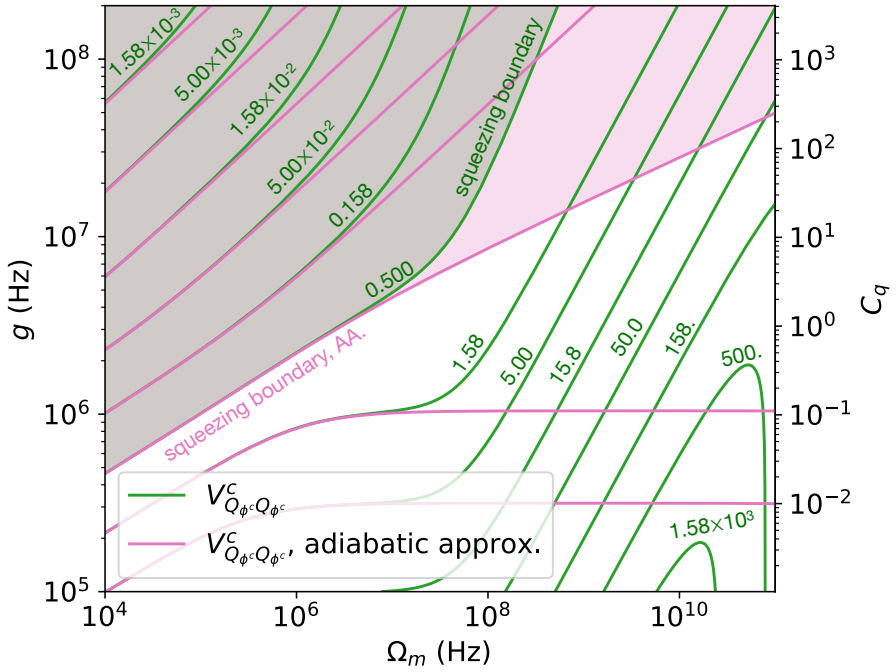

Figure 3.6: Contour plot of the conditional minimum variance $V^c_{Q_{\phi^c}Q_{\phi^c}}$ as a function of Ω_m and g, using either the nonRWA model (green) or the adiabatic approximation used in [45] (pink). marked on the plot are the values of $V^c_{Q_{\phi^c}Q_{\phi^c}}$ that the contours correspond to. The regions at which each of the two models predict mechanical squeezing ($V^c_{Q_{\phi^c}Q_{\phi^c}} < 0.5$) are coloured in with light green or pink, respectively. Parameters used in this plot are $\theta = \pi/2$, $\kappa = 10^8$ Hz, $Q_m = 10^8$, and $\eta = 1$.

fact that the measured output field has interacted with the mechanics over multiple mechanical periods, thereby giving less timely information about the mechanical state. On the other hand, the minimum variance decreases again at even higher frequencies, where the number of thermal phonons is small.

Our next step is to analyze the effect of optimizing the measurement angle, θ, for maximizing the degree of mechanical squeezing. In Figure 3.7. top, the conditional and unconditional minimum variances $V^c_{Q_{\phi^c}Q_{\phi^c}}$ and $V_{Q_\phi Q_\phi}$, respectively, are plotted against $\theta \in [0, \pi]$ for $\Omega_m = 10^4$ Hz and $\Omega_m = 10^6$ Hz. It is clear that squeezing can be produced for a rather large range of local oscillator phases (for this particular choice of parameters), and that the phase for which optimum squeezing is achieved is very different for the conditional and unconditional states. Interestingly, we also see that the squeezing angle ϕ varies continuously with the measurement angle for the conditional state while it stays constant at $\phi = 0$ for the unconditional state. This means that no matter what light quadrature is being measured, the position variable of the mechanics will always attain the smallest variance among all mechanical quadratures for the unconditional state. It is however interesting to note that for other choices of the parameters (e.g. choosing a larger mechanical frequency), the smallest variance will occur in the momentum variable ($\phi = \pi/2$) for certain measurement angles. The changeover from $\phi = 0$ to $\phi = \pi/2$ happens when the conditional squeezing angle ϕ_c reaches $-\pi/4$, which never happens under the

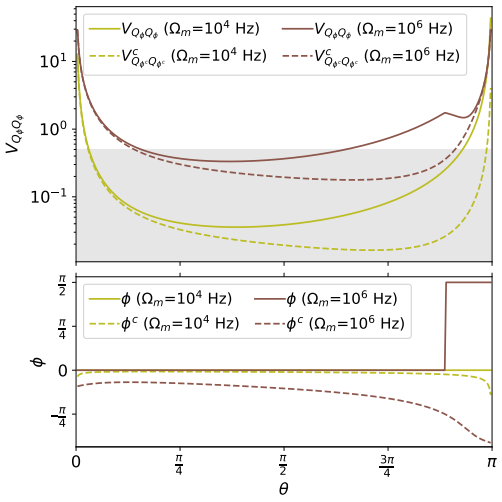

Figure 3.7: Top: Plot of the minimum variance of the mechanics vs measurement angle θ for both the conditional ($V^c_{Q_{\phi^c}Q_{\phi^c}}$, dashed lines) and the unconditional case ($V_{Q_\phi Q_\phi}$, solid lines) for $\Omega_m = 10^4$ Hz and $\Omega_m = 10^6$ Hz. The grey area indicates mechanical squeezing. Bottom: squeezing angles vs θ for the conditional (ϕ_c, dashed lines) and the unconditional case (ϕ, solid lines). Parameters used for these plots are $g = 5 \cdot 10^6$ Hz, $Q_m = 10^8$, $\kappa = 10^8$ Hz, and $\eta = 1$.

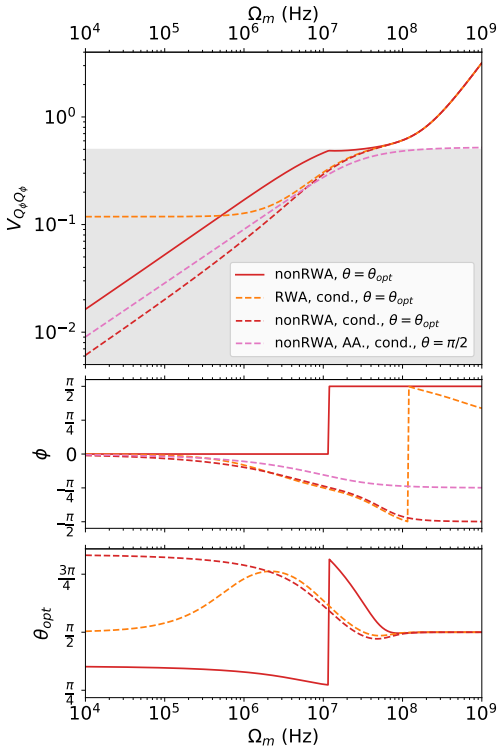

Figure 3.8: Plot of the minimum mechanical variance in both the conditional (cond., dashed lines) and the unconditional (solid lines) case with measurement angles $\theta = \pi/2$ and $\theta = \theta_{\text{opt}}$. versus Ω_m. Top: Minimum variance. Middle: corresponding values of ϕ and ϕ^c. Bottom: corresponding values of θ_{opt}. Parameters used for these plots are $g = 10^7$ Hz, $Q_m = 10^8$ Hz, $\kappa = 10^8$ Hz, and $\eta = 1$.

adiabatic approximation [45]. This is shown in Fig. 3.7, bottom (for $\Omega_m = 10^4$ Hz and $\Omega_m = 10^6$ Hz), where it is clear that the angle corresponding to the minimized variance is a binary function of the measurement angle. Furthermore, for this choice of the mechanical frequency, the range of measurements angles for which squeezing is observed is strongly reduced. The phase space nature of the unconditional state is thus very different from that of the conditional state.

In Figure 3.8 we plot the minimized mechanical variance as a function of the mechanical frequency for the conditional and unconditional states where the variance has been minimized over the measurement angle, θ while the quality factor and coupling strengths are kept constant. It is clear that for mechanical oscillators in the low frequency regime, a significant amount of squeezing can be observed for both the conditional and unconditional case. These squeezing amounts

are invisible if one applies the rotating wave approximation to the environment as illustrated by the dashed curve. In the high frequency regime (at the order of the cavity bandwidth or larger), the cavity dynamics will average out the dynamics of the mechanics, thereby smearing out the squeezing effect. In this case the variances of the conditional and unconditional states overlap, and moreover, the rotating wave approximation to the environment becomes valid.

Finally we make a comparison to the conditional solution found in Ref. [45] where the adiabatic approximation was applied and the measurement angle was set to $\pi/2$. This solution is represented by the dashed pink curves in Fig. 3.8, and it is clear that the adiabatic approximation breaks down at large frequencies as expected, and that the degree of attainable conditional squeezing is underestimated.

3.5 Conclusion

In conclusion, we have developed the formalism for optimal control of a mechanical oscillator without residing to any rotating-wave approximations for the mechanical oscillator. Using this formalism we discuss the resulting opto-mechanical dynamics with measurement and feedback, and deduced the minimal phonon occupancy as well as the minimal quadrature variance of the controlled mechanical oscillator. This was done both for the conditional state (where the measurement record is used to infer the state) and the unconditional state (where the measurement record is actively used to steer the mechanical oscillator into the desired state). We find that the rotating wave approximation of the mechanics to the environment is not valid in a rather large parameter space that is feasibly accessible in current optomechanical systems. Furthermore, we find that as a result of decoherence of the mechanical oscillator during feedback, the purity of the unconditional state is degraded compared to the conditional state. However, ground state cooling and squeezing of the unconditional state is still attainable in a room temperature environment. Indeed, ground state cooling of a room-temperature mechanical oscillator has recently been demonstrated [37].

3.6 S1: Linearisation of the optomechanical Hamiltonian including feedback

To ensure consistency with the full nonlinear cavity-optomechanical Hamiltonian including dissipation and measurement, we here derive from it the linearized Hamiltonian in Equation (3.3.1) in the main text. The section is inspired by many similar derivations in the literature, see e.g. [4].

The full Hamiltonian (disregarding the harmonic oscillator zero-point energies, and in a frame rotating with the laser frequency ω_L relative to the cavity field) is [50]

$$\begin{aligned}\hat{H}(t) =&\hbar\Delta_0\hat{a}^\dagger\hat{a} + \hbar\Omega_m\hat{b}^\dagger\hat{b} + \hbar g_0\hat{a}^\dagger\hat{a}(\hat{b}+\hat{b}^\dagger)\\ &+ i\hbar\sqrt{\kappa_{in}}\left[\epsilon(t)\hat{a}^\dagger - \epsilon^*(t)\hat{a}\right],\end{aligned} \tag{3.6.1}$$

where $\Delta_0 = \omega_c - \omega_L$ is the detuning of the input field, and g_0 is the vacuum optomechanical coupling rate. In order to make the linearisation approximation, we perform the following time-dependent transformation of the density matrix:

$$\rho \to \bar{\rho} = U\rho U^\dagger, \tag{3.6.2}$$

with

$$U = U(t) = D_a(-\alpha(t))D_b(-\beta(t)) \tag{3.6.3}$$

where $D_d(\delta) = e^{\delta d^\dagger - \delta^* d}$ is the standard displacement operator, defined for some annihilation operator d and complex number δ. This transforms the Schrödinger picture operators a and b to

$$\begin{aligned} \bar{a}(t) &:= U(t)aU^\dagger(t) = a + \alpha(t) \\ \bar{b}(t) &:= U(t)bU^\dagger(t) = b + \beta(t), \end{aligned} \tag{3.6.4}$$

which can be shown using the Baker-Hausdorff lemma. Note that we will frequently drop the time argument of the α and β functions in the following. The density matrix evolves according to the master equation:

$$\begin{aligned} d\hat{\rho} = &-\frac{i}{\hbar}[\hat{H}, \hat{\rho}]dt + \mathcal{L}_{\text{env}}\hat{\rho}, dt \\ &+ \kappa\mathcal{D}[\hat{a}]\hat{\rho}dt + \sqrt{\eta\kappa}\mathcal{H}[\hat{a}e^{-i\theta}]\hat{\rho}dW \end{aligned} \tag{3.6.5}$$

where the superoperators $\mathcal{D}$, $\mathcal{H}$ and $\mathcal{L}_{\text{env}}$ are defined as in the main text, i.e. $\mathcal{L}_{\text{env}}$ either equals $\mathcal{L}_{\text{RWA}}$ or $\mathcal{L}_{\text{nonRWA}}$ depending on which model is used.

We will now determine a new Hamiltonian $\bar{H}$ such that the master equation (3.6.5) is fulfilled under the substitutions $\rho \to \bar{\rho}$ and $H \to \bar{H}$.

The master equation of $\bar{\rho}$ is as follows

$$\begin{aligned} d\bar{\rho} &= \bar{\rho}(t + dt) - \bar{\rho}(t) \\ &= U(t + dt)\hat{\rho}(t + dt)U^\dagger(t + dt) - U(t)\hat{\rho}(t)U^\dagger(t) \\ &= dU(t)\hat{\rho}(t)U^\dagger(t) + U(t)d\hat{\rho}U^\dagger(t) + U(t)\hat{\rho}dU^\dagger \\ &= Ud\hat{\rho}U^\dagger + [\dot{\alpha}^* a - \dot{\alpha}a^\dagger + \dot{\beta}^* b - \dot{\beta}b^\dagger, \bar{\rho}]dt \end{aligned} \tag{3.6.6}$$

Where we have used that $\frac{d}{dt}D_a(-\alpha(t)) = [(\dot{\alpha}^* a - \dot{\alpha}a^\dagger) + \frac{1}{2}(\dot{\alpha}^*\alpha - \dot{\alpha}\alpha^*)]D_a(-\alpha(t)$, and similarly for $D_b(-\beta(t))$. These derivatives are found e.g. by using the Taylor expansions of the displacement operator.

The transformation of each of the terms in the expression of $Ud\hat{\rho}U^\dagger$ is:

$$U(\mathcal{D}[a])\hat{\rho}U^\dagger = \mathcal{D}[a]\bar{\rho} - \frac{1}{2}[\alpha a^\dagger - \alpha^* a, \bar{\rho}] \tag{3.6.7}$$

$$U(\mathcal{L}_{\text{RWA}}\hat{\rho})U^\dagger = \mathcal{L}_{\text{RWA}}\bar{\rho} - \frac{\Gamma_m}{2}[\beta b^\dagger - \beta^* b, \bar{\rho}] \tag{3.6.8}$$

$$U(\mathcal{L}_{\text{nonRWA}}\hat{\rho})U^\dagger = \mathcal{L}_{\text{nonRWA}}\bar{\rho} - \frac{\Gamma_m}{2}[(\beta - \beta^*)(b + b^\dagger), \bar{\rho}] \tag{3.6.9}$$

$$U(\mathcal{H}[\hat{a}e^{-i\theta}]\hat{\rho})U^\dagger = \mathcal{H}[\hat{a}e^{-i\theta}]\bar{\rho} \tag{3.6.10}$$

Thus, putting everything together, we obtain:

$$\begin{aligned}\frac{d}{dt}\bar{\rho} = &-\frac{i}{\hbar}[UHU^\dagger, \bar{\rho}] + \mathcal{L}_{\text{env}}\bar{\rho}dt \\ &+ \kappa\mathcal{D}[\hat{a}]\bar{\rho}dt + \sqrt{\eta\kappa}\mathcal{H}[\hat{a}e^{-i\theta}]\bar{\rho}dW \\ &+ \Big[\frac{\kappa}{2}(\alpha^* a - \alpha a^\dagger) + \mathcal{F}_{\text{env}} \\ &+\dot{\alpha}^* a - \dot{\alpha}a^\dagger + \dot{\beta}^* b - \dot{\beta}b^\dagger, \bar{\rho}\Big]\, dt\end{aligned} \tag{3.6.11}$$

with $\mathcal{F}_{\text{env}}$ equaling $\mathcal{F}_{\text{RWA}}$ or $\mathcal{F}_{\text{nonRWA}}$ defined below:

$$\mathcal{F}_{\text{RWA}} = \frac{\Gamma_m}{2}(\beta^* b - \beta b^\dagger) \tag{3.6.12}$$

$$\mathcal{F}_{\text{nonRWA}} = \frac{\Gamma_m}{2}(\beta^* - \beta)(b + b^\dagger) \tag{3.6.13}$$

This yields an expression for $\bar{H}$:

$$\begin{aligned}\bar{H} = UHU^\dagger + i\hbar\Big\{&\frac{\kappa}{2}(\alpha^* a - \alpha a^\dagger) + \frac{\Gamma_m}{2}(\beta^* b - \beta b^\dagger) \\ &+\dot{\alpha}^* a - \dot{\alpha}a^\dagger + \dot{\beta}^* b - \dot{\beta}b^\dagger\Big\}\end{aligned} \tag{3.6.14}$$

Evaluating $UHU^\dagger$ is straightforward, if a bit tedious. In the end we find that, when neglegting terms that are purely complex numbers (and therefore do not add to the dynamics), $\bar{H}$ can be written as

$$\begin{aligned}\bar{H} =&\hbar\Delta a^\dagger a + \hbar\Omega_m b^\dagger b + \hbar g(a^\dagger b + a^\dagger b^\dagger) + \hbar g^*(ab + ab^\dagger) \\ &+ i\hbar\sqrt{\kappa_{in}}(\epsilon_{fb}a^\dagger - \epsilon_{fb}^* a) + \hbar g_0 a^\dagger a(b + b^\dagger),\end{aligned} \tag{3.6.15}$$

with effective detuning $\Delta := \Delta_0 + g_0(\beta + \beta^*)$ and effective coupling $g := g_0\alpha$, all as long as α and β satisfies the following coupled differential equations:

$$\dot{\alpha} = -i[\Delta_0 + g_0(\beta + \beta^*)]\alpha - \frac{\kappa}{2}\alpha + \sqrt{\kappa_{\text{in}}}\epsilon_{\text{probe}} \tag{3.6.16a}$$

$$\dot{\beta} = -i\Omega_m\beta + \mathcal{G}_{\text{env}} - ig_0|\alpha|^2, \tag{3.6.16b}$$

where $\mathcal{G}_{\text{env}}$ equals $\mathcal{G}_{\text{RWA}} = -\frac{\Gamma_m}{2}\beta$ or $\mathcal{G}_{\text{nonRWA}} = -\frac{\Gamma_m}{2}(\beta - \beta^*)$, depending on the approximation. Throughout the calculations in the the main body of the paper, we work in this displaced picture where α and β are chosen to satisfy these equations. Note that if ϵ is substituted with ϵ_{probe}, these values of $\alpha(t), \beta(t)$ are equal to the expectation values $\langle a(t)\rangle, \langle b(t)\rangle$ in the undisplaced picture.

The existence and nature of steady-state solutions to Eqs. (3.6.16) are discussed in e.g. [2]. In the steady state, for constant ϵ_{probe}, Δ and g are approximately constant. In some cases, g will be real, such as when Δ is set to 0 as in this paper. For sufficiently strong driving strengths ϵ_{probe} and not too strong feedback strengths ϵ_{fb}, the nonlinear term $\hbar g_0 a^\dagger a(b + b^\dagger)$ may be neglected from the Hamiltonian. Thus, under these conditions, we obtain the Hamiltonian in Eq. eqrefeq:hamiltonian. It should be noted that we have not given precise requirements or bounds on the values of ϵ_{probe} and ϵ_{fb}. These considerations are left for future studies.

3.7 S2: Deriving the equations of motion

When deriving the covariance matrix elements in Eq. (3.3.7) of the main text, several smaller challenges must be dealt with: First of all, denoting the covariance of two arbitrary operators $\hat{A}$ and $\hat{B}$ by $\mathrm{Cov}[\hat{A},\hat{B}]= V_{AB} = \mathrm{Re}(\langle\hat{A}\hat{B}\rangle) - \langle\hat{A}\rangle\langle\hat{B}\rangle)$, we have that

$$dV_{AB} = \frac{1}{2}(d\langle\hat{A}\hat{B}\rangle + d\langle\hat{B}\hat{A}\rangle) - d(\langle\hat{A}\rangle\langle\hat{B}\rangle) \tag{3.7.1}$$

The last term must be evaluated using the Itō Calculus product rule stating that for two functions f and g evolving according to the stochastic differential equations $df = f_1 dt + f_2 dW$ and $dg = g_1 dt + g_2 dW$, then:

$$d(fg) = fdg + gdf + dfdg \tag{3.7.2}$$

While in normal calculus the term $dfdg$ vanishes, as it is proportional to dt^2, here we have that

$$\begin{aligned} dfdg &= f_1 g_1 dt^2 + (f_1 g_2 + g_2 f_1) dt dW + f_2 g_2 dW^2 \\ &= f_2 g_2 dt \end{aligned} \tag{3.7.3}$$

since $dW^2 = dt$.

Secondly, the differential equations for the variances will contain third order moments of A and B, i.e. $\langle A^2 B\rangle$. However, because the quantum state is assumed to be Gaussian, such products can be expressed in terms of first and second order moments. This property has been noted before in e.g. [32, 2]. It can be shown by the use of *Isserlis' theorem*. A specific instance of this theorem states that for three (classical) stochastic variables X_1, X_2, X_3 that follows a multivariate Gaussian distribution, it holds that [64]

$$\begin{aligned} E[X_1X_2X_3] =& E[X_1X_2]\mu_3 + E[X_1X_3]\mu_2 + E[X_2X_3]\mu_1 \\ &- 2\mu_1\mu_2\mu_3 \end{aligned} \tag{3.7.4}$$

where E is the classical expectation value (strictly different from the expectation value E (non-italicized) used in the main text) defined by

$$E[f(\mathbf{X})] = \int_{\mathbb{R}^n} f(\mathbf{x}) p(\mathbf{x}) d^n\mathbf{x} \tag{3.7.5}$$

and $\mu_i = E[X_i]$, $i = 1, 2, 3$ is the means of X_i. In the above formula, $p(\mathbf{x})$ is the probability density function corresponding to the stochastic vector $\mathbf{X}$ of length n. For a multivariate Gaussian distribution,

$$p(\mathbf{x}) = \frac{1}{\sqrt{(2\pi)^n \det \mathbf{V}}} \exp(-\frac{1}{2}(\mathbf{x}-\boldsymbol{\mu})^T \mathbf{V}^{-1}(\mathbf{x}-\boldsymbol{\mu})) \tag{3.7.6}$$

where $\boldsymbol{\mu} = E[\mathbf{X}]$ and $\mathbf{V} = E[(\mathbf{X}-\boldsymbol{\mu})(\mathbf{X}-\boldsymbol{\mu})^T]$. When working with Gaussian states in quantum information, The above formula exactly equals the form of the Wigner function $W(\mathbf{x})$ of the state $\hat{\rho}$ (See [48] for proper definitions). For the Wigner function, however, the 'expectation value' $E[...]$ is *not* equal to the quantum expectation $\langle ...\rangle$. Rather, we have that for any function f, [65]

$$E[f(\mathbf{X})] = \int_{\mathbb{R}^n} f(\mathbf{x})W(\mathbf{x})d^n\mathbf{x} = \langle \hat{F}(\hat{\mathbf{X}}) \rangle \tag{3.7.7}$$

where, $\hat{F}$ is an operator function of the operators $\hat{\mathbf{X}}$, that symmetrizes f. Specifically, $\hat{F}$ satisfies the properties

1. $\hat{F}(\mathbf{x}) = f(\mathbf{x})$
2. $\hat{F}(P\hat{\mathbf{X}}) = \hat{F}(\hat{\mathbf{X}})$ For all permutations P.

In the above, $P\hat{\mathbf{X}}$ represents a permutation of the elements in the vector of operators $\mathbf{X}$, e.g. swapping two elements.

As an example, if $f(\mathbf{x}) = x^2y$, then $\hat{F}(\hat{\mathbf{X}}) = \frac{1}{3}(\hat{X}^2\hat{Y} + \hat{X}\hat{Y}\hat{X} + \hat{Y}\hat{X}^2)$, i.e. an average over all the ways the operators $(\hat{X}, \hat{X}, \hat{Y})$ can be ordered in a non-commutative product. This gives us:

$$\frac{1}{3}(\langle \hat{X}^2\hat{Y} \rangle + \langle \hat{X}\hat{Y}\hat{X} \rangle + \langle \hat{Y}\hat{X}^2 \rangle) = E[X^2Y] \tag{3.7.8}$$

The above sum of third order moments of $\hat{X}$ and $\hat{Y}$ can now be expressed as a sum of products of first and second order moments by application of Eq. 3.7.4. Applying identities such as the above leads us to the equations of motion for

3.8 S3: Positivity of the density matrix

A real, symmetric, positive-definite matrix $\mathbf{V}$ corresponds to the covariance matrix of a quantum state density matrix $\hat{\rho}$ if and only if [66, 48]

$$\mathbf{V} + \frac{i}{2}\mathbf{\Omega} \geq 0 \tag{3.8.1}$$

where $\mathbf{\Omega}$ is the symplectic form defined in [48, Eq. (2)]. Thus, if a given covariance matrix $\mathbf{V}$ satisfies the above inequality, its associated density matrix must be positive, as this is one of the defining properties of a quantum density matrix.

As mentioned in section 3.3 of the main text, the nonRWA model of the mechanical interaction with its environment as given Eq. (3b) can occasionally produce nonpositive density matrices, which will of course be an invalid result. Therefore, we haved checked that each individual numerically calculated covariance matrix all the figures in the main text that behind the phonon numbers plotted in was verified to fulfil Eq. (3.8.1).

3.9 S4: Asymptotic feedback

In this section we derive the excess covariance matrix elements for $p/q \to \infty$ presented in section 3.3.4 of the main text. We focus on the nonRWA model with feedback that minimize the phonon number. The derivations for the RWA model and for feedback that optimize squeezing are similar and therefore omitted. The following derivations are valid under the conditions $\Gamma_m > 0, \kappa > 0, g > 0, \theta \in \mathbb{R}, p > 0, q > 0$, as well as the condition that the mechanical oscillator is underdamped, i.e. $\Gamma_m < 2\Omega_m$.

We are given the algebraic Riccati equation for the infinite-horizon optimal control problem

$$\mathbf{P} + \mathbf{A}^T\mathbf{Y} + \mathbf{Y}\mathbf{A} - \mathbf{Y}\mathbf{B}\mathbf{Q}^{-1}\mathbf{B}^T\mathbf{Y} = 0, \tag{3.9.1}$$

where $\mathbf{A}$, $\mathbf{B}$, $\mathbf{P}$, $\mathbf{Q}$, and $\mathbf{Y}$ are defined as in the main text. We normalize the equation by writing the rates of the system in units of Ω_m, i.e. by dividing through by Ω_m and then performing the substitution $x \to x\Omega_m$ for $x \in \{\Omega_m, \Gamma_m, g, \kappa\}$.

We solve for the 4×4 matrix $\mathbf{Y}$ by finding eigenvalues and eigenvectors to the following 8×8 Hamiltonian matrix $\mathbf{H}$ (not related to the energy operator):

$$\begin{aligned}\mathbf{H} &= \begin{bmatrix} \mathbf{A} & -\mathbf{B}\mathbf{Q}^{-1}\mathbf{B}^T \\ -\mathbf{P} & -\mathbf{A}^T \end{bmatrix} \\ &= \begin{bmatrix} 0 & 1 & 0 & 0 & 0 & 0 & 0 & 0 \\ -1 & -\Gamma_m & -2g & 0 & 0 & 0 & 0 & 0 \\ 0 & 0 & -\frac{\kappa}{2} & 0 & 0 & 0 & -\frac{\kappa}{q} & 0 \\ -2g & 0 & 0 & -\frac{\kappa}{2} & 0 & 0 & 0 & -\frac{\kappa}{q} \\ -p & 0 & 0 & 0 & 0 & 1 & 0 & 2g \\ 0 & -p & 0 & 0 & -1 & \Gamma_m & 0 & 0 \\ 0 & 0 & 0 & 0 & 0 & 2g & \frac{\kappa}{2} & 0 \\ 0 & 0 & 0 & 0 & 0 & 0 & 0 & \frac{\kappa}{2} \end{bmatrix}\end{aligned} \tag{3.9.2}$$

We find the following characteristic polynomial $ch(\lambda) = \det(\mathbf{H} - \lambda\mathbf{I})$:

$$\begin{aligned} ch(\lambda) = -\frac{1}{8q}\left(\frac{\kappa}{2} - \lambda\right)(\kappa + 2\lambda)\Big[&- 4g\left(4g\kappa p - 4g\kappa\lambda^2 p\right) \\ &- q\left(-\Gamma_m^2\lambda^2 + \lambda^4 + 2\lambda^2 + 1\right)(\kappa - 2\lambda)(\kappa + 2\lambda)\Big] \end{aligned} \tag{3.9.3}$$

it is immediately apparent that

$$\lambda_1^{\pm} = \pm\frac{\kappa}{2} \tag{3.9.4}$$

Are two roots to $ch(\lambda)$ and thus eigenvalues to $\mathbf{H}$. to find the rest of the eigenvalues, we divide out the roots and simplify the characteristic equation $ch(\lambda) = 0$ to find:

$$\begin{aligned} &\left(ch(\lambda) = 0 \ \wedge \ \lambda \neq \lambda_1^{\pm}\right) \\ &\iff -16g^2\kappa p(1 - \lambda^2) - q(\lambda^4 + \lambda^2(2 - \Gamma_m^2) + 1)(\kappa^2 - (2\lambda)^2) = 0 \\ &\iff 4g^2\kappa(\lambda^2 - 1) + \frac{q}{p}(\lambda^4 + \lambda^2(2 - \Gamma_m^2) + 1)\left[\lambda^2 - \left(\frac{\kappa}{2}\right)^2\right] = 0 \end{aligned} \tag{3.9.5}$$

Note that the above is a cubic equation in the variable $\sigma = \lambda^2$, so we can write it as

$$4g^2\kappa(\sigma - 1) + \frac{q}{p}(\sigma^2 + \sigma(2 - \Gamma_m^2) + 1)\left[\sigma - \left(\frac{\kappa}{2}\right)^2\right] = 0 \tag{3.9.6}$$

In principle, we could solve this using the standard formula for a cubic equation. We can however simplify the problem slightly, as we are only interested in the limiting case $q/p \to 0$. Now, the second term on the left hand side of the above equation is directly proportional to q/p

and therefore goes to zero as q/p goes to zero. This suggests that the cubic equation has a root $\sigma = \sigma_2$ for which $\sigma_2 \to 1$ as $q/p \to 0$. To prove this statement, write the root as $\sigma_2 := 1 + r_2$, where r_2, which we call the remainder of σ_2, is a complex number depending on the coefficients of the equation in (3.9.6), in particular on q/p. if we substitute $\sigma = 1 + r_2$ into (3.9.6), we get:

$$4g^2\kappa r_2 + \frac{q}{p}\left[(1+r_2)^2 + (1+r_2)(2-\Gamma_m^2) + 1\right]\left[(1+r_2) - \left(\frac{\kappa}{2}\right)^2\right] = 0 \tag{3.9.7}$$

It is clear that if we set $q/p = 0$ we have that $r_2 = 0$. Note that since the roots of a polynomial depend continuously on its coefficients, r_2 is a continuous function of q/p. Moreover, continuously increasing q/p from zero will also continuously change r_2 (possibly branching into more than one root). equivalently, there must exist at least one root for which its remainder r_2 goes to zero, as desired. We can also show how quickly r_2 goes to zero: multiplying by p/q on both sides of Eq. (3.9.7), we have

$$4g^2\kappa\left(\frac{p}{q}\right)r_2 + \left[(1+r_2)^2 + (1+r_2)(2-\Gamma_m^2) + 1\right]\left[(1+r_2) - \left(\frac{\kappa}{2}\right)^2\right] = 0, \tag{3.9.8}$$

which can be rearranged to show that

$$\lim_{q/p\to 0}\left(\frac{p}{q}\right)r_2 = -\frac{(4-\Gamma_m^2)\left[1-\left(\frac{\kappa}{2}\right)^2\right]}{4g^2\kappa} \tag{3.9.9}$$

We reduce the characteristic equation further by dividing Eq. (3.9.5) by $\sigma - \sigma_2$, which gives:

$$\begin{aligned}\frac{1}{4}\Gamma_m^2\left(\kappa^2-4\right) + \frac{4g^2\kappa p}{q} - \frac{3\kappa^2}{4} + r_2^2 - \frac{1}{4}r_2\left(4\Gamma_m^2+\kappa^2-16\right) + 4 \\ +\sigma\left(-\Gamma_m^2 - \frac{\kappa^2}{4} + r_2 + 3\right) + \sigma^2 = 0\end{aligned} \tag{3.9.10}$$

We find the roots of the above quadratic using the standard procedure: the discriminant d is

$$\begin{aligned}d = -16g^2\kappa\frac{p}{q} + \Gamma_m^4 + \frac{\kappa^4}{16} - 3r_2^2 + \frac{1}{2}\kappa^2\left(-\Gamma_m^2 + r_2 + 3\right) \\ + 2\Gamma_m^2(r_2-1) - 10r_2 - 7r_2.\end{aligned} \tag{3.9.11}$$

In the expression for d, the term $-16g^2\kappa p/q$ is the only term proportional to p/q, while the other terms are constant or proportional to r_2 or r_2^2. Therefore, for sufficiently large values of p/q, d is negative, or at least has negative real part, as we do not yet know whether or not r_2 is real. Thus, the remaining roots to the characteristic equation are

$$\sigma_3 = \frac{1}{2}\left(\Gamma_m^2 + \frac{\kappa^2}{4} - r_2 - 3 - i\sqrt{-d}\right) \tag{3.9.12}$$

$$\sigma_4 = \frac{1}{2}\left(\Gamma_m^2 + \frac{\kappa^2}{4} - r_2 - 3 + i\sqrt{-d}\right) \tag{3.9.13}$$

We can now deduce that for sufficiently large values of p/q, the parameter r_2 is real. This is because, when r_2 is sufficiently small, σ_3 and σ_4 are necessarily complex. since the reduced characteristic equation (3.9.6) has real coefficients, any complex roots must appear in conjugate pairs. The remaining root $\sigma_2 = 1 + r_2$ therefore has to be real, which proves that d is real and negative.

We now have that the eigenvalues to $\mathbf{H}$ with negative real part is $\lambda_1 = -\frac{\kappa}{2}$, $\lambda_i = -\sqrt{\sigma_i}, i = 2, 3, 4$. corresponding eigenvectors are denoted $\mathbf{v}_i$, $i = 1, 2, 3, 4$.

$$\lambda_3 = -\sqrt{\sigma_3} = \sqrt{g}\sqrt[4]{\frac{\kappa p}{q}}(-1+i) + r_3 \tag{3.9.14}$$

$$\lambda_4 = -\sqrt{\sigma_4} = \lambda_3^*, \tag{3.9.15}$$

where r_3 is a number that goes to zero as q/p goes to zero.

It is easy to show that an eigenvector corresponding to λ_1 is $\mathbf{v}_1 = [0\ 0\ 0\ 1\ 0\ 0\ 0\ 0]^T$. Through Gauss-Jordan elimination of $\mathbf{H} - \lambda_i \mathbf{I}$, with $\mathbf{I}$ being the (8×8) identity matrix, we find that

$$\mathbf{v}_2 = \begin{bmatrix} -\frac{1}{p\sqrt{r_2+1}} \\ \frac{1}{p} \\ \frac{\frac{r_2+2}{\sqrt{r_2+1}} - \Gamma_m}{2gp} \\ -\frac{4g}{-\kappa p\sqrt{r_2+1} + 2pr_2 + 2p} \\ -\frac{\frac{\Gamma_m}{\sqrt{r_2+1}} + 2}{\Gamma_m\sqrt{r_2+1} + r_2 + 2} \\ \frac{r_2}{\sqrt{r_2+1}\left(\Gamma_m\sqrt{r_2+1} + r_2 + 2\right)} \\ \frac{q\left(\frac{r_2+2}{\sqrt{r_2+1}} - \Gamma_m\right)\left(\sqrt{r_2+1} - \frac{\kappa}{2}\right)}{2g\kappa p} \\ 0 \end{bmatrix} \tag{3.9.16}$$

$$\mathbf{v}_3 = \begin{bmatrix} \frac{2g}{-(1-i)\Gamma_m\sqrt{g}\sqrt[4]{\frac{\kappa p}{q}} - 2ig\sqrt{\frac{\kappa p}{q}} + r_3\left(\Gamma_m - (2-2i)\sqrt{g}\sqrt[4]{\frac{\kappa p}{q}}\right) + r_3^2 + 1} \\ \frac{2g}{\Gamma_m - (1-i)\sqrt{g}\sqrt[4]{\frac{\kappa p}{q}} + \frac{1}{r_3 - (1-i)\sqrt{g}\sqrt[4]{\frac{\kappa p}{q}}} + r_3} \\ -1 \\ -\frac{8g^2}{\left(-(2-2i)\sqrt{g}\sqrt[4]{\frac{\kappa p}{q}} + \kappa + 2r_3\right)\left(-(1-i)\Gamma_m\sqrt{g}\sqrt[4]{\frac{\kappa p}{q}} - 2ig\sqrt{\frac{\kappa p}{q}} + r_3\left(\Gamma_m - (2-2i)\sqrt{g}\sqrt[4]{\frac{\kappa p}{q}}\right) + r_3^2 + 1\right)} \\ \frac{2gp\left(-\Gamma_m - (2-2i)\sqrt{g}\sqrt[4]{\frac{\kappa p}{q}} + 2r_3\right)}{\left(-(1-i)\Gamma_m\sqrt{g}\sqrt[4]{\frac{\kappa p}{q}} - 2ig\sqrt{\frac{\kappa p}{q}} + r_3\left(\Gamma_m - (2-2i)\sqrt{g}\sqrt[4]{\frac{\kappa p}{q}}\right) + r_3^2 + 1\right)\left((1-i)\Gamma_m\sqrt{g}\sqrt[4]{\frac{\kappa p}{q}} - 2ig\sqrt{\frac{\kappa p}{q}} - r_3\left(\Gamma_m + (2-2i)\sqrt{g}\sqrt[4]{\frac{\kappa p}{q}}\right) + r_3^2 + 1\right)} \\ \frac{2gp\left(-2ig\sqrt{\frac{\kappa p}{q}} - (2-2i)\sqrt{g}r_3\sqrt[4]{\frac{\kappa p}{q}} + r_3^2 - 1\right)}{\left(-(1-i)\Gamma_m\sqrt{g}\sqrt[4]{\frac{\kappa p}{q}} - 2ig\sqrt{\frac{\kappa p}{q}} + r_3\left(\Gamma_m - (2-2i)\sqrt{g}\sqrt[4]{\frac{\kappa p}{q}}\right) + r_3^2 + 1\right)\left((1-i)\Gamma_m\sqrt{g}\sqrt[4]{\frac{\kappa p}{q}} - 2ig\sqrt{\frac{\kappa p}{q}} - r_3\left(\Gamma_m + (2-2i)\sqrt{g}\sqrt[4]{\frac{\kappa p}{q}}\right) + r_3^2 + 1\right)} \\ \frac{q\left(-(2-2i)\sqrt{g}\sqrt[4]{\frac{\kappa p}{q}} + \kappa + 2r_3\right)}{2\kappa} \\ 0 \end{bmatrix} \tag{3.9.17}$$

$$\mathbf{v}_4 = \mathbf{v}_3^* \tag{3.9.18}$$

These expressions all hold for sufficiently small values of r_2 and r_3.

The algebraic Ricatti equation (3.9.1) is now solved as follows: Define an 8×4 matrix $\mathbf{U}$ and two 4×4 matrices $\mathbf{U}_1$ and $\mathbf{U}_2$ by

$$\mathbf{U} :=: \begin{bmatrix}\mathbf{U}_1\\ \mathbf{U}_2\end{bmatrix} := \begin{bmatrix}\mathbf{v}_1 & \mathbf{v}_2 & \mathbf{v}_3 & \mathbf{v}_4\end{bmatrix}. \tag{3.9.19}$$

Then it holds that [67]

$$\mathbf{Y} = \mathbf{U}_2\mathbf{U}_1^{-1} \tag{3.9.20}$$

is the unique stabilizing solution to (3.9.1), i.e. the unique solution that renders the matrix $\mathbf{A} - \mathbf{B}\mathbf{Q}^{-1}\mathbf{B}^T\mathbf{Y}$ asymptotically stable (eigenvalues with all negative real parts) [34].

We find that $\mathbf{Y}$ is of the form

$$\mathbf{Y} = \begin{bmatrix} y_{11} & y_{12} & y_{13} & 0\\ y_{12} & y_{22} & y_{23} & 0\\ y_{13} & y_{23} & y_{33} & 0\\ 0 & 0 & 0 & 0\end{bmatrix} \tag{3.9.21}$$

The above entries y_{ij} are all complicated expressions of the system parameters and r_2 and r_3, and won't be written in full here. We are only interested in their behavior as p/q goes to infinity. Note that we only care about the terms y_{13}, y_{23}, and y_{33}, as they are the only terms appearing in the Kalman Gain matrix $\mathbf{K} = \mathbf{Q}^{-1}\mathbf{B}^T\mathbf{Y} = \frac{\sqrt{\kappa}}{q}\begin{bmatrix} y_{13} & y_{23} & y_{33} & 0\\ 0 & 0 & 0 & 0\end{bmatrix}$.

we find that

$$y_{13} = -q\left(\sqrt{\frac{p}{\kappa q}} + O\left(\sqrt[4]{\frac{p}{q}}\right)\right) \tag{3.9.22}$$

$$y_{23} = -q\left(\sqrt{\frac{p}{\kappa q}} + O\left(\sqrt[4]{\frac{p}{q}}\right)\right) \tag{3.9.23}$$

$$y_{33} = 2q\left(\sqrt{\frac{g}{\kappa}}\sqrt[4]{\frac{p}{\kappa q}} + O(1)\right) \tag{3.9.24}$$

The lower-order terms of $\mathbf{K}$ are not important; note however that, from the fact that $\mathbf{Y}$ is the unique stabilizing solution, it follows that $\mathbf{Y}$ is real, and thus also $\mathbf{K}$ is real.

With the above expression for $\mathbf{K}$, we can now solve the Lyapunov equation for the excess covariance matrix $\mathbf{V}^E_{\mathbf{XX}}$:

$$\mathbf{N}\mathbf{V}^E_{\mathbf{XX}} + \mathbf{V}^E_{\mathbf{XX}}\mathbf{N}^T + \mathbf{F}^T\mathbf{F} = 0, \tag{3.9.25}$$

with $\mathbf{N} = \mathbf{A} - \mathbf{B}\mathbf{Q}^{-1}\mathbf{B}^T\mathbf{Y}$ and $\mathbf{F} = \mathbf{C}\mathbf{V}^c_{\mathbf{XX}} + \mathbf{\Gamma}$. Equation (3.9.25) is a linear system of equations in the entries of $\mathbf{V}_E$ and are therefore straightforwardly solved. We then take the limit of the solutions to these equations as $(p/q) \to \infty$ to obtain the expressions in Sec. II D.

Chapter 4

Measurement-based feedback scheme with squeezed input light

4.1 Introduction

In the previous chapter, we presented and analysed a measurement-based feedback scheme for an optomechanical system that assumed that the probe and feedback input field was in a coherent state. In this chapter, we extend the model to account for an input field in a displaced squeezed state. In contrast to a coherent state, the squeezed state introduces some new correlations in phase space which must be accounted for in the dynamics of the optomechanical coupling. Our model must therefore be extended which will be the subject of this chapter. We find that by using squeezed states in replacement of coherent states, it is possible to feedback cool the mechanical oscillator to the ground state at a lower input power. This is somewhat expected, but we also find that by using squeezed states of light as a probe it is possible to feedback control the mechanical oscillator into a mechanically squeezed state that is significantly more squeezed than if we were using coherent states of light for probing.

4.2 Derivation of the stochastic master equation

In this section, we will derive the master equation for the system with broadband squeezed input light. The derivations follow loosely the notation and playbook of Ref. [42], in which similar master equations are derived.

We start by introducing some notation relevant for squeezed states. For a pure squeezed state of a single-mode optical field, the covariance matrix of its amplitude and phase quadratures is

$$\mathbf{V} = \mathbf{R}_{\nu_{\mathrm{asq}}} \begin{bmatrix} \frac{1}{2}e^{2r} & 0 \\ 0 & \frac{1}{2}e^{-2r}, \end{bmatrix} \mathbf{R}_{\nu_{\mathrm{asq}}}^{T} \tag{4.2.1}$$

where the real number r is called the squeezing parameter that characterizes the strength of the squeezing, while $\mathbf{R}_{\nu_{\mathrm{asq}}}$ is a rotation matrix that rotates by an angle ν_{asq}. This is called the anti-squeezing angle and corresponds to the angle in quadrature phase space along which the anti-squeezing is largest.

A different way of representing the covariance matrix is the following:

$$\mathbf{V} = \begin{bmatrix} \frac{1}{2} + N + \mathrm{Re}[M] & \mathrm{Im}[M] \\ \mathrm{Im}[M] & \frac{1}{2} + N - \mathrm{Re}[M] \end{bmatrix} \tag{4.2.2}$$

where $N \geq 0$ is the mean number of photons in the squeezed state. The number M is in general complex and contains information about the angle and asymmetry of the squeezing. For pure squeezed states, $|M|^2 = N(N+1)$, while for impure states $|M|^2 \leq N(N+1)$. We will however not be considering impure squeezed input fields in this dissertation in order to constrain the discussion. In this chapter, we will mostly be using the parameters N and M for mathematical convenience. We remark that the following relations hold between N,M and r, ν_{asq}:

$$\nu_{\mathrm{asq}} = \arg[M]/2 \tag{4.2.3}$$

$$r = \frac{1}{2}\ln(1 + 2N + 2|M|) \tag{4.2.4}$$

Having the squeezed state notation at hand, we proceed with the actual derivation of the master equation. Our optomechanical system interacts with an external Markovian input field according to the following Hamiltonian:

$$\hat{H} = \hat{H}_0 + \hat{H}_{\mathrm{int}}, \tag{4.2.5}$$

$$\hat{H}_{\mathrm{int}} = i\hbar(\hat{s}\hat{a}^\dagger_{\mathrm{in}}(t) - \hat{s}^\dagger\hat{a}_{\mathrm{in}}(t)) \tag{4.2.6}$$

with $\hat{s} = \sqrt{\kappa}\hat{a}$ being a system operator, and $\hat{a}_{\mathrm{in}}(t)$ input field operators that commute with the system Hamiltonian $\hat{H}_0$ and satisfy the commutation relation $[\hat{a}_{\mathrm{in}}(t), \hat{a}^\dagger_{\mathrm{in}}(t')] = \delta(t-t')$. From this commutation relation, intuitively, one can understand the operator $\hat{a}^\dagger_{\mathrm{in}}(t)\sqrt{dt}$ as the creation operator of an infinitesimally narrow temporal mode at time $[t, t+dt]$. We introduce *quantum* Itō increments: $d\hat{A}_{\mathrm{in}}(t) = \hat{a}_{\mathrm{in}}(t)dt$ which obey the commutation relation $[d\hat{A}_{\mathrm{in}}(t), d\hat{A}^\dagger_{\mathrm{in}}(t)] = dt$. (The rigorous definition of quantum Itō calculus is given in e.g. [61].) Assuming a broadband squeezed input field, the Itō increments obey the rules:

$$d\hat{A}_{\mathrm{in}}(t)d\hat{A}_{\mathrm{in}}(t) = Mdt,\ \ d\hat{A}_{\mathrm{in}}(t)d\hat{A}^\dagger_{\mathrm{in}}(t) = (N+1)dt \tag{4.2.7}$$

$$d\hat{A}^\dagger_{\mathrm{in}}(t)d\hat{A}_{\mathrm{in}}(t) = Ndt,\ \ d\hat{A}^\dagger_{\mathrm{in}}(t)d\hat{A}^\dagger_{\mathrm{in}}(t) = M^*dt, \tag{4.2.8}$$

with M, N being scalars such that $N > 0$ and $|M|^2 \leq N(N+1)$, with equality holding for a pure squeezed state as mentioned above. The operators $d\hat{A}_{\mathrm{in}}(t)$ and $d\hat{A}^\dagger_{\mathrm{in}}(t)$ commute with all other operators at different times $t' \neq t$.

The time evolution operator $\hat{U}(t)$ under the Hamiltonian $\hat{H}$ in Eq. (4.2.5) obeys the following Itō equation:

$$\begin{aligned} d\hat{U}(t) &= \hat{U}(t+dt) - \hat{U}(t) \\ &= \left[\exp\left(-\frac{i}{\hbar}\hat{H}dt\right) - 1\right]U(t) \\ &= \left[\exp\left(-\frac{i}{\hbar}\hat{H}_0 dt + \hat{s}d\hat{A}^\dagger_{\mathrm{in}}(t) - \hat{s}^\dagger d\hat{A}_{\mathrm{in}}(t)\right) - 1\right]\hat{U}(t) \end{aligned} \tag{4.2.9}$$

By Taylor expanding the above exponential to second order around 0 and using the Itō rules (4.2.7) as well as the rules $d\hat{A}_{\text{in}}(t)dt \propto dt^2 = 0$, we obtain

$$d\hat{U}(t) = \left[-\frac{i}{\hbar}\hat{H}_{\text{eff}}dt + \hat{s}d\hat{A}^\dagger_{\text{in}}(t) - \hat{s}^\dagger d\hat{A}_{\text{in}}(t)\right]\hat{U}(t), \tag{4.2.10}$$

where

$$\hat{H}_{\text{eff}} = \hat{H}_0 - \frac{i\hbar}{2}\left[\hat{s}\hat{s}^\dagger N + \hat{s}^\dagger\hat{s}(N+1) - \hat{s}^2M^* - (\hat{s}^\dagger)^2M\right] \tag{4.2.11}$$

is the *effective Hamiltonian*. Note that this Hamiltonian is not Hermitian.

4.2.1 Pure squeezed input, $\hat{x}$-quadrature measurement

We assume that the input field is in a pure broadband squeezed vacuum state $|M\rangle$, satisfying the eigenvalue equation [34]

$$\left[(N+M^*+1)\hat{a}_{\text{in}}(t) - (N+M)\hat{a}^\dagger_{\text{in}}(t)\right]|M\rangle = 0 \tag{4.2.12}$$

for all times t. (The relations (4.2.7) may be derived from this eigenvalue equation, the commutation relations $[d\hat{A}_{\text{in}}(t), d\hat{A}^\dagger_{\text{in}}(t)] = dt$, and that $|M|^2 = N(N+1)$ for a pure squeezed state.) Assuming that the quantum state $|\phi(t)\rangle$ of the full system starts in the (pure) product state $|\phi(0)\rangle = |\psi(0)\rangle \otimes |M\rangle$, we get that

$$\begin{aligned} d|\phi(t)\rangle &= \left[-\frac{i}{\hbar}\hat{H}_{\text{eff}}dt + \hat{s}d\hat{A}^\dagger_{\text{in}}(t) - \hat{s}^\dagger d\hat{A}_{\text{in}}(t)\right]|\phi(t)\rangle \\ &= \left[-\frac{i}{\hbar}\hat{H}_{\text{eff}}dt + \hat{O}(d\hat{A}_{\text{in}}(t) + d\hat{A}^\dagger_{\text{in}}(t))\right]|\phi(t)\rangle\,, \end{aligned} \tag{4.2.13}$$

with $\hat{O} = [(N+M^*+1)\hat{s} - (N+M)\hat{s}^\dagger]/L$, where $L = 2N + 2\text{Re}(M) + 1$. The last line can be derived from adding multiples of $(N+M^*+1)d\hat{A}_{\text{in}}(t) - (N+M)d\hat{A}^\dagger_{\text{in}}(t)\,|\phi(t)\rangle = 0$ to the right hand side.

A subsequent measurement of the amplitude ($\hat{x}$) quadrature of the output field projects the input field state onto one of the eigenstates $|I_x(t)\rangle$ of the operator $(\hat{a}_{\text{in}}(t) + \hat{a}^\dagger_{\text{in}}(t))$ with respective eigenvalues $I_x(t)$. Performing this measurement continuously over time projects the system into the conditional state $|\psi(t)\rangle$. Under time evolution and subsequent measurement of $|\phi(t)\rangle$, we are left with the unnormalized state $|\tilde{\phi}(t+dt)\rangle$ at time $t+dt$:

$$\begin{aligned} |\phi(t)\rangle \to |\tilde{\phi}(t+dt)\rangle &:= |I_x(t)\rangle\langle I_x(t)|\phi(t+dt)\rangle \\ &= |I_x(t)\rangle\langle I_x(t)|\left[1 - \frac{i}{\hbar}\hat{H}_{\text{eff}}dt + \hat{O}(d\hat{A}_{\text{in}}(t) + d\hat{A}^\dagger_{\text{in}}(t))\right]|\phi(t)\rangle \\ &= |I_x(t)\rangle\langle I_x(t)|M\rangle\left[1 - \frac{i}{\hbar}\hat{H}_{\text{eff}}dt + \hat{O}I_x(t)dt\right]|\psi(t)\rangle\,. \end{aligned} \tag{4.2.14}$$

We thus have that the unnormalized conditional state $|\tilde{\psi}(t+dt)\rangle$ evolves according to the differential equation:

$$\begin{aligned} d\left|\tilde{\psi}(t)\right\rangle &= \left|\tilde{\psi}(t+dt)\right\rangle - \left|\psi(t)\right\rangle \\ &= \left[-\frac{i}{\hbar}\hat{H}_{\text{eff}}dt + \hat{O}I_x(t)dt\right]\left|\psi(t)\right\rangle \end{aligned} \tag{4.2.15}$$

Using Eq. (4.2.12), it can be shown that

$$\left|\left\langle I_x(t)|M\right\rangle\right|^2 = \sqrt{\frac{dt}{2\pi L}}\exp\left(-\frac{I_x^2 dt}{2L}\right). \tag{4.2.16}$$

As $I_x(t)dt$ and $d\hat{A}_{\text{in}}(t) + d\hat{A}_{\text{in}}^\dagger(t)$ obey the same statistics, we find that $(I_x(t)dt)^2 = Ldt$. From this, we can show that

$$\langle\tilde{\psi}(t+dt)|\tilde{\psi}(t+dt)\rangle = 1 + \frac{I_x(t)dt}{L}\left\langle\hat{s}+\hat{s}^\dagger\right\rangle, \tag{4.2.17}$$

where $\langle\cdot\rangle = \langle\psi(t)|\cdot|\psi(t)\rangle$. The probability of measuring the photocurrent $I_x(t)$ at time $t+dt$ is

$$\begin{aligned} \Pr(I_x(t)dt) &= \langle\tilde{\phi}(t+dt)|\tilde{\phi}(t+dt)\rangle \\ &= \left|\left\langle I_x(t)|M\right\rangle\right|^2\langle\tilde{\psi}(t+dt)|\tilde{\psi}(t+dt)\rangle \\ &= \sqrt{\frac{dt}{2\pi L}}\exp\left(-\frac{I_x(t)^2dt}{2L}\right)\left(1+\frac{I_x(t)dt}{L}\left\langle\hat{s}+\hat{s}^\dagger\right\rangle\right) \end{aligned} \tag{4.2.18}$$

Since the photocurrent $I_x(t)$ comes from an $\hat{x}$-measurement on a squeezed environment, it must have a Gaussian probability distribution with mean and variance given by μ and σ^2/dt, respectively. That is,

$$\begin{aligned} \Pr(I_x(t)dt) &= \sqrt{\frac{dt}{2\pi\sigma^2}}\exp\left(-\frac{(I_x-\mu)^2dt}{2\sigma^2}\right) \\ &= \sqrt{\frac{dt}{2\pi\sigma^2}}\exp\left(\frac{-I_x^2dt}{2\sigma^2}\right)\exp\left(-\frac{\mu^2dt}{2\sigma^2}+\mu\frac{I_xdt}{\sigma^2}\right) \\ &= \sqrt{\frac{dt}{2\pi\sigma^2}}\exp\left(\frac{-I_x^2dt}{2\sigma^2}\right)\left[1-\frac{\mu^2dt}{2\sigma^2}+\mu\frac{I_xdt}{\sigma^2}+\frac{1}{2}\left(\mu\frac{I_xdt}{\sigma^2}\right)^2\right] \\ &= \sqrt{\frac{dt}{2\pi\sigma^2}}\exp\left(\frac{-I_x^2dt}{2\sigma^2}\right)\left[1-\frac{\mu^2dt}{2\sigma^2}+\frac{I_xdt}{\sigma^2}\mu+\mu^2\frac{Ldt}{2\sigma^4}\right], \end{aligned} \tag{4.2.19}$$

where we again used that $(I_xdt)^2 = Ldt$. Comparing Eqs. (4.2.18) and (4.2.19), we find that $\mu = \langle\hat{s}+\hat{s}^\dagger\rangle$ and $\sigma^2 = L$. We can now write the incremental photocurrent $I_x(t)dt$ as an Itō equation:

$$\begin{aligned} I_x(t)dt &= \mu dt + \sigma dW(t) \\ &= \left\langle\hat{s}+\hat{s}^\dagger\right\rangle dt + \sqrt{L}dW(t), \end{aligned} \tag{4.2.20}$$

where $dW(t)$ is a Wiener increment.

We are now in a position to derive an explicit equation for the time evolution normalized, conditional density matrix $\hat{\rho}_c(t) = |\psi(t)\rangle\langle\psi(t)|$. We have that

$$d\hat{\rho}_c(t) = \frac{\tilde{\rho}_c(t+dt)}{\mathrm{Tr}[\tilde{\rho}_c(t+dt)]} - \hat{\rho}_c(t), \tag{4.2.21}$$

where $\tilde{\rho}_c(t+dt) := |\tilde{\psi}(t+dt)\rangle\langle\tilde{\psi}(t+dt)|$ is the unnormalized density matrix and $\mathrm{Tr}[\tilde{\rho}_c(t+dt)] = \langle\tilde{\psi}(t+dt)|\tilde{\psi}(t+dt)\rangle = 1 + \frac{1}{L}\langle\hat{s}+\hat{s}^\dagger\rangle^2 dt + \frac{1}{\sqrt{L}}\langle\hat{s}+\hat{s}^\dagger\rangle dW(t)$, cf. Eqs. (4.2.17) and (4.2.20). Expanding the above equation and using Itō calculus, we arrive at the following conditional master equation:

$$\begin{aligned} d\hat{\rho}(t) =& -\frac{i}{\hbar}(\hat{H}_{\mathrm{eff}}\hat{\rho}(t) - \hat{\rho}(t)\hat{H}_{\mathrm{eff}}^\dagger)dt + L\hat{O}\hat{\rho}(t)\hat{O}^\dagger dt \\ &+ \sqrt{L}\left[\hat{O}\hat{\rho}(t) + \hat{\rho}(t)\hat{O}^\dagger - \frac{1}{L}\langle\hat{s}+\hat{s}^\dagger\rangle\hat{\rho}(t)\right]dW(t) \\ =& \left(-\frac{i}{\hbar}[\hat{H}_0,\hat{\rho}] + (N+1)\mathcal{D}[\hat{s}]\hat{\rho} + N\mathcal{D}[\hat{s}^\dagger]\hat{\rho}\right)dt \\ &- \left(M^*\mathcal{D}^\circ[\hat{s}]\hat{\rho} + M\mathcal{D}^\circ[\hat{s}^\dagger]\hat{\rho}\right)dt \\ &+ \sqrt{L}\left[\hat{O}\hat{\rho}(t) + \hat{\rho}(t)\hat{O}^\dagger - \frac{1}{L}\langle\hat{s}+\hat{s}^\dagger\rangle\hat{\rho}(t)\right]dW(t), \end{aligned} \tag{4.2.22}$$

where the superoperators $\mathcal{D}$ and $\mathcal{D}^\circ$ are defined by

$$\mathcal{D}[\hat{c}]\hat{\rho}dt = \hat{c}\hat{\rho}\hat{c}^\dagger - \frac{1}{2}(\hat{c}^\dagger\hat{c}\hat{\rho} - \hat{\rho}\hat{c}^\dagger\hat{c}). \tag{4.2.23}$$

$$\mathcal{D}^\circ[\hat{c}]\hat{\rho}dt = \hat{c}\hat{\rho}\hat{c} - \frac{1}{2}(\hat{c}\hat{c}\hat{\rho} - \hat{\rho}\hat{c}\hat{c}). \tag{4.2.24}$$

The master equation presented in Eq. (4.2.22) is well-known and also derived in e.g. Ref. [34]. While it is important to note that the master equation is only valid at $\eta = 1$ detetion efficiency of the output field, it is fairly simple to show [32] that a non-unit detection efficiency η can be accounted for simply by multiplying the terms proportional to $dW(t)$ by $\sqrt{eta}$. However, as this chapter only considers the case $\eta = 1$, we will simply ignore this parameter here.

4.2.2 Pure squeezed input, $\hat{x}_\theta$-quadrature measurement

In the previous section, we considered the time evolution under continuous measurement of the $\hat{x}$ quadrature of the light field. We here present the results for a general rotated quadrature $x_\theta(t) = \hat{a}_{\mathrm{in}}(t)e^{-i\theta} + \hat{a}_{\mathrm{in}}^\dagger(t)e^{i\theta}$.

The Schrödinger time evolution of the full system, Eq. (4.2.13), can be rewritten as follows:

$$d|\phi(t)\rangle = \left[-\frac{i}{\hbar}\hat{H}_{\mathrm{eff}}dt + \hat{O}_\theta(d\hat{A}_{\mathrm{in}}(t)e^{-i\theta} + d\hat{A}_{\mathrm{in}}^\dagger(t)e^{+i\theta})\right]|\phi(t)\rangle, \tag{4.2.25}$$

with

$$\hat{O}_\theta = \frac{(N+M^*+1)\hat{s} - (N+M)\hat{s}^\dagger}{(N+M^*+1)e^{i\theta} + (N+M)e^{-i\theta}} \tag{4.2.26}$$

Through measurements of the photocurrent, $I_\theta(t)$, projects the state onto $|I_\theta(t)\rangle$, where $\hat{x}_\theta |I_\theta(t)\rangle = I_\theta(t) |I_\theta(t)\rangle$. We then have that

$$\begin{aligned} d|\tilde{\psi}(t)\rangle &= |\tilde{\psi}(t+dt)\rangle - |\psi(t)\rangle \\ &= \left[-\frac{i}{\hbar}\hat{H}_{\text{eff}}dt + \hat{O}_\theta I_\theta(t)dt\right]|\psi(t)\rangle\,, \end{aligned} \tag{4.2.27}$$

and the probability of obtaining a given photocurrent is

$$|\langle I_\theta(t)|M\rangle|^2 = \sqrt{\frac{dt}{2\pi L_\theta}}\exp\left(-\frac{I_\theta^2 dt}{2L_\theta}\right), \tag{4.2.28}$$

with $L_\theta = 2N + 2\text{Re}\{Me^{-2i\theta}\} + 1$. Thus, the Itō time evolution of the photocurrent may be written as

$$I_\theta(t)dt = \langle \hat{s}_\theta + \hat{s}_\theta^\dagger\rangle\, dt + \sqrt{L_\theta}dW(t), \tag{4.2.29}$$

In the end, this leaves us with the conditional master equation

$$\begin{aligned} d\hat{\rho}(t) = &\left(-\frac{i}{\hbar}[\hat{H}_0,\hat{\rho}] + (N+1)\mathcal{D}[\hat{s}]\hat{\rho} + N\mathcal{D}[\hat{s}^\dagger]\hat{\rho}\right)dt \\ &- \left(M^*\mathcal{D}^\circ[\hat{s}]\hat{\rho} + M\mathcal{D}^\circ[\hat{s}^\dagger]\hat{\rho}\right)dt \\ &+ \sqrt{L_\theta}\left[\hat{O}_\theta\hat{\rho}(t) + \hat{\rho}(t)\hat{O}_\theta^\dagger - \frac{1}{L_\theta}\langle \hat{s}_\theta + \hat{s}_\theta^\dagger\rangle\,\hat{\rho}(t)\right]dW(t). \end{aligned} \tag{4.2.30}$$

4.2.3 State space matrices

From Eq. (4.2.30), we may now derive the state space matrices pertaining to the optomechanical system described in Chapter 3, but with a squeezed input field instead of a coherent input field. To that end, we set the system Hamiltonian to

$$\hat{H}_0 = \hbar\frac{\Omega_m}{2}(\hat{Q}^2 + \hat{P}^2) + 2\hbar g\hat{Q}\hat{X} + \hbar\sqrt{\kappa}\left[x_{fb}(t)\hat{Y} - y_{fb}(t)\hat{X}\right], \tag{4.2.31}$$

as in Eq. (3.3.1) but with $\Delta = 0$. We remind the reader that $\hat{Q} = (\hat{b} + \hat{b}^\dagger)/\sqrt{2}$ and $\hat{P} = (\hat{b} - \hat{b}^\dagger)/(i\sqrt{2})$ are the mechanical mode position and momentum quadratures, while $\hat{X} = (\hat{a}+\hat{a}^\dagger)/\sqrt{2}$ and $\hat{Y} = (\hat{a} - \hat{a}^\dagger)/(i\sqrt{2})$ are the cavity field amplitude and phase quadratures; Ω_m is the mechanical resonance frequency, g is the effective optomechanical coupling strength, and κ is the cavity linewidth, assumed to be equal to the cavity input mirror coupling rate; finally, $x_{fb}(t)$ and $y_{fb}(t)$ are controllable time-dependent feedback parameters, although in this chapter we will not consider the effect of adding feedback, but only look at the conditional state.

With this choice of $\hat{H}_0$, the optomechanical system can almost directly be modeled by the master equation in Eq. (4.2.30) with $\hat{s} = \sqrt{\kappa}\hat{a}$. The only missing part is the mechanical interaction with the environment. In this chapter, we will be exclusively consider the nonRWA model, as the comparison with the RWA model has already been discussed in Chapter 3. We add this interaction by simply adding to Eq. (4.2.30) the term $\mathcal{L}_{\text{nonRWA}}\hat{\rho}(t)$ as given in Eq. (3.3.3).

We find the state space matrices for the means and variances of the quadratures $[\hat{Q}\ \ \hat{P}\ \ \hat{X}\ \ \hat{Y}]$ using the same procedure as in Chapter 3. We find that $\mathbf{A}_{\text{nonRWA}}$ and $\mathbf{B}$ are unchanged and as in Eqs. (3.3.9a) and (3.3.10a), while $\mathbf{D}_{\text{nonRWA}}$, $\mathbf{C}$, and $\mathbf{\Gamma}$ now take the following form:

$$\mathbf{D}_{\text{nonRWA}} = \begin{bmatrix} 0 & 0 & 0 & 0 \\ 0 & 2\Gamma_m(\bar{n}+1/2) & 0 & 0 \\ 0 & 0 & \kappa(N+1/2+\text{Re}[M]) & \kappa\text{Im}[M] \\ 0 & 0 & \kappa\text{Im}[M] & \kappa(N+1/2-\text{Re}[M]) \end{bmatrix} \tag{4.2.32}$$

$$\mathbf{C} = \frac{\sqrt{2\kappa L_\theta}L}{\cos^2(\theta)\left[L+2\text{Im}[M]\tan(\theta)\right]^2+\sin^2(\theta)} \begin{bmatrix} 0 & 0 & \cos(\theta) & \sin(\theta) \end{bmatrix} \tag{4.2.33}$$

$$\begin{aligned} \mathbf{\Gamma} = &\left(\frac{-\sqrt{\frac{\kappa L_\theta}{2}}L}{\cos^2(\theta)\left[L+2\text{Im}[M]\tan(\theta)\right]^2+\sin^2(\theta)} \right) \\ &\times \begin{bmatrix} 0 & 0 & \text{Re}\{e^{i\theta}(1+2N+2Me^{-2i\theta})\} & \text{Im}\{e^{i\theta}(1+2N+2Me^{-2i\theta})\} \end{bmatrix} \end{aligned} \tag{4.2.34}$$

As mentioned we do not present results regarding the unconditional mechanical state when feedback is applied in this chapter. The main reason for this is that the asymptotic excess variances that we showed in Chapter 3 become significantly more complicated to when the squeezed probe and its associated parameters is introduced. These considerations are left for future studies.

4.3 Numerical results

In this section, we discuss the effect on the conditional phonon number and the conditional minimum variance (as defined in Chapter 3) on using a squeezed probe field based on numerical results of applying the state space model.

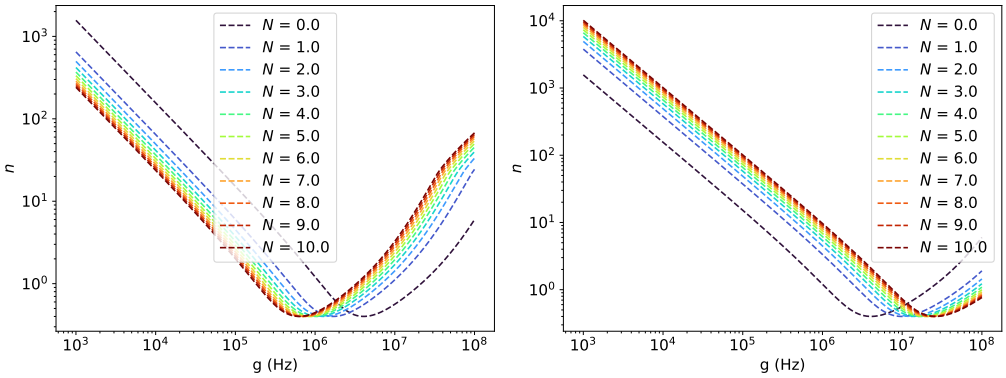

Figure 4.1: Conditional phonon number n vs coupling strength g for different squeezing numbers N. **Left:** anti-squeezing angle is $\nu_{\text{asq}} = 0$. **Right:** anti-squeezing angle is $\nu_{\text{asq}} = \pi/2$. . Using the nonRWA model and optimizing the homodyne measurement angle, $\theta = \theta_{\text{opt}}$. Other parameters used for this plot is $\Omega_m = 10^6\,\text{Hz}$, $\kappa = 10^8\,\text{Hz}$, $Q_m = 10^8$, $\eta = 1$, and $T = 300\,\text{K}$.

in Fig. 4.1, the conditional phonon number is plotted for a range values of the squeezing number N, for two choices of the anti-squeezing angle: $\nu_{\text{asq}} = 0$ and $\nu_{\text{asq}} = \pi/2$. Note that in both cases, the homodyne measurement angle θ is optimized. for $\nu_{\text{asq}} = 0$ it is clear that for low

coupling strengths g, the phonon number decreases when N is increased. However, the minimum phonon number with respect to g remains the same; the minimum value is simply attained at a lower value of g. For $\nu_{\mathrm{asq}} = \pi/2$, one observes the opposite behaviour, i.e. that the phonon number increases with N until the optimal phonon number reached, which will be at a higher optimal value of g than for $N = 0$. In other words, of these two choices, $\nu_{\mathrm{asq}} = 0$ is clearly preferred. The reason is that the mechanical position is imprinted in the phase quadrature of the output field, which is therefore where one should lower the measurement imprecision noise. $\nu_{\mathrm{asq}} = 0$ achieves exactly this, since this means squeezing and thus less noise in the phase quadrature, while $\nu_{\mathrm{asq}} = \pi/2$ achieves the opposite.

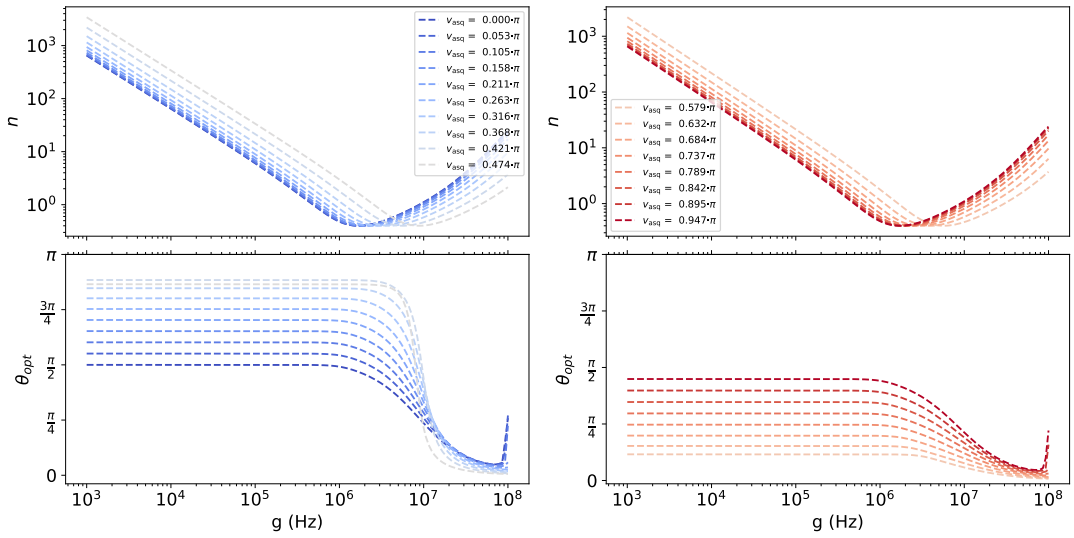

Figure 4.2: The conditional phonon number n_C and corresponding optimal measurement angle θ_{opt} vs coupling strength g for different anti-squeezing angles ν_{asq}. NonRWA model is used. **Left:** ν_{asq} in a range between 0 and $\pi/2$. **Right:** ν_{asq} in a range between $\pi/2$ and π. In both plots, the color is darker for larger values of ν_{asq} as shown on the legends. Parameters used for this plot is $N = 1$, $\Omega_m = 10^6$ Hz, $\kappa = 10^8$ Hz, $Q_m = 10^8$, $\eta = 1$, and $T = 300$ K.

One might ask if $\nu_{\mathrm{asq}} = 0$ is the optimal choice of anti-squeezing angle. This question is explored in figure Fig. 4.2, where the conditional phonon number vs coupling strength is plotted a range of ν_{asq} in the range 0 to $\pi/2$. It is evident from the plot. that $\nu_{\mathrm{asq}} = 0$ is still the best choice. It is however interesting to look at the optimal measurement angles θ, which are plotted as well in Fig. 4.2. For low coupling strengths, the optimal values of θ change completely in step with ν_{asq}; for example, when $\nu_{\mathrm{asq}} = 0.211\pi$, we find that $\theta_{\mathrm{opt}} = \pi/2 + 0.211 \cdot \pi$. The only exception to this is when ν_{asq} is near $\pi/2$. The explanation here is as follows: When a rotated quadrature $\hat{X}_\theta = \hat{X}\cos(\theta) + \hat{Y}\sin(\theta)$ of the cavity field is measured, the information from the measurement is proportional to $\sin(\theta)\hat{Q} + (\text{noise})$, so it would appear that it is always better to choose $\sin(\theta) = \pi/2$. On the other hand, the noise term is the lowest whenever θ matches the squeezing angle, i.e. when $\theta = \nu_{\mathrm{asq}} + \pi/2$. It turns out that minimizing the noise term is much more important, at least for this degree of squeezing ($N = 1$), as any deviation from a matched measurement angle comes at a penalty of a large amount of anti-squeezing noise. The only thing that this explanation ignores is the effect of backaction noise. However, the backaction noise is

negligible until the optimal value of g and the minimal value of the phonon number is reached. The effect of backaction noise is clear from the figure, as we observe the optimal angles θ_{opt} to all decrease below $\pi/2$ at coupling strengths near or above the optimum.

Nevertheless, it is clear that, at least for this parameter space, the optimal choice of anti-squeezing angle is $\nu_{\text{asq}} = 0$.

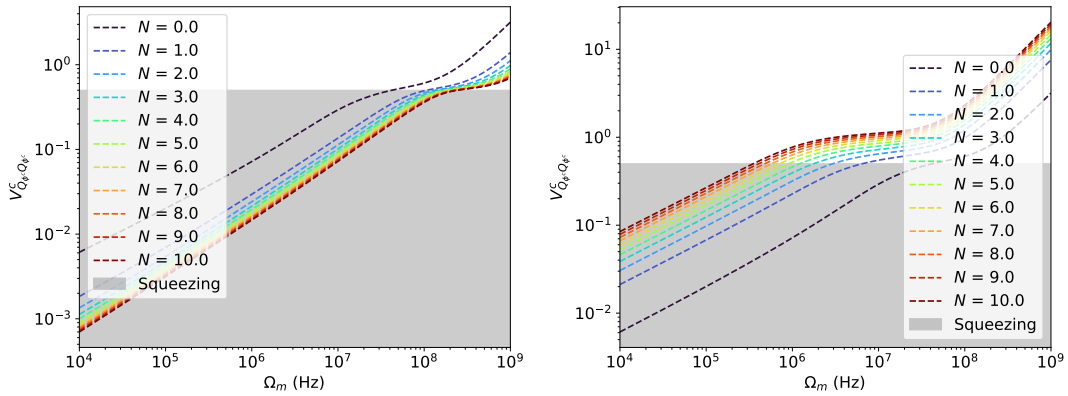

Figure 4.3: The conditional minimum variance $V^c_{Q_{\phi^c} Q_{\phi^c}}$ vs mechanical frequency Ω_m for different squeezing numbers N. **Left:** Anti-squeezing angle is $\nu_{\text{asq}} = 0$. **Right:** Anti-squeezing angle is $\nu_{\text{asq}} = \pi/2$. . Using the nonRWA model and optimizing the homodyne measurement angle, $\theta = \theta_{\text{opt}}$. The grey area indicates mechanical squeezing. Other parameters used for this plot is $g = 10^7$ Hz, $\kappa = 10^8$ Hz, $Q_m = 10^8$, $\eta = 1$, and $T = 300$ K.

We now move on to briefly discuss how introducing a squeezed probe field affects the conditional minimum mechanical variance $V^c_{Q_{\phi^c} Q_{\phi^c}}$. In Fig. 4.3, $V^c_{Q_{\phi^c} Q_{\phi^c}}$ is plotted at a fixed coupling strength for versus mechanical frequencies Ω_m, for a range of squeezing numbers N for $\nu_{\text{asq}} = 0, \pi/2$. Again, we observe that $\nu_{\text{asq}} = 0$ is the better choice, as the conditional variance then decreases as a function of N, whereas it increases when $\nu_{\text{asq}} = \pi/2$. The explanation is exactly the same as for the conditional phonon number, and we also here find that $\nu_{\text{asq}} = 0$ is the optimal choice.

4.4 Conclusion

In this section, we have extended the model for optomechanical measurement and conditional cooling and squeezing in Chapter 3 to the case where the probe field is in a pure squeezed state. We have presented numerical simulations of the conditional phonon number and conditional minimum variance of the mechanics under this squeezed probe field. In general, we find that a probe field with an anti-squeezing angle of $\nu_{\text{asq}} = 0$ (corresponding to phase-squeezed light) is optimal in both cases, and presents clear improvements over the coherent probe field: For the conditional phonon number, the overall minimal phonon number remains the same, but is achievable at a signicantly reduced coupling strength. The conditional minimum mechanical variance is significantly reduced overall across all mechanical frequencies, thereby making mechanical squeezing possible at lower coupling strengths than with a coherent probe. We have not calculated the effect on the unconditional state including feedback, but we expect similar conclusions to hold in this case.

Chapter 5

Coherent feedback cooling

5.1 Introduction

In this chapter we turn to a markedly different feedback scheme from the previous chapters. Instead of measuring the output field from the cavity and then using the measurement outcome as a basis for a feedback beam, we feed the output field directly back into the cavity. In other words, we use the output beam as the feedback beam. This setup has the advantage of being slightly simpler, as it bypasses the need for measurement equipment, and it also eliminates detection inefficiencies as a source of loss. It may also have an additional advantage of not collapsing the output field into a single number from the measurement. This means that the full quantum information is retained in the feedback beam, which is potentially useful.

On the other hand, in order for the feedback scheme to work, some manipulation of the output beam is still necessary before it will work suitably as a feedback force. While for a measurement-based feedback scheme, this manipulation can be done using digital FPGA filters, our current physical tools for a direct feedback scheme are less sophisticated. In this chapter, the manipulation of the output field that we propose is a delay line along with a rotation and displacement of the field. The delay time is set to a quarter mechanical period, such that the position information in the output field will be converted to negative momentum information. Through The rotation and displacement of the output field, this information is converted to a negative feedback force in the momentum quadrature. The delay line is implemented simply by running the output through a long line of free space or fiber, and the displacement operation may easily be carried out by mixing the output with a local oscillator in a highly transmissive beamsplitter, similarly to what is done in unbalanced homodyne detection. The rotation operation is essentially a phase shift and can in principle be implemented with a second cavity, but we will show that this operation is not strictly necessary for the scheme to work. The setup is sketched in Fig. 5.1.

The chapter is structured as follows: In Section 5.2, we establish the quantum Langevin equations used to analyze the feedback scheme, and we the equations are linearised. In Section 5.3, we solve the linearised quantum Langevin equations and derive expressions of the mechanical power spectral density and phonon number. In Section 5.4, we discuss some numerical results in the form of phonon numbers, including comparisons with the results in the previous chapters and discussions on which experimental parameter values are the most favourable. The chapter

is concluded in Section 5.5.

5.2 The theoretical model

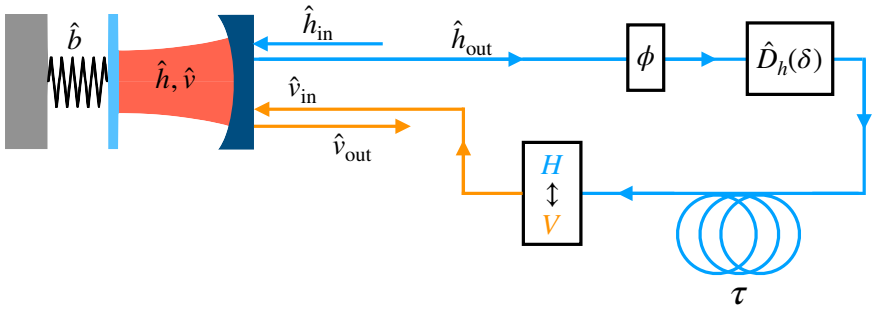

Figure 5.1: Sketch of the setup: A mechanical element represented by its annihilation operator $\hat{b}$ is interacting with horizontally and vertically polarized cavity fields with annihilation opeartors $\hat{h}$ and $\hat{v}$, respectively. the cavity is driven by an external horizontally polarized input field $\hat{h}_{\text{in}}$. The horizontal output field $\hat{h}_{\text{out}}$ is sent through a phase shift by an angle ϕ, a displacement operation $\hat{D}_h(\delta)$, a delay line of temporal length τ, and finally a half-wave plate converts the light to vertically polarized light. The resulting field $\hat{v}_{\text{in}}$ is then fed back into the cavity. The vertical output field $\hat{v}_{\text{out}}$ is not used in the analysis but is included in the sketch for the sake of completeness.

5.2.1 Langevin equations: Empty cavity

In order to fully appreciate the theoretical model of the direct feedback scheme, we consider first the setup in Fig. 5.1 except for an empty cavity without the mechanical element. We are dealing with horizontally and a vertically polarized cavity fields with annihilation operators $\hat{h}(t)$, and $\hat{v}(t)$, respectively. The cavity fields couple in and out of the cavity with rates κ_h and κ_v. $\hat{h}_{\text{in}}(t)$ represents the horizontal input field, with commutation relations $[\hat{h}_{\text{in}}(t), \hat{h}_{\text{in}}(t')] = 0$ and $[\hat{h}_{\text{in}}(t), \hat{h}^\dagger_{\text{in}}(t')] = \delta(t - t')$.

The input-output relations give us $\hat{h}_{\text{out}}(t) = -\hat{h}_{\text{in}}(t) + \sqrt{\kappa_h} h(t)$. On this output field, we apply a fixed rotation in phase space by the angle ϕ, followed by a displacement by the complex amplitude δ, followed by a delay line with a fixed delay of duration τ. In total, this gives us the transformation

$$\hat{h}_{\text{out}}(t) \to e^{-i\phi} \hat{h}_{\text{out}}(t - \tau) + \delta. \tag{5.2.1}$$

For notational convenience, we will introduce the time delay superoperator $T_{t'}$ defined by $T_{t'} \hat{A}(t) := \hat{A}(t - t')$, for any time-dependent operator $\hat{A}$ and delay time t'. Using this notation, the above transformation can be written as $\hat{h}_{\text{out}}(t) \to e^{-i\phi} T_\tau \hat{h}_{\text{out}}(t) + \delta$.

Finally, the output field is converted to a vertical polarization by sending it through a half-wave plate, and it is then fed into the cavity. This means that the vertical mode inside the cavity interacts with a vertical input field operator given by $\hat{v}_{\text{in}}(t) = e^{-i\phi} T_\tau \hat{h}_{\text{out}}(t) + \delta$.

With all of these considerations, the Langevin equations of the two cavity modes are:

$$\dot{\hat{h}} = -\frac{\kappa_h}{2}\hat{h} + \sqrt{\kappa_h}\hat{h}_{\text{in}} \tag{5.2.2}$$

$$\dot{\hat{v}} = -\frac{\kappa_v}{2}\hat{h} + \sqrt{\kappa_v}\delta + \sqrt{\kappa_v}e^{-i\phi}T_\tau(-\hat{h}_{\text{in}} + \sqrt{\kappa_h}\hat{h}) \tag{5.2.3}$$

Note that we have dropped the time argument in the above equations, e.g. we write $\hat{h}$ instead of $\hat{h}(t)$. This notation will be used repeatedly throughout this chapter.

It can be shown that the expected commutation relations of $h(t)$ and $v(t)$ are conserved over time. This is most straightforwardly done by showing that $[\hat{h}_{\text{out}}(t), \hat{h}_{\text{out}}(t')] = \delta(t-t')$. The model may be extended to include optical loss by performing the substitution $\sqrt{\kappa_h}h_{\text{in}}(t) \to \sqrt{\kappa_h^{\text{in}}}h_{\text{in}}(t) + \sqrt{\kappa_h^{\text{loss}}}h_{\text{loss}}(t)$, with $\kappa_h^{\text{in}} + \kappa_h^{\text{loss}} = \kappa_h$. Note that this modifies the input-output relation to $\hat{h}_{\text{out}}(t) = -\hat{h}_{\text{in}}(t) + \sqrt{\kappa_h}h(t) \to -\hat{h}_{\text{in}}(t) + \sqrt{\kappa_h^{\text{in}}}\hat{h}(t)$ [2].

5.2.2 Langevin equations: Cavity w. optomechanical coupling

We now insert a mechanical element into the cavity described in the previous section, with annihilation operator $\hat{b}$. Both the horizontally and the vertically polarized fields couple to the mechanics with vacuum coupling rates s_h and s_v, respectively. The system Hamiltonian (with driving terms absorbed into input operators) is now given by:

$$\begin{aligned}\hat{H} = \hbar\Omega_m\hat{b}^\dagger\hat{b} + \hbar\Delta_h\hat{h}^\dagger\hat{h} + \hbar s_h\hat{h}^\dagger\hat{h}(\hat{b}+\hat{b}^\dagger) \\ + \hbar\Delta_v\hat{v}^\dagger\hat{v} + \hbar s_v\hat{v}^\dagger\hat{v}(\hat{b}+\hat{b}^\dagger),\end{aligned} \tag{5.2.4}$$

where Δ_h and Δ_v are the detunings of the cavity fields with respect to the laser fequency. We model mechanical losses by letting the mechanical oscillator interact with a thermal environment in a Markovian non-rotating wave approximation with damping rate Γ_m and thermal phonon number $\bar{n}$. The system thus evolves according to the following quantum Langevin equations:

$$\dot{\hat{Q}} = \Omega_m\hat{P} \tag{5.2.5}$$

$$\dot{\hat{P}} = -\Omega_m\hat{Q} - \sqrt{2}s_h\hat{h}^\dagger\hat{h} - \sqrt{2}s_h\hat{v}^\dagger\hat{v} - \Gamma_m\hat{P} + \sqrt{2\Gamma_m}\hat{P}_{\text{in}} \tag{5.2.6}$$

$$\dot{\hat{h}} = -i\Delta_h\hat{h} - i\sqrt{2}s_h\hat{Q}\hat{h} - \frac{\kappa_h}{2}\hat{h} + \sqrt{\kappa_h^{\text{in}}}\hat{h}_{\text{in}} + \sqrt{\kappa_h^{\text{loss}}}\hat{h}_{\text{loss}} \tag{5.2.7}$$

$$\dot{\hat{v}} = -i\Delta_v\hat{v} - i\sqrt{2}s_v\hat{Q}\hat{v} - \frac{\kappa_h}{2}\hat{v} + \sqrt{\kappa_v^{\text{in}}}e^{-i\phi}T_\tau\left(\hat{h}_{\text{in}} - \sqrt{\kappa_h^{\text{in}}}\hat{h}\right) + \sqrt{\kappa_v^{\text{in}}}\delta + \sqrt{\kappa_h^{\text{loss}}}\hat{v}_{\text{loss}} \tag{5.2.8}$$

5.2.3 Linearising the model

Having established the quantum Langevin equations of the full model, we move on to linearise the equations to simplify the calculations. We will restrict the analysis to steady-state dynamics, as this is sufficient for the purpose of mechanical cooling.
The first step in the linearisation procedure is to consider the equations for the expectation values $\langle Q\rangle$, $\langle P\rangle$, $\langle h\rangle$, $\langle v\rangle$:

$$\langle \dot{Q} \rangle = \Omega_m \langle P \rangle \tag{5.2.9}$$

$$\langle \dot{P} \rangle = -\Omega_m \langle Q \rangle - \sqrt{2} s_h \langle h^\dagger h \rangle - \sqrt{2} s_v \langle v^\dagger v \rangle - \Gamma_m \langle P \rangle \tag{5.2.10}$$

$$\langle \dot{h} \rangle = -i\Delta_h \langle h \rangle - i\sqrt{2} s_h \langle Qh \rangle - \frac{\kappa_h}{2} \langle h \rangle + \sqrt{\kappa_h^{\text{in}}} \langle h_{\text{in}} \rangle \tag{5.2.11}$$

$$\langle \dot{v} \rangle = -i\Delta_v \langle v \rangle - i\sqrt{2} s_v \langle Qv \rangle - \frac{\kappa_h}{2} \langle v \rangle + \sqrt{\kappa_v^{\text{in}}} e^{-i\phi} \left(\langle T_\tau h_{\text{in}} \rangle - \sqrt{\kappa_h^{\text{in}}} \langle T_\tau h \rangle \right) + \sqrt{\kappa_v^{\text{in}}} \delta \tag{5.2.12}$$

We have used $\langle P_{\text{in}} \rangle = \langle h_{\text{loss}} \rangle = \langle v_{\text{loss}} \rangle = 0$. We linearize the dynamics by reducing second order moments in the above equation. For the second order moment $\langle Qh \rangle$, we have that

$$\begin{aligned} \langle Qh \rangle &= \langle (\langle Q \rangle + \delta Q)(\langle h \rangle + \delta h) \rangle \\ &= \langle Q \rangle \langle h \rangle + \langle Q \rangle \langle \delta h \rangle + \langle \delta Q \rangle \langle h \rangle + \langle \delta Q \delta h \rangle \\ &= \langle Q \rangle \langle h \rangle + \langle \delta Q \delta h \rangle , \end{aligned} \tag{5.2.13}$$

where we have introduced the notation $\delta \hat{A} := \hat{A} - \langle A \rangle$ for any operator $\hat{A}$. In the differential equations for the first moments, we now perform the approximation

$$\langle Qh \rangle \approx \langle Q \rangle \langle h \rangle , \tag{5.2.14}$$

under the assumption that the term $\langle \delta Q \delta h \rangle$ will have a negligible effect on the dynamics. This is known as the linearisation approximation, and is broadly valid when $|\langle h \rangle| \gg 1$. We perform similar approximations of the terms $\langle h^\dagger h \rangle$, $\langle v^\dagger v \rangle$, and $\langle Qv \rangle$.
We assume that constant, steady-state solutions to Eq. (5.2.9) exists. Such solutions will satisfy the relations $\langle \dot{Q} \rangle = \langle \dot{P} \rangle = \langle \dot{h} \rangle = \langle \dot{v} \rangle = 0$, and also $\langle T_\tau h_{\text{in}} \rangle = \langle h_{\text{in}} \rangle$ and $\langle T_\tau h \rangle = \langle h \rangle$. This gives us the steady-state equations

$$0 = \Omega_m \langle P \rangle \tag{5.2.15}$$

$$0 = -\Omega_m \langle Q \rangle - \Gamma_m \langle P \rangle - \sqrt{2} s_h |\langle h \rangle|^2 - \sqrt{2} s_v |\langle v \rangle|^2 \tag{5.2.16}$$

$$0 = -i\Delta_h^{\text{eff}} \langle h \rangle - \frac{\kappa_h}{2} \langle h \rangle + \sqrt{\kappa_h^{\text{in}}} \langle h_{\text{in}} \rangle \tag{5.2.17}$$

$$0 = -i\Delta_v^{\text{eff}} \langle v \rangle - \frac{\kappa_h}{2} \langle v \rangle + \sqrt{\kappa_v^{\text{in}}} e^{-i\phi} \left[\langle h_{\text{in}} \rangle - \sqrt{\kappa_h^{\text{in}}} \langle h \rangle \right] + \sqrt{\kappa_v^{\text{in}}} \delta, \tag{5.2.18}$$

where we have introduced the definitions

$$\Delta_h^{\text{eff}} := \Delta_h + \sqrt{2} s_h \langle Q \rangle \tag{5.2.19}$$

$$\Delta_v^{\text{eff}} := \Delta_v + \sqrt{2} s_v \langle Q \rangle . \tag{5.2.20}$$

$$\tag{5.2.21}$$

Furthermore, for this coherent feedback scheme, we wish to drive the two input beams on resonance, thereby setting $\Delta_h^{\text{eff}} = \Delta_v^{\text{eff}} = 0$. In this case, the steady-state solutions are:

$$\langle h\rangle = \frac{2\sqrt{\kappa_h^{\text{in}}}}{\kappa_h}\langle h_{\text{in}}\rangle \tag{5.2.22}$$

$$\langle v\rangle = \frac{2\sqrt{\kappa_v^{\text{in}}}}{\kappa_v}\left[\delta + e^{-i\phi}\left(1-\frac{2\kappa_h^{\text{in}}}{\kappa_h}\right)\langle h_{\text{in}}\rangle\right] \tag{5.2.23}$$

$$\langle Q\rangle = \frac{\sqrt{2}}{\Omega_m}\left(s_h|\langle h\rangle|^2 + s_v|\langle v\rangle|^2\right) \tag{5.2.24}$$

$$\langle P\rangle = 0 \tag{5.2.25}$$

We also introduce the effective coupling strengths:

$$g_h := s_h\langle h\rangle \tag{5.2.26}$$

$$g_v := s_v\langle v\rangle \tag{5.2.27}$$

$$\tag{5.2.28}$$

We furthermore choose the drive strength $\langle h_{\text{in}}\rangle$ to be a real number, in which case $\langle h\rangle$ and thus g_h will be real as well. On the other hand, we will allow g_v to be complex and write it as

$$g_v = |g_v|e^{ix}, \tag{5.2.29}$$

where $x = \arg(g_v)$. Note that the value of g_v is fully controlled by the displacement term δ.

We are now in a position to give equations for the fluctuation terms. In a similar fashion to earlier, we make linearisation approximations on second order fluctuation terms:

$$\begin{aligned}\delta(\hat{Q}\hat{h}) &:= \hat{Q}\hat{h} - \langle Qh\rangle \\ &= \delta\hat{Q}\langle h\rangle + \langle Q\rangle\delta\hat{h} + \delta\hat{Q}\delta\hat{h} - \langle\delta Q\delta h\rangle \\ &\approx \delta\hat{Q}\langle h\rangle + \langle Q\rangle\delta\hat{h}\end{aligned} \tag{5.2.30}$$

and similar for $\delta(\hat{Q}\hat{v}), \delta(\hat{h}^\dagger\hat{h})$, and $\delta(\hat{v}^\dagger\hat{v})$. This finally gives us the following set of equations:

$$\dot{\delta\hat{Q}} = \Omega_m\delta\hat{P} \tag{5.2.31}$$

$$\dot{\delta\hat{P}} = -\Omega_m\delta\hat{Q} - \Gamma_m\delta\hat{P} - \sqrt{2}g_h(\delta\hat{h} + \delta\hat{h}^\dagger) - \sqrt{2}|g_v|(e^{-ix}\delta\hat{v} + e^{ix}\delta\hat{v}^\dagger) + \sqrt{2\Gamma_m}\hat{P}_{\text{in}} \tag{5.2.32}$$

$$\dot{\delta\hat{h}} = -i\sqrt{2}g_h\delta\hat{Q} - \frac{\kappa_h}{2}\delta\hat{h} + \sqrt{\kappa_h^{\text{in}}}\delta\hat{h}_{\text{in}} + \sqrt{\kappa_h^{\text{loss}}}\delta\hat{h}_{\text{loss}} \tag{5.2.33}$$

$$\dot{\delta\hat{v}} = -i\sqrt{2}g_v\delta Q - \frac{\kappa_v}{2}\delta\hat{v} + \sqrt{\kappa_v^{\text{loss}}}\delta\hat{v}_{\text{loss}} + \sqrt{\kappa_v^{\text{in}}}e^{-i\phi}T_\tau(\delta\hat{h}_{\text{in}} - \sqrt{\kappa_h^{\text{in}}}\delta\hat{h}) \tag{5.2.34}$$

The linearisation of the model is now complete. The set of equations above are referred to as the linearised quantum Langevin equations.

5.3 Solving the linearised Langevin equations

We will now solve for the fluctuation terms $\delta\hat{Q}, \delta\hat{P}, \delta\hat{h}, \delta\hat{v}$, which we from here on in this section will denote simply as $\hat{Q}, \hat{P}$, etc. We also work with dimensionless parameters by redefining all

rates to be given in units of Ω_m. For example, we replace Ω_m by 1 and Γ_m by $\tilde{\Gamma}_m = \Gamma_m/\Omega_m$, and subsequently drop the tilde. Since the input field operators $\hat{h}_{\rm in}$, $\hat{h}_{\rm loss}$ and $v_{\rm loss}$ have units $\sqrt{\rm Hz}$, these are normalized by diving by $\sqrt{\Omega_m}$. We also introduce quadrature operators of the optical fields. With $a \in \{h, v\}$ below, we define:

$$\hat{X}_a = \frac{1}{\sqrt{2}}(\hat{a} + \hat{a}^\dagger), \qquad \hat{Y}_a = \frac{1}{i\sqrt{2}}(\hat{a} - \hat{a}^\dagger) \tag{5.3.1}$$

$$\hat{X}_a^{\rm in} = \frac{1}{\sqrt{2}}(\hat{a}_{\rm in} + \hat{a}_{\rm in}^\dagger), \qquad \hat{Y}_a^{\rm in} = \frac{1}{i\sqrt{2}}(\hat{a}_{\rm in} - \hat{a}_{\rm loss}^\dagger) \tag{5.3.2}$$

$$\hat{X}_a^{\rm in} = \frac{1}{\sqrt{2}}(\hat{a}_{\rm loss} + \hat{a}_{\rm loss}^\dagger), \qquad \hat{Y}_a^{\rm loss} = \frac{1}{i\sqrt{2}}(\hat{a}_{\rm loss} - \hat{a}_{\rm loss}^\dagger) \tag{5.3.3}$$

We Fourier transform with the convention $f(\omega) = \int_{-\infty}^{\infty} f(t)e^{i\omega t}dt$ the equations of the fluctuation terms to get the following:

$$-i\omega\hat{\mathbf{X}}(\omega) = \mathbf{A}(\omega)\hat{\mathbf{X}}(\omega) + \hat{\mathbf{b}}(\omega) \tag{5.3.4}$$

with

$$\hat{\mathbf{X}}(\omega) = \begin{bmatrix} \hat{Q}(\omega) \\ \hat{P}(\omega) \\ \hat{X}_h(\omega) \\ \hat{Y}_h(\omega) \\ \hat{X}_v(\omega) \\ \hat{Y}_v(\omega) \end{bmatrix}, \quad \hat{\mathbf{b}}(\omega) = \begin{bmatrix} 0 \\ \sqrt{2\Gamma_m}\hat{P}_{\rm in}(\omega) \\ \sqrt{\kappa_h^{\rm in}}\hat{X}_h^{\rm in}(\omega) + \sqrt{\kappa_h^{\rm loss}}\hat{X}_h^{\rm loss}(\omega) \\ \sqrt{\kappa_h^{\rm in}}\hat{Y}_h^{\rm in}(\omega) + \sqrt{\kappa_h^{\rm loss}}\hat{Y}_h^{\rm loss}(\omega) \\ \sqrt{\kappa_v^{\rm loss}}\hat{X}_v^{\rm loss}(\omega) + \sqrt{\kappa_v^{\rm in}}e^{i\tau\omega}(\hat{X}_h^{\rm in}(\omega)\cos(\phi)) + \hat{Y}_h^{\rm in}(\omega)\sin(\phi)) \\ \sqrt{\kappa_v^{\rm loss}}\hat{Y}_v^{\rm loss}(\omega) + \sqrt{\kappa_v^{\rm in}}e^{i\tau\omega}(-\hat{X}_h^{\rm in}(\omega)\sin(\phi) + \hat{Y}_h^{\rm in}(\omega)\cos(\phi)) \end{bmatrix} \tag{5.3.5}$$

$$\mathbf{A}(\omega) = \begin{bmatrix} 0 & 1 & 0 & 0 & 0 & 0 \\ -1 & -\Gamma_m & -2g_h & 0 & -2|g_v|\cos(x) & -2|g_v|\sin(x) \\ 0 & 0 & -\frac{\kappa_h}{2} & 0 & 0 & 0 \\ -2g_h & 0 & 0 & -\frac{\kappa_h}{2} & 0 & 0 \\ 2|g_v|\sin(x) & 0 & -\sqrt{\kappa_h^{\rm in}\kappa_v^{\rm in}}\cos(\phi)e^{i\tau\omega} & -\sqrt{\kappa_h^{\rm in}\kappa_v^{\rm in}}\sin(\phi)e^{i\tau\omega} & -\frac{\kappa_v}{2} & 0 \\ -2|g_v|\cos(x) & 0 & \sqrt{\kappa_h^{\rm in}\kappa_v^{\rm in}}\sin(\phi)e^{i\tau\omega} & -\sqrt{\kappa_h^{\rm in}\kappa_v^{\rm in}}\cos(\phi)e^{i\tau\omega} & 0 & -\frac{\kappa_v}{2} \end{bmatrix} \tag{5.3.6}$$

The solution is $\hat{\mathbf{X}}(\omega) = -(\mathbf{A}(\omega) + i\omega\mathbf{I})^{-1}\hat{\mathbf{b}}(\omega)$, where $\mathbf{I}$ denotes the identity matrix. In particular, we find that

$$\hat{Q}(\omega) = \chi(\omega)\hat{\xi}(\omega) \underbrace{\begin{bmatrix} -\sqrt{2\Gamma_m}(\kappa_h/2 - i\omega)(\kappa_v/2 - i\omega) \\ g_h\sqrt{\kappa_h^{\text{in}}}(\kappa_v - 2i\omega) + |g_v|\sqrt{\kappa_v^{\text{in}}}e^{i\tau\omega}(\kappa_h - 2\kappa_h^{\text{in}} - 2i\omega)\cos(x+\phi) \\ |g_v|\sqrt{\kappa_v^{\text{in}}}e^{i\tau\omega}(\kappa_h - 2\kappa_h^{\text{in}} - 2i\omega))\sin(x+\phi) \\ g_h\sqrt{\kappa_h^{\text{loss}}}(\kappa_v - 2i\omega) - 2|g_v|e^{i\tau\omega}\sqrt{\kappa_h^{\text{in}}\kappa_h^{\text{loss}}\kappa_v^{\text{in}}}\cos(x+\phi) \\ -2|g_v|e^{i\tau\omega}\sqrt{\kappa_h^{\text{in}}\kappa_h^{\text{loss}}\kappa_v^{\text{in}}}\sin(x+\phi) \\ |g_v|\sqrt{\kappa_v^{\text{loss}}}(\kappa_h - 2i\omega)\cos(x) \\ |g_v|\sqrt{\kappa_v^{\text{loss}}}(\kappa_h - 2i\omega)\sin(x) \end{bmatrix}}_{=:\mathbf{T}(\omega)}, \tag{5.3.7}$$

with

$$\hat{\xi}(\omega) := \begin{bmatrix} \hat{P}_{\text{in}}(\omega) & \hat{X}_h^{\text{in}}(\omega) & \hat{Y}_h^{\text{in}}(\omega) & \hat{X}_h^{\text{loss}}(\omega) & \hat{Y}_h^{\text{loss}}(\omega) & \hat{X}_v^{\text{loss}}(\omega) & \hat{Y}_v^{\text{loss}}(\omega) \end{bmatrix}, \tag{5.3.8}$$

and

$$[\chi(\omega)]^{-1} := \left(i\Gamma_m\omega + \omega^2 - 1\right)\left(\frac{\kappa_h}{2} - i\omega\right)\left(\frac{\kappa_v}{2} - i\omega\right) - 4g_h|g_v|\sqrt{\kappa_h^{\text{in}}\kappa_v^{\text{in}}}e^{i\tau\omega}\sin(x+\phi). \tag{5.3.9}$$

The stability of the system is determined by the poles of the system susceptibility function $\chi(\omega)$. Namely, in order for the system to be asymptotically stable, all poles, i.e. all ω_p such that $[\chi(\omega_p)]^{-1} = 0$ must satisfy the criterion $\text{Im}(\omega_p) < 0$. [1]

The elements of the input noise vector $\hat{\xi}(\omega)$ are delta-correlated: For a mechanical thermal environment with average phonon number $\bar{n}$ and vaccuum or coherent input fields, they satisfy the following relations [2]:

$$\langle[\xi(\omega)]^T\xi(\omega')\rangle = \underbrace{\begin{bmatrix} \bar{n}+1/2 & 0 & 0 & 0 & 0 & 0 & 0 \\ 0 & 1/2 & i/2 & 0 & 0 & 0 & 0 \\ 0 & -i/2 & 1/2 & 0 & 0 & 0 & 0 \\ 0 & 0 & 0 & 1/2 & i/2 & 0 & 0 \\ 0 & 0 & 0 & -i/2 & 1/2 & 0 & 0 \\ 0 & 0 & 0 & 0 & 0 & 1/2 & i/2 \\ 0 & 0 & 0 & 0 & 0 & -i/2 & 1/2 \end{bmatrix}}_{=:\mathbf{M}_\xi} 2\pi\delta(\omega+\omega') \tag{5.3.10}$$

From Eq. (5.3.7), and the above relations, we find the power spectral density

$$\begin{aligned} S_{QQ}(\omega) &= \int_{-\infty}^{\infty}\langle Q(t)Q(0)\rangle\, e^{i\omega t}dt = \frac{1}{2\pi}\int_{-\infty}^{\infty}\langle Q(\omega)Q(\omega')\rangle\, d\omega' \\ &= \chi(\omega)\chi(-\omega)[\mathbf{T}(\omega)]^T\mathbf{M}_\xi\mathbf{T}(-\omega) \end{aligned} \tag{5.3.11}$$

[1] Traditionally, the stability criterion is formulated in terms of the Laplace transform of the transfer function: A linear, causal, time-invariant input $X(t)$ and output $Y(t) = \int_{-\infty}^{\infty} h(\tau)X(t-\tau)d\tau$ is defined to be asymptotically (or BIBO) stable when every bounded input $X(t)$ gives rise to a bounded output $Y(t)$. This is the case if and only if the Laplace transform $\mathcal{L}h(s) = \int_0^\infty h(t)e^{-st}dt$ of $h(t)$ only has poles s_p s.t. $\text{Re}(s_p) < 0$ [68]. Note that since h is causal, i.e. $h(t) = 0$ for $t < 0$, the lower bound of the integral can be extended to $-\infty$ instead of 0. We therefore have that its Fourier transform is related to the Laplace transform by $\mathcal{F}h(\omega) = \int_{-\infty}^{\infty} h(t)e^{i\omega t}dt = \mathcal{L}h(-i\omega)$. Hence the stability condition $\text{Im}(\omega_p) < 0$ for all poles ω_p of $\mathcal{F}h$.

The full expression of $S_{QQ}(\omega)$ is fairly long and wont be written out in full here; it may instead be found in the appendix in Section 5.6. It is however important to point out that one observes that the angles x and ϕ appear only as the sum $x+\phi$ in the expression of $S_{QQ}(\omega)$. This means that it is not necessary to do both a displacement and a rotation of the horizontal output field before it is fed back into the cavity. As we will argue at the end of this section and later show numerically, it is generally favourable to set $x+\phi = -\pi/2$, and this is likely most easily accomplished experimentally by not doing a rotation, thereby setting $\phi = 0$ and then choosing the displacement δ such that $x = -\pi/2$. On the other hand, if ϕ can be varied, it may be favourable to optimize x and ϕ such as to maximize the vertical coupling strength g_v given by eqs. (5.2.23) and (5.2.27). We will however not explore this further.

Having obtained an expression of $S_{QQ}(\omega)$, we are now in a position to find the steady-state mechanical phonon number. From the equation $-i\omega Q(\omega) = P(\omega)$, one finds that the momentum power spectral density is $S_{PP}(\omega) = \omega^2 S_{QQ}(\omega)$. From this, we find the steady-state mechanical phonon number by performing the inverse Fourier transforms of the power spectral densities:

$$\begin{aligned} n &= \frac{1}{2}(\langle Q^2\rangle + \langle P^2\rangle) - \frac{1}{2} \\ &= \frac{1}{4\pi}\int_{-\infty}^{\infty}(1+\omega^2)S_{QQ}(\omega)d\omega - \frac{1}{2} \end{aligned} \tag{5.3.12}$$

For a system with time delays such as in our case, the above integral is difficult if not impossible to evaluate analytically. It can however be evaluated numerically.

We conclude this section by giving some intuition for why it is favourable to set $x+\phi = -\pi/2$ in most cases. The main reason is that it results in the negative feedback force in the momentum quadrature that we want, which we will argue in the following. We will for simplicity assume that $\phi = 0$ as well as the bad cavity limit $\kappa_h \gg 1$ (recall that we use normalized units). We then have that

$$\dot{\hat{Y}}_h = -2g_h\hat{Q} - \frac{\kappa_h}{2}\hat{Y}_h + \sqrt{\kappa_h^{\text{in}}}\hat{Y}_h^{\text{in}}. \tag{5.3.13}$$

In an adiabatic approximation, we then find that

$$\hat{Y}_h(t) \simeq -\frac{4g_h}{\kappa_h}Q(t) + \frac{2\sqrt{\kappa_h^{\text{in}}}}{\kappa_h}\hat{Y}_h^{\text{in}}(t). \tag{5.3.14}$$

Consider the evolution of the position quadrature $\hat{Q}(t)$ after the period $\tau = \pi/2$, a quarter mechanical period. If we consider only the harmonic oscillations and neglect damping and optomechanical coupling, we have that $Q(t-\tau) = Q(t-\pi/2) \simeq P(t)$. Thus,

$$\hat{Y}_h(t-\tau) \simeq \frac{4g_h}{\kappa_h}\hat{P}(t) + (\text{noise terms}), \tag{5.3.15}$$

where 'noise terms' encompasses everything that is not directly proportional to $P(t)$ or $Q(t)$ or is irrelevant in the short term. We will keep accumulating irrelevant terms into this expression as this derivation continues. When $\phi = 0$, the $\hat{Y}_v(t)$ quadrature carries the information about $\hat{Y}_h(t-\tau)$, while the $\hat{X}_v$ quadrature does not. We have

$$\dot{\hat{Y}}_v(t) = -2|g_v|\cos(x)\hat{Q}(t) - \sqrt{\kappa_h^{\text{in}}\kappa_v^{\text{in}}}\hat{Y}_h(t-\tau) - \frac{\kappa_v}{2}\hat{Y}_v(t) + \sqrt{\kappa_v^{\text{loss}}}\hat{Y}_v^{\text{loss}}(t) + \sqrt{\kappa_v^{\text{in}}}\hat{Y}_h^{\text{in}}(t-\tau) \quad (5.3.16)$$

Again, using an adiabatic approximation and substituting the approximate expression for $Y_h(t-\tau)$, we find that

$$\hat{Y}_v(t) \simeq -\frac{4|g_v|\cos(x)}{\kappa_v}\hat{Q}(t) - \frac{8\sqrt{\kappa_h^{\text{in}}\kappa_v^{\text{in}}}g_h}{\kappa_h\kappa_v}\hat{P}(t) + (\text{noise terms}). \quad (5.3.17)$$

We are finally in a position to evaluate the feedback force $\hat{F}_{\text{fb}}(t)$ on the momentum, namely

$$\begin{aligned}\hat{F}_{\text{fb}}(t) &= -2|g_v|\left(\cos(x)\hat{X}_v(t) + \sin(x)\hat{Y}_v(t)\right) \\ &\simeq -2|g_v|\cos(x)\hat{X}_v(t) + \frac{8|g_v|^2\cos(x)\sin(x)}{\kappa_v}\hat{Q}(t) + \frac{16\sqrt{\kappa_h^{\text{in}}\kappa_v^{\text{in}}}g_h|gv|\sin(x)}{\kappa_h\kappa_v}\hat{P}(t) + (\text{noise terms})\end{aligned} \quad (5.3.18)$$

In order for F_{fb} to provide a negative feedback force, the coefficient in front of $P(t)$ must be negative and preferably as large as possible. It is clear that $x = -\pi/2$ achieves this goal, while also eliminating other unwanted contributions to the feedback force.

5.4 Numerical results

In this section, we discuss the behavior of the phonon number by numerically evaluating the integral in Eq. (5.3.12). This is done in Mathematica using the built-in function `NIntegrate`. Note that as $S_{QQ}(\omega)$ is sharply peaked at the points $\omega/\Omega_m \in \{-1, 1\}$, care must be taken to make sure that the numerical algorithm's integration mesh is fine enough around these point in order to get a trustworthy value. Throughout this section, we will keep the following parameters constant unless explicitly stated otherwise:

$$\begin{gathered}\Omega_m = 10^6 \text{ Hz}, \;\; Q_m = 10^8, \;\; T = 300 \text{ K}, \;\; \bar{n} = \{\exp[\hbar\Omega_m/(k_{\text{B}}T)] - 1\}^{-1} = 3.93 \cdot 10^7, \\ \kappa_h = \kappa_v = \kappa_h^{\text{in}} = \kappa_v^{\text{in}} = 100\Omega_m, \;\; \kappa_h^{\text{loss}} = \kappa_v^{\text{loss}} = 0, \\ g_h = 10^{-2}\Omega_m, \;\; |g_v| = 10^{-2}\Omega_m, \\ x + \phi = -\frac{\pi}{2}, \;\; \tau = \frac{\pi}{2\Omega_m}\end{gathered} \quad (5.4.1)$$

The parameters are chosen so as to compare with the performance of the measurement-based feedback schemes discussed in earlier chapters. Notice that in this section, we no longer work with dimensionless parameters (unless explicitly stated so).

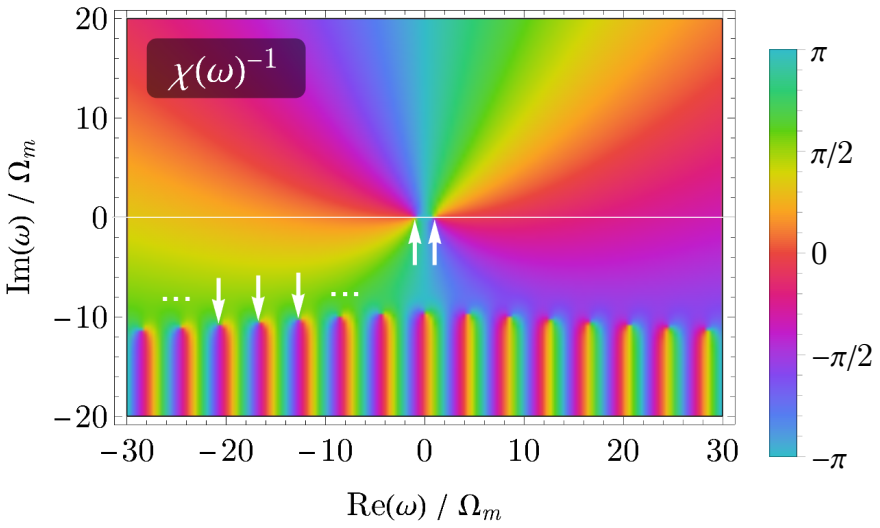

Figure 5.2: Plot of $[\chi(\omega)]^{-1}$ in the complex plane. The colors denote the complex phase of $[\chi(\omega)]^{-1}$ according to the scale on the right. Since $[\chi(\omega)]^{-1}$ is a holomorphic function, zeros of $[\chi(\omega)]^{-1}$ are identified as points where any circle drawn around them hits all colors on the scale. The white arrows show the location of some of these points. The white ellipses next to the arrows indicate that the zeros extends infinitely in both directions. The white horizontal line indicate $\mathrm{Im}(\omega) = 0$, below which all zeros must lie in order for the system to be stable. Parameters used for this plot are given in Eq. (5.4.1).

Until now, we have not considered for what parameters the system is stable. As previously stated, the system is stable when all zeros of $[\chi(\omega)]^{-1}$ have negative imaginary parts. In Fig. 5.2, $[\chi(\omega)]^{-1}$ is plotted in a section of complex ω-space. The figure shows that for this set of parameters, all zeros satisfy $\mathrm{Im}(\omega) < 0$, indicating that the system is stable. Note that the two roots close to the origin are numerically found to be at $\omega_\pm/\Omega_m = \pm 1 - 8.00 \cdot 10^{-6} i$. There are seemingly infinitely many roots below these two points, as indicated in the figure, which is to be expected for a time-delay system [68]. While we have not been able to prove that none of these roots ever cross the $\mathrm{Im}(\omega) = 0$ line, we generally observe that the roots decrease downwards as $|\mathrm{Re}(\omega)|$ increases. We also have not observed any other roots above the $\mathrm{Im}(\omega) = 0$ line for these parameters. Before we move on, we remark that if $x + \phi \in [0, \pi]$, we observe that the two roots near the origin have positive real part, rendering the system unstable. We also observe that if either g_h or g_v is increased, the 'pillars' and their roots at the bottom of the plot move upwards near the $\mathrm{Im}(\omega) = 0$ line. We generally find that at a certain threshold value of g_h or g_v, a root with $\mathrm{Re}(\omega) = 0$ will be the first to cross the line, rendering the system unstable. In other words, the system becomes unstable when the coupling strengths are sufficiently high. This point may be identified exactly by solving the equation

$$[\chi(0)]^{-1} = -\frac{\kappa_h \kappa_v}{2} - 4 g_h |g_v| \sqrt{\kappa_h^{\mathrm{in}} \kappa_v^{\mathrm{in}}} \sin(x + \phi) = 0 \tag{5.4.2}$$

with respect to g_h or $|g_v|$. Note that the parameters are normalized in units of Ω_m in the equation above.
To conclude the stability discussion, we have found that roots that violate the stability condition

typically appear first near $\omega = \pm\Omega_m$ or $\omega = 0$. In other words, looking for roots near these three values of ω should be a sufficient test of stability in most cases.

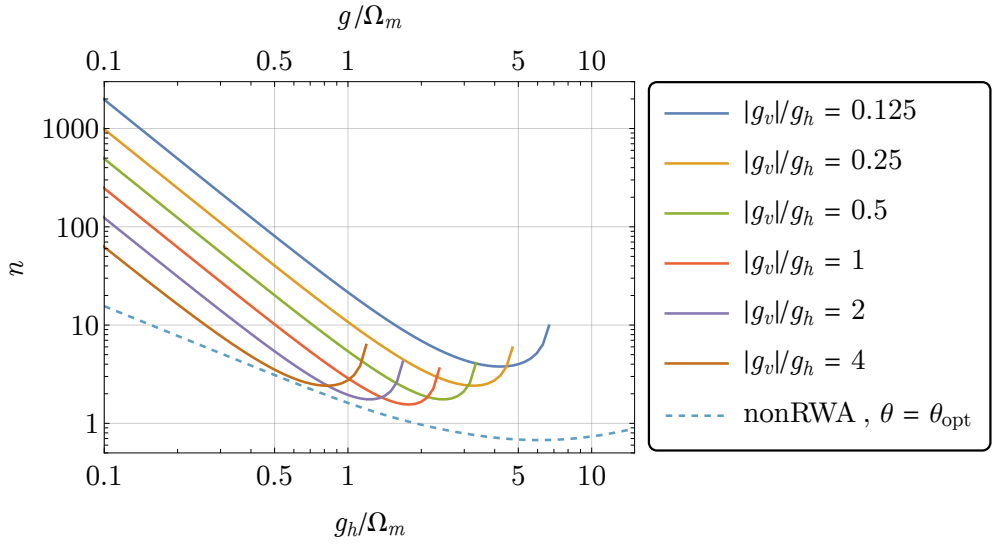

Figure 5.3: Mechanical phonon number n vs g_h for a range of values of $|g_v|/g_h$. The dashed curve is the unconditional phonon number vs g using the measurement-based feedback scheme described in Chapter 3 using the nonRWA model with $\theta = \theta_{\text{opt}}$. the Each of the solid curves ends to the right just before their point of instability. Parameters used for this plot are given in Eq. (5.4.1) except for g_h and $|g_v|$.

We now turn our attention towards the dependence of n on the coupling strengths g_h and $|g_v|$. Although $|g_v|$ may be controlled somewhat independently of g_h by tuning the displacement term δ (see Eq. (5.2.23)), we still expect these two parameters to be roughly proportional in an experimental setting. We therefore plot n versus g_h for a selection of values of $|g_v|/g_h$ in Fig. 5.3. For comparison, Fig. 5.3 also includes the unconditional phonon number vs g using the measurement-based feedback scheme described in Chapter 3 using the nonRWA model with $\theta = \theta_{\text{opt}}$. One observes from the plot that, as usual, n decreases versus g_h until it reaches a minimum, after which it increases again until an instability point is reached shortly after. One also observes from the figure that n decreases with $|g_v|/g_h$, but this parameter reaches an optimal value as well. One may think of the parameter $|g_v|/g_h$ as the feedback strength, as it characterizes the strength of the feedback force from the vertically polarized field relative to the probe of the horizontally polarized field. Thus, in some sense, the observed behavior is contrasting the measurement-based scheme using optimal control, where one can increase the feedback strength and/or the coupling strength arbitrarily without reaching instabilities.
From numerical optimization, the minimal value of n with respect to g_h and $|g_v|$ is $n = 1.55$ at $g_h = |g_v| = 1.78\Omega_m$. The fact that $g_h = |g_v|$ is optimal is not a coincidence, but may be shown analytically from the expression of $S_{QQ}(\omega)$ for the specific choice of parameters $\kappa_h = \kappa_v = \kappa_h^{\text{in}} = \kappa_v^{\text{in}}$, and $\kappa_h^{\text{loss}} = \kappa_v^{\text{loss}} = 0$. For comparison, the measurement-based model reaches a minimum of $n = 0.676$ at $g/\Omega_m = 6.19$, a reduction of the optimal n by a little over 50%.

From Fig. 5.3, it is evident that, although it comes close, the coherent feedback cooling scheme is not as effective as the measurement-based cooling scheme. On one hand, it is disappointing

that carrying coherent information about the system in the feedback beam does not provide an advantage compared to carrying measurement information. On the other hand, in some sense, it is not surprising that the performance of the coherent scheme is worse since as mentioned in the introduction to this chapter, the 'filtering' of the probe beam is not as sophisticated as with the measurement-based scheme. All this being said, it must be mentioned that we have not explored the effect of introducing optical losses into the models (e.g. setting $\kappa_h^{\text{in}} < \kappa_h$ and $\kappa_h^{\text{loss}} > 0$). It might be that the coherent feedback scheme outperforms the measurement-based scheme in this case.

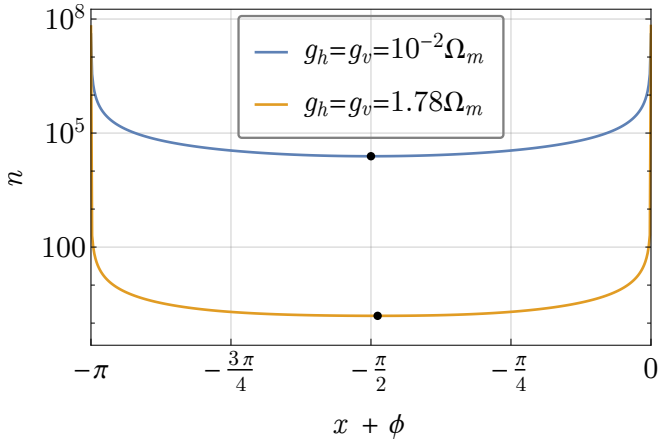

Figure 5.4: Mechanical phonon number n vs $x+\phi$ for the coupling strengths $g_h = |g_v| = 10^{-2}\Omega_m$ and $g_h = |g_v| = 1.78\Omega_m$, the latter of which is the optimal value of the pair $(g_h, |g_v|)$ for this set of parameters. The black dots indicate minimal values of n w.r.t $x + \phi$, which are located at $(x + \phi, n) = (-1.57, 2.46 \cdot 10^4)$ and $(x + \phi, n) = (-1.53, 1.55)$ for $g_h = |g_v| = 10^{-2}\Omega_m$ and $1.78\Omega_m$, respectively. Parameters used for this plot are given in Eq. (5.4.1) except for g_h, g_v, and $x + \phi$.

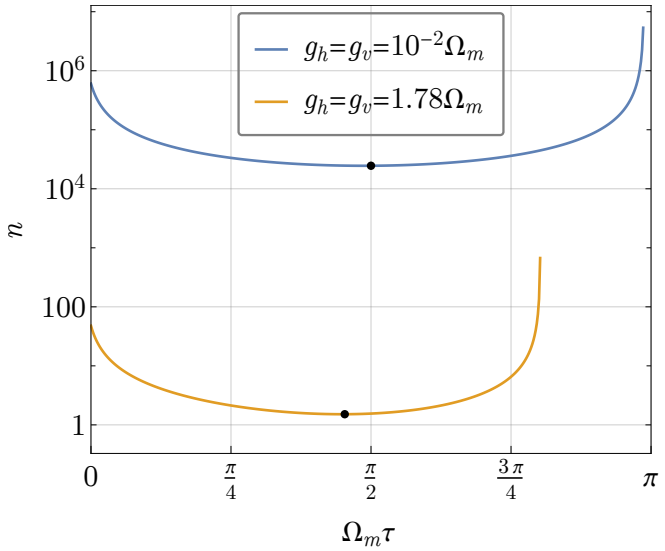

Figure 5.5: Mechanical phonon number n vs τ for the coupling strengths $g_h = |g_v| = 10^{-2}\Omega_m$ and $g_h = |g_v| = 1.78\Omega_m$, the latter of which is the optimal value of the pair $(g_h, |g_v|)$ for this set of parameters. Each of the solid curves ends to the right just before their point of instability. The black dots indicate minimal values of n w.r.t τ, which are located at $(\tau, n) = (1.57, 2.46 \cdot 10^4)$ and $(\tau, n) = (1.42, 1.51)$ for $g_h = |g_v| = 10^{-2}\Omega_m$ and $1.78\Omega_m$, respectively. Parameters used for this plot are given in Eq. (5.4.1) except for g_h, g_v, and τ.

Finally, we consider whether it is worth optimizing the parameters x, the argument of g_v and τ, the delay time.
Fig. 5.4 shows n versus $x + \phi$ for a selection of coupling strengths. For $g_h = |g_v| = 10^{-2}\Omega_m$, $x + \phi = -\pi/2$ is exactly the optimal value for minimizing n, while for $g_h = |g_v| = 1.78\Omega_m$, $x+\phi = -1.53$ is optimal, slightly to the left - although the minimal phonon number is unchanged at 1.55 within 3 significant digits from $x + \phi = -\pi/2$. In summary, It is clear from Fig. 5.4 that n is not very sensitive to $x + \phi$.

Fig. 5.5 shows n vs τ for the same values of $g_h = |g_v|$. Here, optimizing τ does yield a small improvement at $g_h = |g_v| = 1.78\Omega_m$, bringing n down by 2.6% to 1.51 by adjusting τ to $1.42 \cdot \Omega_m^{-1}$. It is not entirely clear why adjusting τ away from $\pi/(2\Omega_m)$ improves the phonon number, but we ascribe the effect to a modified effective mechanical frequency at strong feedback. We finally remark that for $g_h = |g_v| = 1.78\Omega_m$, minimizing n w.r.t $x + \phi$ and τ simultaneously yields $n = 1.49$ at $x + \phi = -1.33$, $\tau = 1.32/\Omega_m$, a 4% improvement.

In summary, optimizing these parameters only leads to very insignificant improvements. On the positive side, the results also show that the experiment are not too sensitive to these parameters.

5.5 Conclusion

We have analysed a model of all-optical coherent feedback cooling in an optomechanical system. We have derived the appropriate equations of motion in a linearized regime, and provided analytical expressions for the steady-state solution to the system in Fourier space and the power

spectral density. We have investigated the model's ability to cool the mechanical phonon number. Through numerical analysis, we have shown that the model comes close to, but does not outperform the measurement-based feedback scheme described in earlier chapters, at least when all optical sources of noise are eliminated (but the quantum noise). We expect that this model may still be useful, in particular because it may pose a simpler way to perform feedback experimentally.

5.6 Appendix: Analytical expression of $S_{QQ}(\omega)$

In this section, the full analytical expression of the power spectral density $S_{QQ}(\omega)$ is written out. From Eq. (5.3.11), we find that:

$$\begin{aligned}
S_{QQ}(\omega) =& \chi(\omega)\chi(-\omega)\Bigg[\\
&\frac{1}{16}\Gamma_m(2\bar{n}+1)\left(\kappa_h^2+4\omega^2\right)\left(\kappa_v^2+4\omega^2\right) \\
&+\frac{1}{2}g_h^2(\kappa_h^{\mathrm{in}}+\kappa_h^{\mathrm{loss}})\left(\kappa_v^2+4\omega^2\right) \\
&+\frac{1}{2}|g_v|^2\left(\kappa_h^2(\kappa_v^{\mathrm{in}}+\kappa_v^{\mathrm{loss}})+4\kappa_h^{\mathrm{in}}\kappa_v^{\mathrm{in}}(\kappa_h^{\mathrm{in}}+\kappa_h^{\mathrm{loss}}-4\kappa_h)+4\omega^2(\kappa_v^{\mathrm{in}}+\kappa_v^{\mathrm{loss}})\right) \\
&+g_h|g_v|\cos(-\tau\omega+x+\phi) \\
&\quad\times\left(\kappa_h\kappa_v\sqrt{\kappa_h^{\mathrm{in}}\kappa_v^{\mathrm{in}}}-2\kappa_v\sqrt{(\kappa_h^{\mathrm{in}})^3\kappa_v^{\mathrm{in}}}-2\kappa_h^{\mathrm{loss}}\kappa_v\sqrt{\kappa_h^{\mathrm{in}}\kappa_v^{\mathrm{in}}}+4\omega^2\sqrt{\kappa_h^{\mathrm{in}}\kappa_v^{\mathrm{in}}}\right) \\
&-2g_h|g_v|\omega\sin(-\tau\omega+x+\phi) \\
&\quad\times\left(\sqrt{\kappa_h^{\mathrm{in}}\kappa_v^{\mathrm{in}}}(-\kappa_h+2\kappa_h^{\mathrm{loss}}+\kappa_v)+2\sqrt{(\kappa_h^{\mathrm{in}})^3\kappa_v^{\mathrm{in}}}\right)\Bigg]
\end{aligned} \tag{5.6.1}$$

where the definition of the susceptibility $\chi(\omega)$ is given in Eq. (5.3.9), but repeated here for the sake of convenience:

$$[\chi(\omega)]^{-1}=\left(i\Gamma_m\omega+\omega^2-1\right)\left(\frac{\kappa_h}{2}-i\omega\right)\left(\frac{\kappa_v}{2}-i\omega\right)-4g_h|g_v|\sqrt{\kappa_h^{\mathrm{in}}\kappa_v^{\mathrm{in}}}e^{i\tau\omega}\sin(x+\phi) \tag{5.6.2}$$

Chapter 6

Conclusion

In this chapter, we review the results presented in this dissertation.

In Chapter 3, we investigated an optomechanical measurement-based conditional estimation-based optimal control strategy for mechanical cooling and squeezing, assuming either a rotating-wave approximation (RWA) or non-rotating-wave approximation (nonRWA) of the mechanical interaction with its thermal environment. We showed parameter regimes in which cooling and squeezing is possible, and where the RWA disagrees with the RWA model. We also compared the model to the model in [45], in which an adiabatic approximation is assumed, and showed where this approximation breaks down. We also showed the important difference between the conditional and the unconditional phonon numbers and squeezing levels, and emphasized why the conditional and unconditional states cannot in general coincide in an optomechanical experiment using optimal feedback control. Finally, we discussed the effect of optimizing the homodyne measurement angle θ.

In Chapter 4, we derived an extension of the model in Chapter 3 to allow for squeezed probe fields, and used this model to calculate how this changes the conditional phonon number and conditional squeezing values. We found that improvements in both the phonon numbers and squeezing values are found when using phase-squeezed light in the probe field and discussed the reasons why phase squeezing is optimal in this case.

Finally, in Chapter 5, we investigated a model for so-called coherent feedback cooling, in which the output field from the cavity is run through a delay line before being fed back directly into the cavity, without any intermediate measurement. We discussed the points at which this feedback system is stable, and calculated the obtainable phonon numbers for a selection of parameters. We found that when the optomechanical coupling strengths in the model are tuned appropriately, the performance of the scheme comes close to, but does not outperform the scheme in Chapter 3, at least when optical losses are neglected. This is in general promising, as the this latter experiment will most often be easier to carry out than that in Chapter 3, since one does not need to worry about optimizing the feedback filter and measurement efficiencies.

In summary, we expect these results to be useful when designing optomechanical feedback cooling experiments. They show to a certain extent which parameters are important and which are not, and show which phonon numbers and squeezing levels one can expect under different physical conditions and design constraints. This work thus helps paving the way for generating interesting non-classical and non-Gaussian states in optomechanics, where the mechanical noise needs to be reduced as much as possible.

Chapter 7

Bibliography

[1] M. Aspelmeyer, T. J. Kippenberg, and F. Marquardt, "Cavity optomechanics," *Reviews of Modern Physics*, vol. 86, no. 4, pp. 1391–1452, 2014.

[2] W. P. Bowen and G. J. Milburn, *Quantum Optomechanics*. CRC Press, 2016.

[3] S. Barzanjeh, A. Xuereb, S. Gröblacher, M. Paternostro, C. A. Regal, and E. M. Weig, "Optomechanics for quantum technologies," *Nature Physics*, vol. 18, no. 1, pp. 15–24, 2022.

[4] S. G. Hofer, W. Wieczorek, M. Aspelmeyer, and K. Hammerer, "Quantum entanglement and teleportation in pulsed cavity optomechanics," *Physical Review A - Atomic, Molecular, and Optical Physics*, vol. 84, no. 5, pp. 1–10, 2011.

[5] T. A. Palomaki, J. W. Harlow, J. D. Teufel, R. W. Simmonds, and K. W. Lehnert, "Coherent state transfer between itinerant microwave fields and a mechanical oscillator," *Nature*, vol. 495, no. 7440, pp. 210–214, 2013.

[6] R. Y. Teh, S. Kiesewetter, M. D. Reid, and P. D. Drummond, "Simulation of an optomechanical quantum memory in the nonlinear regime," *Physical Review A*, vol. 96, no. 1, 2017.

[7] A. Wallucks, I. Marinković, B. Hensen, R. Stockill, and S. Gröblacher, "A quantum memory at telecom wavelengths," *Nature Physics*, vol. 16, no. 7, pp. 772–777, 2020.

[8] A. I. Lvovsky, P. Grangier, A. Ourjoumtsev, V. Parigi, M. Sasaki, and R. Tualle-Brouri, "Production and applications of non-Gaussian quantum states of light," pp. 1–50, 2020.

[9] M. V. Larsen, X. Guo, C. R. Breum, J. S. Neergaard-Nielsen, and U. L. Andersen, "Deterministic generation of a two-dimensional cluster state," *Science*, vol. 366, no. 6463, pp. 369–372, 2019.

[10] H. S. Zhong, Y. H. Deng, J. Qin, H. Wang, M. C. Chen, L. C. Peng, Y. H. Luo, D. Wu, S. Q. Gong, H. Su, Y. Hu, P. Hu, X. Y. Yang, W. J. Zhang, H. Li, Y. Li, X. Jiang, L. Gan, G. Yang, L. You, Z. Wang, L. Li, N. L. Liu, J. J. Renema, C. Y. Lu, and J. W. Pan, "Phase-Programmable Gaussian Boson Sampling Using Stimulated Squeezed Light," *Physical Review Letters*, vol. 127, no. 18, p. 180502, 2021.

[11] A. Deshpande, A. Mehta, T. Vincent, N. Quesada, M. Hinsche, M. Ioannou, L. Madsen, J. Lavoie, H. Qi, J. Eisert, D. Hangleiter, B. Fefferman, and I. Dhand, "Quantum computational advantage via high-dimensional gaussian boson sampling," *Science Advances*, vol. 8, no. 1, p. eabi7894, 2022.

[12] S. Hong, R. Riedinger, I. Marinković, A. Wallucks, S. G. Hofer, R. A. Norte, M. Aspelmeyer, and S. Gröblacher, "Hanbury Brown and Twiss interferometry of single phonons from an optomechanical resonator," *Science*, vol. 358, no. 6360, pp. 203–206, 2017.

[13] Y. Tsaturyan, A. Barg, E. S. Polzik, and A. Schliesser, "Ultracoherent nanomechanical resonators via soft clamping and dissipation dilution," *Nature Nanotechnology*, vol. 12, no. 8, pp. 776–783, 2017.

[14] D. Høj, F. Wang, W. Gao, U. B. Hoff, O. Sigmund, and U. L. Andersen, "Ultra-coherent nanomechanical resonators based on inverse design," *Nature Communications*, vol. 12, no. 1, pp. 1–8, 2021.

[15] R. Riedinger, A. Wallucks, I. Marinković, C. Löschnauer, M. Aspelmeyer, S. Hong, and S. Gröblacher, "Remote quantum entanglement between two micromechanical oscillators," *Nature*, vol. 556, no. 7702, pp. 473–477, 2018.

[16] K. C. Lee, M. R. Sprague, B. J. Sussman, J. Nunn, N. K. Langford, X. M. Jin, T. Champion, P. Michelberger, K. F. Reim, D. England, D. Jaksch, and I. A. Walmsley, "Entangling macroscopic diamonds at room temperature," *Science*, vol. 334, no. 6060, pp. 1253–1256, 2011.

[17] I. Marinković, A. Wallucks, R. Riedinger, S. Hong, M. Aspelmeyer, and S. Gröblacher, "Optomechanical Bell Test," *Physical Review Letters*, vol. 121, no. 22, pp. 1–6, 2018.

[18] G. Enzian, J. J. Price, L. Freisem, J. Nunn, J. Janousek, B. C. Buchler, P. K. Lam, and M. R. Vanner, "Single-Phonon Addition and Subtraction to a Mechanical Thermal State," *Physical Review Letters*, vol. 126, no. 3, p. 33601, 2021.

[19] R. Abbott et al. (LIGO Scientific Collaboration and Virgo Collaboration), "Approaching the motional ground state of a 10-kg object," *Science*, vol. 372, no. 6548, pp. 1333–1336, 2021.

[20] P. Kharel, G. I. Harris, E. A. Kittlaus, W. H. Renninger, N. T. Otterstrom, J. G. Harris, and P. T. Rakich, "High-frequency cavity optomechanics using bulk acoustic phonons," *Science Advances*, vol. 5, no. 4, pp. 1–9, 2019.

[21] S. Bose, K. Jacobs, and P. L. Knight, "Preparation of nonclassical states in cavities with a moving mirror," *Physical Review A*, vol. 56, pp. 4175–4186, nov 1997.

[22] U. B. Hoff, J. Kollath-Bönig, J. S. Neergaard-Nielsen, and U. L. Andersen, "Measurement-Induced Macroscopic Superposition States in Cavity Optomechanics," *Physical Review Letters*, vol. 117, no. 14, pp. 1–6, 2016.

[23] I. Shomroni, L. Qiu, and T. J. Kippenberg, "Optomechanical generation of a mechanical catlike state by phonon subtraction," *Physical Review A*, vol. 101, no. 3, 2020.

[24] U. Delić, M. Reisenbauer, K. Dare, D. Grass, V. Vuletić, N. Kiesel, and M. Aspelmeyer, "Cooling of a levitated nanoparticle to the motional quantum ground state," *Science*, vol. 367, pp. 892–895, feb 2020.

[25] S. Mancini, D. Vitali, and P. Tombesi, "Optomechanical Cooling of a Macroscopic Oscillator by Homodyne Feedback," *Physical Review Letters*, vol. 80, pp. 688–691, jan 1998.

[26] C. Genes, D. Vitali, P. Tombesi, S. Gigan, and M. Aspelmeyer, "Ground-state cooling of a micromechanical oscillator: Comparing cold damping and cavity-assisted cooling schemes," *Phys. Rev. A*, vol. 77, p. 033804, Mar 2008.

[27] H. Habibi, E. Zeuthen, M. Ghanaatshoar, and K. Hammerer, "Quantum feedback cooling of a mechanical oscillator using variational measurements: tweaking heisenberg's microscope," *Journal of Optics*, vol. 18, p. 084004, jul 2016.

[28] S. Zippilli, N. Kralj, M. Rossi, G. Di Giuseppe, and D. Vitali, "Cavity optomechanics with feedback-controlled in-loop light," *Physical Review A*, vol. 98, no. 2, pp. 1–19, 2018.

[29] M. Rossi, D. Mason, J. Chen, Y. Tsaturyan, and A. Schliesser, "Measurement-based quantum control of mechanical motion," *Nature*, vol. 563, no. 7729, pp. 53–58, 2018.

[30] F. Tebbenjohanns, M. L. Mattana, M. Rossi, M. Frimmer, and L. Novotny, "Quantum control of a nanoparticle optically levitated in cryogenic free space," *Nature*, vol. 595, no. 7867, pp. 378–382, 2021.

[31] H. M. Wiseman and G. J. Milburn, "Quantum theory of field-quadrature measurements," *Physical Review A*, vol. 47, no. 1, pp. 642–662, 1993.

[32] K. Jacobs and D. A. Steck, "A straightforward introduction to continuous quantum measurement," *Contemporary Physics*, vol. 47, no. 5, pp. 279–303, 2006.

[33] A. C. Doherty and K. Jacobs, "Feedback control of quantum systems using continuous state estimation," *Physical Review A - Atomic, Molecular, and Optical Physics*, vol. 60, no. 4, pp. 2700–2711, 1999.

[34] H. M. Wiseman and G. J. Milburn, *Quantum measurement and control*, vol. 9780521804. Cambridge University Press, 2010.

[35] W. Wieczorek, S. G. Hofer, J. Hoelscher-Obermaier, R. Riedinger, K. Hammerer, and M. Aspelmeyer, "Optimal State Estimation for Cavity Optomechanical Systems," *Physical Review Letters*, vol. 114, no. 22, pp. 1–6, 2015.

[36] A. Setter, M. Toroš, J. F. Ralph, and H. Ulbricht, "Real-time Kalman filter: Cooling of an optically levitated nanoparticle," *Physical Review A*, vol. 97, no. 3, pp. 1–8, 2018.

[37] L. Magrini, P. Rosenzweig, C. Bach, A. Deutschmann-Olek, S. G. Hofer, S. Hong, N. Kiesel, A. Kugi, and M. Aspelmeyer, "Real-time optimal quantum control of mechanical motion at room temperature," *Nature*, vol. 595, no. 7867, pp. 373–377, 2021.

[38] M. Rossi, D. Mason, J. Chen, and A. Schliesser, "Observing and Verifying the Quantum Trajectory of a Mechanical Resonator," *Physical Review Letters*, vol. 123, no. 16, p. 163601, 2019.

[39] R. A. Thomas, M. Parniak, C. Østfeldt, C. B. Møller, C. Bærentsen, Y. Tsaturyan, A. Schliesser, J. Appel, E. Zeuthen, and E. S. Polzik, "Entanglement between distant macroscopic mechanical and spin systems," *Nature Physics*, vol. 17, no. 2, pp. 228–233, 2021.

[40] A. C. Doherty, A. Szorkovszky, G. I. Harris, and W. P. Bowen, "The quantum trajectory approach to quantum feedback control of an oscillator revisited," in *Philosophical Transactions of the Royal Society A: Mathematical, Physical and Engineering Sciences*, vol. 370, pp. 5338–5353, 2012.

[41] M. G. Genoni, J. Zhang, J. Millen, P. F. Barker, and A. Serafini, "Quantum cooling and squeezing of a levitating nanosphere via time-continuous measurements," *New Journal of Physics*, vol. 17, no. 7, 2015.

[42] S. G. Hofer and K. Hammerer, "Entanglement-enhanced time-continuous quantum control in optomechanics," *Physical Review A*, vol. 91, p. 033822, mar 2015.

[43] N. Yamamoto and T. Mikami, "Entanglement-assisted quantum feedback control," *Quantum Information Processing*, vol. 16, no. 7, pp. 1–23, 2017.

[44] A. Di Giovanni, M. Brunelli, and M. G. Genoni, "Unconditional mechanical squeezing via backaction-evading measurements and nonoptimal feedback control," *Physical Review A*, vol. 103, no. 2, p. 22614, 2021.

[45] C. Meng, G. A. Brawley, J. S. Bennett, M. R. Vanner, and W. P. Bowen, "Mechanical Squeezing via Fast Continuous Measurement," *Physical Review Letters*, vol. 125, no. 4, p. 43604, 2020.

[46] J. Guo, R. Norte, and S. Gröblacher, "Feedback Cooling of a Room Temperature Mechanical Oscillator close to its Motional Ground State," *Physical Review Letters*, vol. 123, no. 22, p. 223602, 2019.

[47] S. A. Saarinen, N. Kralj, E. C. Langman, Y. Tsaturyan, and A. Schliesser, "Laser cooling a membrane-in-the-middle system close to the quantum ground state from room temperature," pp. 8–11, 2022.

[48] C. Weedbrook, S. Pirandola, R. García-Patrón, N. J. Cerf, T. C. Ralph, J. H. Shapiro, and S. Lloyd, "Gaussian quantum information," *Reviews of Modern Physics*, vol. 84, no. 2, pp. 621–669, 2012.

[49] C. C. Gerry and P. L. Night, *Introductory Quantum Optics*. Cambridge University Press, 2005.

[50] C. K. Law, "Interaction between a moving mirror and radiation pressure: A Hamiltonian formulation," *Physical Review A*, vol. 51, pp. 2537–2541, mar 1995.

[51] F. W. Isaksen, "Quantum state transfer in optomechanics," Master's thesis, Technical University of Denmark, 2019.

[52] G. W. Ford, J. T. Lewis, and R. F. O'Connell, "Quantum langevin equation," *Phys. Rev. A*, vol. 37, pp. 4419–4428, Jun 1988.

[53] C. W. Gardiner and M. J. Collett, "Input and output in damped quantum systems: Quantum stochastic differential equations and the master equation," *Physical Review A*, vol. 31, pp. 3761–3774, jun 1985.

[54] F. W. Isaksen and U. L. Andersen, "Mechanical cooling and squeezing using optimal control," 2022. *arXiv preprint at https://arxiv.org/abs/2207.07785*.

[55] J. Chan, T. P. Alegre, A. H. Safavi-Naeini, J. T. Hill, A. Krause, S. Gröblacher, M. Aspelmeyer, and O. Painter, "Laser cooling of a nanomechanical oscillator into its quantum ground state," *Nature*, vol. 478, no. 7367, pp. 89–92, 2011.

[56] A. A. Clerk, F. Marquardt, and K. Jacobs, "Back-action evasion and squeezing of a mechanical resonator using a cavity detector," *New Journal of Physics*, vol. 10, 2008.

[57] V. P. Belavkin, "Theory of the control of observable quantum systems," *Remote Control*, vol. 44, p. 178, 1983.

[58] V. P. Belavkin, "Nondemolition measurements, nonlinear filtering and dynamic programming of quantum stochastic processes," in *Modeling and Control of Systems* (A. Blaquiére, ed.), pp. 245–265, Springer Berlin Heidelberg, 1989.

[59] V. P. Belavkin, "Measurement, filtering and control in quantum open dynamical systems," *Rep. Math. Phys.*, vol. 43, p. 405, 1999.

[60] R. Hamerly and H. Mabuchi, "Coherent controllers for optical-feedback cooling of quantum oscillators," *Physical Review A*, vol. 87, p. 013815, jan 2013.

[61] C. W. Gardiner and P. Zoller, *a handbook of Markovian and non-Markovian quantum stochastic methods with applications to quantum optics*, vol. 16. Springer-Verlag Berlin Heidelberg, 2nd enl. ed., 2000.

[62] A. O. Caldeira and A. J. Leggett, "Path integral approach to quantum Brownian motion," *Physica A: Statistical Mechanics and its Applications*, vol. 121, no. 3, pp. 587–616, 1983.

[63] V. Giovannetti and D. Vitali, "Phase-noise measurement in a cavity with a movable mirror undergoing quantum Brownian motion," *Physical Review A*, vol. 63, p. 023812, jan 2001.

[64] L. Isserlis, "On a Formula for the Product-Moment Coefficient of any Order of a Normal Frequency Distribution in any Number of Variables," *Biometrika*, vol. 12, no. 1/2, p. 134, 1918.

[65] U. Leonhardt and M. Beck, "Measuring the Quantum State of Light," *American Journal of Physics*, vol. 66, no. 6, pp. 550–551, 1998.

[66] R. Simon, N. Mukunda, and B. Dutta, "Quantum-noise matrix for multimode systems: U(n) invariance, squeezing, and normal forms," *Physical Review A*, vol. 49, no. 3, pp. 1567–1583, 1994.

[67] A. Laub, "A schur method for solving algebraic Riccati equations," in *1978 IEEE Conference on Decision and Control including the 17th Symposium on Adaptive Processes*, pp. 60–65, IEEE, jan 1978.

[68] K. Gu, V. L. Kharitonov, and J. Chen, *Stability of Time-Delay Systems*. Boston, MA: Birkhäuser Boston, 1 ed., 2003.